UNIVERSITY OF CALIFORNIA, SAN DIEGO

Molecular Gating Dynamics of the Cytoplasmic Domains Of Inwardly Rectifying Potassium (Kir) Channels

A dissertation submitted in partial satisfaction of the

requirements for the degree Doctor of Philosophy

in

Chemistry

by

Scott Dusan Pegan

Committee in charge:

Professor Senyon Choe, Chair
Professor Elizabeth A. Komives, Co-Chair
Professor Partho Ghosh
Professor Douglas Magde
Professor Julian I. Schroeder

2006

The dissertation of Scott Dusan Pegan is approved, and it is acceptable in quality and form for publication on microfilm:

_____

_____

_____

_____

_____

Chair

University of California, San Diego

2006

Dedicated to:

Clarence O. Muskopf (1900-1982), beloved grandfather, who inspired my love of nature and served as a role model of humanity and generosity.

Nelson Fong & Eric Lyons, teachers, who first inspired my love of both mathematics and science.

Kristi Hull (1978-1998), friend, who lit the fire of my passion for biochemistry.

Kathryn L. Pegan, beloved wife, whose love and support have made her my everything.

TABLE OF CONTENTS

LIST OF SYMBOLS AND ABBREVIATIONS

KIR: Potassium Inwardly Rectifying Channel

IRK1: Inwardly Rectifying Potassium Channel (Kir2.1)

GIRK1: G-protein Gated Inwardly Rectifying Potassium Channel (Kir3.1)

K_{ATP}: ATP inhibited Channel (Kir6.2)

PIP_2: Phosphatidylinositol 4, 5 Bisphosphate

AS: Andersen's Syndrome

Kv: voltage-gated potassium (K)

MPD: 2-methyl-2,4-pentanediol

$Kir2.1_L$: Kir2.1 Cytoplasmic Domains (44-64; 189-428)

$Kir2.1_S$: Kir2.1 Cytoplasmic Domains (44-64; 189-371)

IPTG: isopropyl-beta-D-thiogalactopyranoside

DTT: dithiothreitol; wt: wild-type

LIST OF FIGURES

Chapter One Figures

Chapter Two Figures

Chapter Three Figures

Chapter Four Figures

Chapter Five Figures

Chapter Six Figures

LIST OF TABLES

Chapter One Tables

Chapter Two Tables

Chapter Three Tables

ACKNOWLEDGEMENTS

First and foremost, I would like to thank Dr. Senyon Choe for his guidance and support of my research through the last five and half years. Only with his assistance and understanding was I able to serve our Country in Baghdad, Iraq as part of Operation Iraqi Freedom for over a year while still being able to complete this dissertation within the departmental average. I would also like to thank my co-authors, Christine Arrabit, Wei Zhou, Witek Kwiatkowski, Anthony Collins, Paul Slesinger, and Roland Riek, for their contribution of unique talents and perspectives that made this research possible. One particular colleague I would like to highlight is Kent Baker. Although he did not directly contribute to this work, his council I regard as indispensable in making me the scientist I am today. My thanks goes out to the American Heart Association and National Institute of Health Molecular Biophysics Training Grant (GM 08326) for their support of my research.

Just as important to the completion of research, if not more, is family. I want to thank my wonderful wife Kathryn for her understanding and support through these last few years. Her love and support knew no bounds as she would bring me company and sustenance many times throughout the long nights and weekends that it takes for these types of undertakings. I would also like to thank my parents Gregory and Joyce for their love and support throughout the journey of the past 28 years.

Chapter 2 is in part a reprint of the material as it appears in Pegan, S., Arrabit, C., Zhou W., Kwiatkowski W., Collins A., Slesinger PA., Choe, S. (2005) *Cytoplasmic domain structures of Kir2.1 and Kir3.1 shows sites for modulating gating and rectification.* Nat Neurosci. **8**: 279-287. Chapter 3 is in part a reprint of the material that has been submitted for publication as Pegan, S., Arrabit, C., Slesinger, P. A., and Choe, S. (2006). *Andersen's Syndrome Mutation Effects on the Structure and Assembly of the Cytoplasmic Domains of Kir2.1.* Submitted. Chapter 6 is in part a reprint of the material as it appears in Pegan, S., Kwiatkowski, W., Choe, S., Riek, R. (2003) *High-throughput backbone resonance assignment of small ^{13}C, ^{15}N labeled proteins by a triple resonance experiment with four sequential connectivity pathways using chemical shift-dependent apparent $^{1}J(^{1}H,^{13}C)$: HNCACB^{coded}HAHB.* J. Magn. Reson., **165**: 315-319. The dissertation author was the primary research and author of these publications.

VITA

Education

1992-1996	Livermore High School, CA, USA
1996-1997	California State University Hayward, CA, GPA: 3.6
1997-2000	B.S. with Honors in Biochemistry Molecular Biology, University of California Santa Barbara, CA, GPA: 3.4
2000-2002	M.S. in Chemistry Biochemistry, University of California San Diego, CA
2002-2006	Ph.D. in Chemistry Biochemistry, University of California San Diego, CA

Awards

Academic

1999	University California Santa Barbara Dean's List
1999, 2000	ROTC Scholastic Award
1999, 2000	American Legion Award for Scholastic Excellence
2006	Keystone Symposia Structural Biology; Linking Cardiac Arrhythmia to Gene Defects; Scholarship Winner; Poster Winner; Short Talk Speaker
2003-2006	Molecular Biophysics Training Grant Recipient

Military Awards

2 U.S. Army Commendation Medal; 1 National Defense Medal; 1 U.S. Defense Medal; 2 U.S. Army Reserve Achievement Medal; 3 Overseas Reserve Training Ribbon; 1 Reserve Mobilization Ribbon; 1 Global War on Terrorism Expeditionary Medal

PUBLICATIONS

Articles

Pegan, S., Arrabit, C., Slesinger, P. A., and Choe, S. (2006). *Andersen's Syndrome Mutation Effects on the Structure and Assembly of the Cytoplasmic Domains of Kir2.1.* Submitted.

Pegan, S., Arrabit, C., Zhou W., Kwiatkowski W., Collins A., Slesinger PA., Choe, S. (2005) *Cytoplasmic domain structures of Kir2.1 and Kir3.1 shows sites for modulating gating and rectification.* Nat Neurosci. **8**: 279-287

Pegan, S., Kwiatkowski, W., Choe, S., Riek, R. (2003) *High-throughput backbone resonance assignment of small ^{13}C, ^{15}N labeled proteins by a triple resonance experiment with four sequential connectivity pathways using chemical shift-dependent apparent $^{1}J(^{1}H,^{13}C)$: HNCACB^{coded}HAHB.* J. Magn. Reson., **165**: 315-319

FIELDS OF STUDY

Major Field: Biochemistry

Biochemistry: Studies in Structural Components of Ion Channel Gating

ABSTRACT OF THE DISSERTATION

Molecular Gating Dynamics of the Cytoplasmic Domains Of Inwardly Rectifying Potassium (Kir) Channels

by

Scott Dusan Pegan

Doctor of Philosophy in Chemistry

University of California, San Diego, 2006

Professor Senyon Choe, Chair

My research focuses on understanding the mechanisms of eukaryotic inwardly rectifying potassium channels (Kir), which are responsible for creating membrane potential stability. N- and C-terminal cytoplasmic domains of inwardly rectifying K (Kir) channels control the ion-permeation pathway through diverse interactions with small molecules and protein ligands in the cytoplasm. Two crystal structures of the cytoplasmic domains of Kir2.1 ($Kir2.1_L$) and the G protein-sensitive Kir3.1 ($Kir3.1_S$) channels in the absence of PIP_2 show the cytoplasmic ion-permeation pathways occluded by four cytoplasmic loops that form a girdle around the central pore (G-loop). Significant flexibility of the pore-facing G-loop of $Kir2.1_L$ and $Kir3.1_S$ suggest a

possible role as a diffusion barrier between cytoplasmic and transmembrane pores. Consistent with this, mutations of the G-loop disrupted gating or inward rectification. Structure comparison reveals a di-aspartate cluster on the distal end of the cytoplasmic pore of $Kir2.1_L$ that is important for modulating inward rectification. The $Kir2.1_L$ structural allows us the first structural look at the potential causes of Andersen's Syndrome, which is caused by defects in the inwardly rectifying potassium channel 2.1 (Kir2.1). We have characterized individual Andersen's Syndrome mutants R218Q, G300V, E303K, and Δ314-315 and have shown that they have multiple affects on the ability of Kir2.1 channel's cytoplasmic domains to assemble into proper tetrameric assemblies. The 2.0 Å x-ray crystal structure of the N- and C-terminal cytoplasmic domains of Kir2.1 R218Q combined with T309K, reveals the G-loop and CD loop disruptions by the R218Q mutation. We show that E303 plays an important role in gating. Moreover, we demonstrate a novel DE loop stabilizing 2-methyl-2,4-pentanediol binding site, and cytoplasmic bound potassium ion, the first identified for this class of K channels. We have also conducted NMR studies on the last 58 residues of Kir2.1 to show the flexibility of this region and binding footprint of PSD95 PDZ domains, which tethers the channels to the cell's cytoskeleton. Taken together, these results demonstrate that cytoplasmic domains of Kir channels are structurally significant components of the channel and undergo structural changes to modulate gating and inward rectification.

SECTION I

CHAPTER ONE

Introduction

1.1 INTRODUCTION

Ion channels are a diverse group of proteins with the sole function of manipulating an organism's excitable cells electrochemical gradients in order to maintain ion homeostasis and control cell signaling. These ion movements have been harnessed by eukaryotic organisms to provide a host of beneficial functions that includes but are not limited to the coordination of muscular movement, secretion of neurotransmitters in the brain, and pancreatic secretion of insulin (Hille, 2001). One of the key components of this signaling system is the Potassium Inwardly Rectifying (Kir) Channels. In this chapter, I will give a brief synopsis of the biophysics involved in use of use of electrochemical gradients by cells, a simplistic brief view on action potential generation and propagation, a look into the diversity of the Kir Channels, and the use of Kir2.1 as a model system for the Kir Family.

Basis for the Function of Ion Channels. Through the use of the giant squid neuron in the 1940s and 1950s, Hodgkin and Huxeley were the first to link electrical currents to the membrane permeability of Na^+, K^+, and Ca^{2+} ions (Hodgkin and Huxley, 1952). The underlying mechanism for generation and propagation of electrical current in cells is based on these cells being able to develop and control a trans-membrane electrochemical gradient. In order to better understand electrochemical gradients and how they are formed, we can view their formation in the context of a beaker sectioned into two halves, which is separated by a cation

permeable membrane (Figure 1.1). The addition of a certain amount of cation (C^+) and anion (A^-) to the right side and double of that to the left side creates an equilibrium force for both the cation and anion to travel to side one. However, the membrane is only permeable to the cation. As a result, the cation will travel via thermal forces through the membrane making right side contain more positive ions than left side. This translates into a voltage difference that will grow until an equal force; the electrical force attracting the cations to the anions prevents them. The voltage difference at this equilibrium is referred to as equilibrium potential for that ion (Hille, 2001). The equilibrium potential (E_x) can be calculated by Nernst equation:

$$E_x = (RT/F) \ln (X_o/X_i); \text{ where } X = \text{ion of concern}$$

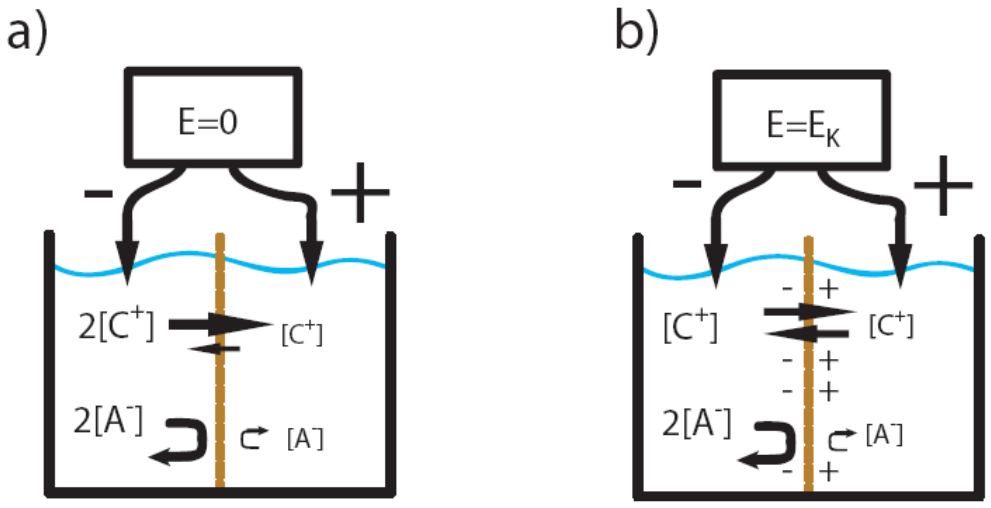

Figure 1.1 Theoretical Model of Equilibrium Potential. C+ and A^- represent cations and anions respectively. (a) System at time of addition of C^+A^-. (b) Beaker after System at equilibrium.

Using the mammalian muscle cell as an example of this model applied in nature, we can clearly see how the different ion equilibrium potentials play a role in determining the overall equilibrium potential of a cell at rest, also known as the resting potential. The typical muscle cell contains a low amount of sodium internally compared with the extracellular environment, which translates into an E_{Na}= +67 mV (Table 1.1). Potassium concentration on the other hand, is high in the cell and low outside creating an E_k= -98 mV. Ca^{2+} can also potentially influence the trans-membrane potential; however, most of this ion is trapped in internal cellular stores for intercellular signally and indirectly affects the resting potential through more complicated pathways. This leaves Na^+ and K^+ as the major players involved with the generation and propagation of membrane potential (Hille, 2001).

Table 1.1: Ion Concentrations and Equilibrium Potentials for Mammalian Skeletal Muscle.

Ion	Extracellular Concentration (mM)	Intracellular Concentration (mM)	(Hodgkin and Huxley)$_o$/(Hodgkin and Huxley)$_i$	Equilibrium Potential[a] (mV)
Na^+	145	12	12	+67
K^+	4	155	.026	-98
Ca^{2+}	1.5	100nM	15,000	+129
Cl^-	123	4.2[b]	29[b]	-90[b]

[a]Calculated from Nernst equation; E_x = (RT/F) ln ((Hodgkin and Huxley)$_o$/(Hodgkin and Huxley)$_i$), where X = ion of concern; T=310 K; R= 8.3145 V C mol^{-1} K^{-1}; F = 9.6485 e4 C mol^{-1}

[b]Calculated assuming a -90 mV resting potential for the muscle membrane
Data from (Hille, 2001)

Na^+ Action Potential Generation and Propagation. In the muscle cell, the cellular membrane serves the role of the semi permeable membrane of the model. In contrast to the model; however, the cellular membrane is not statically fixed on what ions can transverse it (Alberts et al., 1994). Although the lipid bi-layer is not very permeable to ions, ion channels present in the membrane can open or close to create selective pores for ions to travel though. Excitable types of cells utilize this flexibility in order to generate electric currents in the form of action potentials to propagate signal. Normally excitable cells have resting potentials in the range of -40 mV to -95 mV (Hille, 2001).

Electrical signals are generated by the ability of intracellular signal molecules, such as acetylcholine, to trigger plasma membrane receptors that allow the influx of Na^+ ions along their steep equilibrium gradient. The subsequent depolarization (voltage becomes more positive) triggers local Na^+ voltage gated (Na_v) channels to open briefly, thus furthering the depolarization in the local region. The neighboring Na_V channels detect the voltage change and open, thus propagating the electrical signal along the cell membrane (Alberts et al., 1994).

Once a cell is depolarized it must repolarize quickly to the resting potential in order to conduct the next action potential. Although the Na^+/K^+ ATP Pump, which pumps three Na^+ out, two K^+ in, and at the cost of one ATP, resets the ion

concentrations to the resting state and can help restore the resting potential, it only directly contributes 10% to repolarization and maintenance (Alberts et al., 1994). The other 90% is mostly comprised of the presence and function of potassium channels. The class of potassium channel that directly contributes to the restoration of membrane potential are the voltage-gated potassium (Kv) channels. These channels, also known as the delayed K^+ channels, open after the Na_V channels close in order allow K^+ out of the cell rapidly repolarizing it to resting state (Hille, 2001). However, they only restore the resting potential and are not the major force that maintains the resting membrane potential.

Potassium Inwardly Rectifier (Kir) Channels. Maintaining excitable cells at their resting potential falls to the potassium inwardly rectifying (Kir) channels (Enkvetchakul et al., 2005). They perform this duty by allowing K^+ to flow into the cell directionally opposite to the physiological outward flow of the K_v channels. This rectification occurs due to the binding of intracellular polyamines and Mg^{2+} ions that block the channel, preventing the outward flow of potassium ions (Figure 1.1; (Jan and Jan, 1997)). This phenomenon has been widely studied through electrophysiology method of patch clamping Xenopus oocytes injected with Kir Channel mRNA.

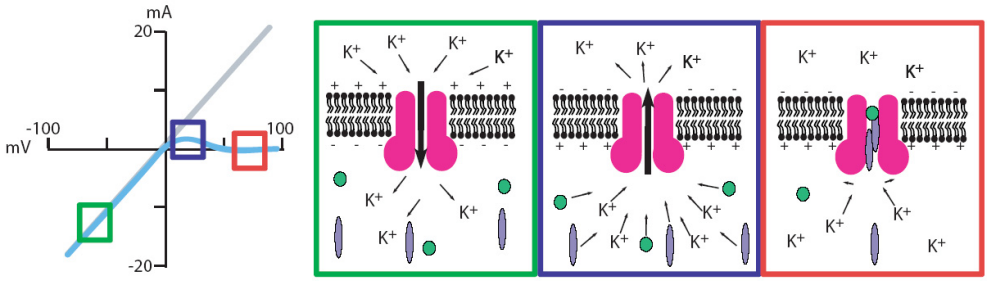

Figure 1.2. Electrophysiology Current Voltage schemes for an open pore channel vs. a generic Kir channel. The K+ ion concentration is the same in and outside of this system. The teal line is a generic Kir channel, gray an open pore, green balls Mg2+, purple ovals are polyamines (spermidine or spermine).

As seen in Figure 1.2, these channels have a unique current-voltage curve that is only generated when a channel conducts large fluxes of ions in one direction and not the other. If the channels were just a simple open selective pore that ions could move through feeling either in or out of the cell when open, they would have a current voltage scheme that was linear with an x-intercept coupled to the ion concentration of the extracellular and intercellular environment and a slope tied to the gating of the channel. If the ion concentration of the outside and inside the cell is equal, and the ions are solely driven by the electrical gradient, the line would pass through zero. This linear profile does not occur however, with Kir channels. Their current voltage scheme curves cross ~ -90 mV, close to E_K due to the inside and outside concentrations of K^+, and rapidly curves horizontal representing the closing, or blocking, of these channels. The ability of these channels to allow only K^+ to a large extent into the cell has the general effect of driving the cell to the E_K of potassium. Some of the Kir family members capitalize on this ability to hyperpolarize the cell in

order to increase the difficulty of an action potential being formed in the cell (Enkvetchakul et al., 2005). As a result, the cell needs more extracelluar stimuli in order to fire.

Structure of the Transmembrane Region of Kir Channels. As with all potassium selective channels, Kir channels are tetrameric, contain an ion selectivity filter for potassium, a pore helix and two trans-membrane helices (Hille, 2001). The selectivity filter of these channels allow only potassium ions to pass through the channel by coordinating the dehydrated potassium ion state while blocking both the dehydrated and hydrated sodium ions (Figure 1.3; (Doyle et al., 1998). Flanking the selectivity filter in the amino acid sequence are the two trans-membrane helices that are the pore forming element of the channel. These helices, M1 and M2, are similar to the fifth and sixth helices in the Kv channel. Like the Kv channels and other prokaryotic channels, Kir channels are also proposed to contain a key glycine residue in its inner M2 helix that allows the bending of helix, which contains a hydrophobic residue whose side chain occludes the pore in the channel's closed state (Doyle et al., 1998). In addition to the two trans-membrane helices common to all K^+ channels, the Kir family also has a slider helix (SH) located on the N-terminal end of the trans-membrane region. The overall trans-membrane regions of the eukaryotic Kir channels are most likely to be homologous to the notably prokaryotic crystallized KcsA channel fragment and eukaryotic Kir like KirBac1.1 (Figure 1.3; (Doyle et al., 1998).

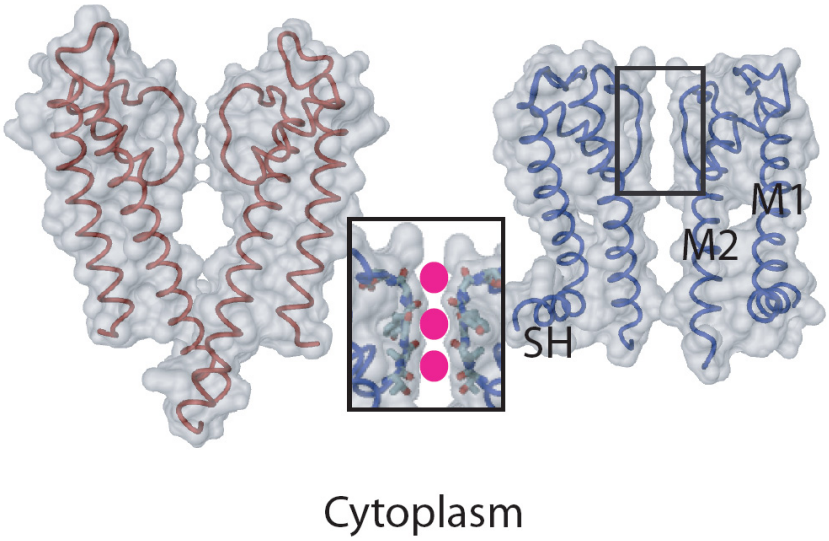

Figure 1.3. Homologous Transmembrane Structures of Procaryotic K+ Channels. In red; KcsA channel (22-124) x-ray crystal structure with two monomers removed (Zhou and MacKinnon, 2003). In blue; KirBac1.1 channel x-ray trans-membrane portion (46-153) crystal structure with two monomers removed. Blow-up is of the K+ selectivity filter of KirBac1.1 (110-115) (Doyle et al., 1998). K^+ in pink.

Diversity of Function in the Kir Channel Family. The Kir family contains seven subfamilies with several channels in each (Kir1.x-Kir7.x) (Hille, 2001). Although the trans-membrane regions of Kir channels are proposed to be functionally equivalent in all Kir Channels and K^+ channels at large, their cytoplamic domains are not. Kir family members all bind phyosphylinositol 4, 5 bisphosphate (PIP_2) in their cytoplasmic / trans-membrane interface in order to open. This is unique to eukaryotic Kir Channels as is seen with the PIP_2 inhibitory effect on the prokaryote, eukaryotic like KirBac1.1 (Enkvetchakul et al., 2005). However, most family members bind other ligands to their cytoplasmic domains to regulate function. As a result, the cytoplasmic domains are the major source of diversity in Kir channels function and

strongly suggest the cytoplasmic domains play a critical role in gating beyond that of the M2 outer helix. Along the lines of their gating in response to other ligands, the Kir family can be broken down into three general subgroups: G-protein gated, ATP-sensitive, and classic (Hille, 2001).

The G-protein gated subgroup (GIRK) contains four members (Kir 3.1-3.4) that form hetero-tetramers between Kir3.1 and other Kir3.(2-4) members and some homo-tetramers of Kir3.2 and Kir3.4 in some tissues through specificity mediated by both the trans-membrane and cytoplamic domains (Corey and Clapham, 1998; Finley et al., 2004; Inanobe et al., 1999; Silverman et al., 1996). Kir3.x channels, in addition to binding PIP_2, need to form protein-protein interactions, which are targeted by $G_{\alpha i/o}$, with the $G_{\beta\gamma}$ subunits in order to open (Clancy et al., 2005). These $G_{\beta\gamma}$ are dissociated from activated G protein-coupled receptors (GPCR) such as dopamine 2 receptor (d2R). The Kir3.x channels are inhibited by a pathway that involves phospholipase C (PLC) via a different type of GPCR, m1 muscarinic acetylcholine receptor (mAChR) (Hill and Peralta, 2001). Furthermore, small-molecule anesthetics, such as lidocaine and bupivacaine, also regulate Kir3.x channels by inhibiting their gating (Zhou et al., 2001). The main function of Kir3.x is to hyperpolarize the excitable cells located in the heart and the brain by allowing K^+ into the cell. As a result, these cells are hyperpolarize, which inhibits action potential formation. Abolishment of the function

of Kir3.x channels in these tissues leads to cardiac abnormalities and brain seizures (Signorini et al., 1997; Wickman et al., 1998).

Unlike the Kir3.x channels, ATP-sensitive channel (Kir 6.1-6.2) subgroup is inhibited by binding a ligand to its cytoplasmic domain. These channels also known as the K_{ATP} channels form homo-tetramers and interact with sulfonylurea receptor (SUR) protein that contains an ATP-binding cassette (Jan and Jan, 1997). Although the binding of ATP to the SUR protein creates an inhibitory effect on the gating of the channel though a protein-protein interaction, ATP has been shown also to directly inhibit the channel (Vanoye et al., 2002). These channels are primarily located in heart, muscular, and neuronal types of tissues. They couple the metabolic state of the cell to its membrane potential. Their involvement in cellular processes includes but is not limited to: inhibition of insulin secretion, neuronal glucose sensing, vascular smooth muscle tone, and response to cardiac arrhythmias (Trapp et al., 2003).

The classic subgroup of Kir channels contains the bulk of the Kir family members to include Kir1.x, Kir2.x, Kir4.x, Kir5.x, and Kir7.x (Hille, 2001). All of these channels are gated by their affinity for PIP_2 and pH with the exception of the Kir2.1 family, which solely responds PIP_2. Of these channels, Kir1.x, Kir4.x, Kir5.x, and Kir7.x are primarily proposed to control fluid transport in epithelia tissues (Schulze et al., 2003; Tateno et al., 2006). Kir2.1 is present in all excitable tissues and serves as the primary Kir that drives channels to E_K. All of the classic Kir

channels readily form homo-tetramers and small amount of hetero-tetramers within their own classical subfamily (Fakler et al., 1996; Hille, 2001; Preisig-Muller et al., 2002).

Kir2.1 Cytoplasmic Domains a Model System for Kir Gating, Rectification, and Kir Disease States. Of all the inward rectifiers, the Kir2.1 channel serves as a model system for study of these channels. The Kir2.1 channel possesses the most simplistic cytoplasmic triggered gating mechanism within the Kir families. It does not require extra protein ligands or pH change in order to open, only the presence of PIP_2 (Enkvetchakul et al., 2005). This allows us to easily study the core mechanism that the cytoplasmic domain utilizes in gating Kir channels. Furthermore, the Kir2.1 channel in found in nature as primarily a homotetrameric channel, removing the need to express multiple proteins to produce a functional channel or study a non-naturally occurring channel such as Kir3.1 that will be discussed in Chapter 2. Kir2.1 also is the strongest rectifier of the Kir channels providing us all the key residues involved with this process. In addition, the Kir2.1 channel sequence contains a PDZ binding motif that allows the study of how the Kir channels localize themselves in the post synaptic density area via protein-protein interactions (Nehring et al., 2000).

The study of the Kir2.1 channel also addresses the key issue how Kir channel family members are affected by mutations that cause disease, such as Andersen's Syndrome (AS). AS is debilitating dominate negative Kir2.1 linked developmental disease. AS was one of the first diseases to be shown to be directly attributed to ion channel (Plaster et al., 2001). This disease is caused when mutations at one of fifteen sites, or two deletions have occurred in Kir2.1. These changes result in non-conducting channels. Patients with this disease present with neurological and cardiac symptoms of a prolonged QT interval, periodic paralysis, and ventricular arrhythmias. The phenotype of AS patients also includes distinct physical anomalies such as clinodactyly, scoliosis, hypertelorism, and micrognathia (Figure 1.4; (Plaster et al., 2001)

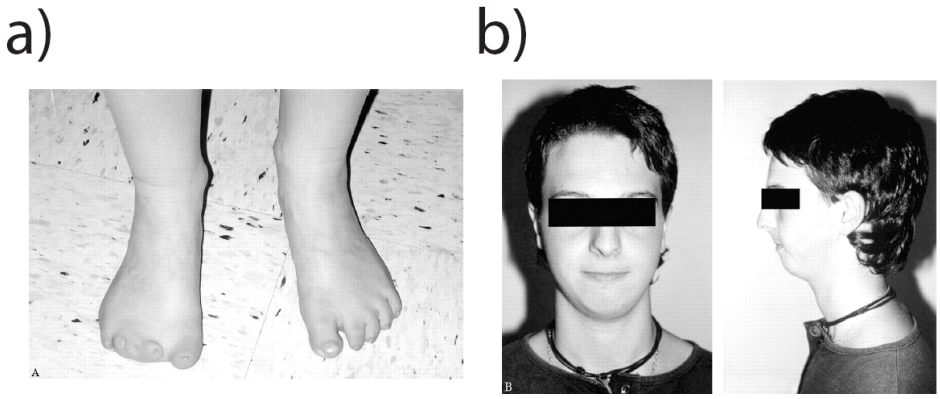

Figure 1.4. Andersen's Syndrome Physical Phenotype. AS patients physical deformities include the following **(a)** clinodactyly (curvature of the fingers and feet). **(b)** micrognathia (small chin), small or prominent ears that are low set or slanted (Plaster et al., 2001). Photos from (Donaldson et al., 2003).

AS is not the only disease that occurs in the Kir family of channels, mutations in Kir1.1 and Kir3.1 resulting in Antenatal Bartter Syndrome in the Kidney's and

cardiac abnormalities respectively (Enkvetchakul et al., 2005; Wickman et al., 1998). However, AS is one of the best studied diseases and has the most pronounce phenotype. This has allowed the location of several potential disease causing sites in Kir2.1. Of these sites, nine of fifteen and one deletion are located in the cytoplasmic region of Kir.2.1 allowing us to gain a significant understanding of how these channel's cytoplasmic domains gating mechanism is affected by these mutations.

Overview of the Coming Chapters. In the upcoming chapters, we study the role of the cytoplasmic domains of the Kir channel Family in gating and the affects of disease inducing mutations on that gating mechanism via structural biology and electrophysiology approaches. We will report on the elucidation of the Kir2.1 and Kir3.1 cytoplasmic domain structures, the discovery of a gating loop (G-loop) in Kir2.1 and the loop's overall role in gating the channel in Chapter 2. Furthermore, Chapter 2 will also discuss the role that the cytoplasmic domains play in the ability of certain Kir family members to rectify more strongly then the others. In Chapter 3, we will show how Andersen's Syndrome mutations affect the ability of the channel's cytoplasmic domains to form proper symmetric tetramers, provide a structural look at why these mutations result in non-conducting channels, elucidate a possible drug lead for Kir Channels, and visualize the first K^+ ion trapped in the cytoplasmic domain of Kir2.1. The molecular structural basis via NMR for localization of Kir2.1 in the post synaptic density region will be discussed in Chapter 4. We will culminate the first

four chapter's points and discoveries in Chapter 5. Chapter 6 contains a method development paper utilizing N-terminal Domain of Vaccinia Topoisomerase as a test bed for learning and developing NMR methods, some of which were used for the Kir Channel portions of this work. Overall, we will show the Kir cytoplasmic domain performs a dynamic role in gating this key family of eukaryotic ion channels.

1.2 REFERENCES

Alberts, B., Bray, D., Lewis, J., Raff, M., Roberts, K., and Watson, J. (1994). Molecular Biology of the Cell, Third edn (New York: Garland Publishing).

Clancy, S. M., Fowler, C. E., Finley, M., Suen, K. F., Arrabit, C., Berton, F., Kosaza, T., Casey, P. J., and Slesinger, P. A. (2005). Pertussis-toxin-sensitive Galpha subunits selectively bind to C-terminal domain of neuronal GIRK channels: evidence for a heterotrimeric G-protein-channel complex. Mol Cell Neurosci *28*, 375-389.

Corey, S., and Clapham, D. E. (1998). Identification of native atrial G-protein-regulated inwardly rectifying K+ (GIRK4) channel homomultimers. J Biol Chem *273*, 27499-27504.

Donaldson, M. R., Jensen, J. L., Tristani-Firouzi, M., Tawil, R., Bendahhou, S., Suarez, W. A., Cobo, A. M., Poza, J. J., Behr, E., Wagstaff, J.*, et al.* (2003). PIP2 binding residues of Kir2.1 are common targets of mutations causing Andersen syndrome. Neurology *60*, 1811-1816.

Doyle, D. A., Morais Cabral, J., Pfuetzner, R. A., Kuo, A., Gulbis, J. M., Cohen, S. L., Chait, B. T., and MacKinnon, R. (1998). The structure of the potassium channel: molecular basis of K+ conduction and selectivity. Science *280*, 69-77.

Enkvetchakul, D., Jeliazkova, I., and Nichols, C. G. (2005). Direct modulation of Kir channel gating by membrane phosphatidylinositol 4,5-bisphosphate. J Biol Chem *280*, 35785-35788.

Fakler, B., Bond, C. T., Adelman, J. P., and Ruppersberg, J. P. (1996). Heterooligomeric assembly of inward-rectifier K+ channels from subunits of different subfamilies: Kir2.1 (IRK1) and Kir4.1 (BIR10). Pflugers Arch *433*, 77-83.

Finley, M., Arrabit, C., Fowler, C., Suen, K. F., and Slesinger, P. A. (2004). betaL-betaM loop in the C-terminal domain of G protein-activated inwardly rectifying K(+) channels is important for G(betagamma) subunit activation. J Physiol *555*, 643-657.

Hill, J. J., and Peralta, E. G. (2001). Inhibition of a Gi-activated potassium channel (GIRK1/4) by the Gq-coupled m1 muscarinic acetylcholine receptor. J Biol Chem *276*, 5505-5510.

Hille, B. (2001). Ion Channels of Excitable Membranes, Third edn (Sunderland, MA: Sinauer Associates, Inc.).

Hodgkin, A. L., and Huxley, A. F. (1952). A quantitative description of membrane current and its application to conduction and excitation in nerve. J Physiol *117*, 500-544.

Inanobe, A., Yoshimoto, Y., Horio, Y., Morishige, K. I., Hibino, H., Matsumoto, S., Tokunaga, Y., Maeda, T., Hata, Y., Takai, Y., and Kurachi, Y. (1999). Characterization of G-protein-gated K+ channels composed of Kir3.2 subunits in dopaminergic neurons of the substantia nigra. J Neurosci *19*, 1006-1017.

Jan, L. Y., and Jan, Y. N. (1997). Cloned potassium channels from eukaryotes and prokaryotes. Annu Rev Neurosci *20*, 91-123.

Nehring, R. B., Wischmeyer, E., Doring, F., Veh, R. W., Sheng, M., and Karschin, A. (2000). Neuronal inwardly rectifying K(+) channels differentially couple to PDZ proteins of the PSD-95/SAP90 family. J Neurosci *20*, 156-162.

Plaster, N. M., Tawil, R., Tristani-Firouzi, M., Canun, S., Bendahhou, S., Tsunoda, A., Donaldson, M. R., Iannaccone, S. T., Brunt, E., Barohn, R.*, et al.* (2001). Mutations in Kir2.1 cause the developmental and episodic electrical phenotypes of Andersen's syndrome. Cell *105*, 511-519.

Preisig-Muller, R., Schlichthorl, G., Goerge, T., Heinen, S., Bruggemann, A., Rajan, S., Derst, C., Veh, R. W., and Daut, J. (2002). Heteromerization of Kir2.x potassium channels contributes to the phenotype of Andersen's syndrome. Proc Natl Acad Sci U S A *99*, 7774-7779.

Schulze, D., Krauter, T., Fritzenschaft, H., Soom, M., and Baukrowitz, T. (2003). Phosphatidylinositol 4,5-bisphosphate (PIP2) modulation of ATP and pH sensitivity in Kir channels. A tale of an active and a silent PIP2 site in the N terminus. J Biol Chem *278*, 10500-10505.

Signorini, S., Liao, Y. J., Duncan, S. A., Jan, L. Y., and Stoffel, M. (1997). Normal cerebellar development but susceptibility to seizures in mice lacking G protein-coupled, inwardly rectifying K+ channel GIRK2. Proc Natl Acad Sci U S A *94*, 923-927.

Silverman, S. K., Lester, H. A., and Dougherty, D. A. (1996). Subunit stoichiometry of a heteromultimeric G protein-coupled inward-rectifier K+ channel. J Biol Chem *271*, 30524-30528.

Tateno, T., Nakamura, N., Hirata, Y., and Hirose, S. (2006). Role of C-terminus of Kir7.1 potassium channel in cell-surface expression. Cell Biol Int *30*, 270-277.

Trapp, S., Haider, S., Jones, P., Sansom, M. S., and Ashcroft, F. M. (2003). Identification of residues contributing to the ATP binding site of Kir6.2. Embo J *22*, 2903-2912.

Vanoye, C. G., MacGregor, G. G., Dong, K., Tang, L., Buschmann, A. S., Hall, A. E., Lu, M., Giebisch, G., and Hebert, S. C. (2002). The carboxyl termini of K(ATP) channels bind nucleotides. J Biol Chem *277*, 23260-23270.

Wickman, K., Nemec, J., Gendler, S. J., and Clapham, D. E. (1998). Abnormal heart rate regulation in GIRK4 knockout mice. Neuron *20*, 103-114.

Zhou, W., Arrabit, C., Choe, S., and Slesinger, P. A. (2001). Mechanism underlying bupivacaine inhibition of G protein-gated inwardly rectifying K+ channels. Proc Natl Acad Sci U S A *98*, 6482-6487.

Zhou, Y., and MacKinnon, R. (2003). The occupancy of ions in the K+ selectivity filter: charge balance and coupling of ion binding to a protein conformational change underlie high conduction rates. J Mol Biol *333*, 965-975.

CHAPTER TWO

Kir2.1 and Kir3.1 cytoplasmic domain structures reveal sites for modulating gating and rectification

2.1 ABSTRACT

N- and C-terminal cytoplasmic domains of inwardly rectifying K (Kir) channels control the ion-permeation pathway through diverse interactions with small molecules and protein ligands in the cytoplasm. Two new crystal structures of the cytoplasmic domains of Kir2.1 ($Kir2.1_L$) and the G protein-sensitive Kir3.1 ($Kir3.1_S$) channels in the absence of PIP_2 show the cytoplasmic ion-permeation pathways occluded by four cytoplasmic loops that form a girdle around the central pore (G-loop). Significant flexibility of the pore-facing G-loop of $Kir2.1_L$ and $Kir3.1_S$ suggest a possible role as a diffusion barrier between cytoplasmic and trans-membrane pores. Consistent with this, mutations of the G-loop disrupted gating or inward rectification. Structural comparison reveals a di-aspartate cluster on the distal end of the cytoplasmic pore of $Kir2.1_L$ that is important for modulating inward rectification. Taken together, these results suggest the cytoplasmic domains of Kir channels undergo structural changes to modulate gating and inward rectification.

2.2 INTRODUCTION

The family of inwardly rectifying potassium (Kir) channels of eukaryotic cells is unique in that the channels conduct K^+ ions better in the inward direction than in the outward direction. In native tissues, the small outward K^+ current through Kir channels influences the resting membrane potential and membrane excitability. The major structural mechanism underlying inward rectification involves a physical occlusion of the pore by polyamines and Mg^{2+} from the cytoplasmic side of the channel (Lopatin et al., 1994; Matsuda et al., 1987). In addition to being inwardly rectifying, Kir channels respond to a variety of intracellular messengers, including G proteins (Kir3 channels) and ATP (Kir6 channels), and respond to changes in pH (Kir1 channels; (Enkvetchakul et al., 2005). Aberrant activity of Kir channels has been linked to a variety of endocrine, cardiac and neurological disorders: for instance, the loss of Kir3 channels leads to hyper-excitability and seizures in the brain, cardiac abnormalities, hyperactivity and reduced anxiety (Signorini et al., 1997; Wickman et al., 1998). Mutations in Kir1 and Kir 2.1 channels have been implicated for Bartter syndrome and Andersen syndrome, respectively (Derst et al., 1997; Plaster et al., 2001). Therefore, elucidating the molecular mechanisms of inward rectification and gating will be instrumental to discovering means to treat these diseases.

The Kir family is composed of seven different subfamilies, Kir1−Kir7 (Enkvetchakul et al., 2005). All Kir channels are tetrameric and contain two trans-

membrane helix domains (M1 and M2), the ion-selective P-loop between M1 and M2, and cytoplasmic N- and C-terminal domains. The extent of rectification varies among the different subfamilies, ranging from weak (Kir1) to strong (Kir2). The stronger rectification of Kir2 can be partly explained by charge negativity in the M2 domain (Kir2.1 Asp172) and a pair of acidic amino acids (Kir2.1 Glu224 and Glu299) in the cytoplasmic domain (Kubo and Murata, 2001; Vanoye et al., 2002; Yang et al., 1995). However, the degree of rectification among different Kir channels does not directly relate to the presence of these negative charges. For example, Kir7.1 shows weak rectification but has the negative charge in the M2 domain (Doring et al., 1998). Kir3.2 shows strong rectification but lacks the same negative charge (Zhou et al., 2001). There is also little consensus on the mechanism by which Mg^{2+} and polyamines produce inward rectification (John et al., 2004). Together, these studies raise the possibility that other previously unknown sites may be involved in regulating inward rectification.

In addition to rectification, another common feature of Kir channels is regulation by the membrane phospholipid PIP_2. Opening of Kir channels requires PIP_2 binding to basic and polar amino acids in the cytoplasmic domains, whereas depletion of PIP_2 seems to close the channel (Huang et al., 1998; Lopes et al., 2002; Shyng et al., 2000). The high degree of sequence similarity in the cytoplasmic domains suggests there should be a common structural means for gating among Kir

channels, yet the cytoplasmic domains respond differently to intracellular regulatory signals. For example, Kir2.1 channels remain constitutively open through endogenous PIP_2 binding, whereas Kir3 channels are opened by G proteins and Kir6 channels are closed by intracellular ATP, respectively (Huang et al., 1998).

Recently, structures of two Kir channels, rat Kir3.1 and bacterial KirBac1.1, have been reported; they show a central water-filled 'cytoplasmic pore' that extends ~ 60 Å coaxially from the trans-membrane pore domain (Doyle et al., 1998; Nishida and MacKinnon, 2002). The structure of KirBac1.1, which contains both trans-membrane and cytoplasmic pore domains, also shows a long pore (Doyle et al., 1998). In the KirBac1.1 structure, a phenylalanine (Phe146) located within the pore-facing M2 helices is postulated to form a barrier to ion permeation, similar to the 'helix bundle crossing' in KcsA or in Kir3.4, to control the pore aperture. However, gating of eukaryotic Kir channels (Kir1, Kir3 and Kir6) requires additional elements such as ATP and $G_{\beta\gamma}$ G protein subunits binding to the channels' cytoplasmic domain (Proks et al., 2003; Vanoye et al., 2002). To better understand mechanisms underlying inward rectification and gating, a structural comparison of different mammalian Kir channels is needed.

Here, we have determined the crystal structures of the cytoplasmic domains of mouse Kir2.1 and rat Kir3.1. Structural comparison has showed an intrinsically

flexible cytoplasmic pore−facing loop. These loops constrict the cytoplasmic pore to ~3 Å, forming a girdle around the central pore axis. This girdle, which we refer to as the G-loop, forms the narrowest portion of the cytoplasmic pathway, reminiscent of the narrow pore-forming girdle of the acetylcholine receptor channel (Miyazawa et al., 2003). Additionally, we have discovered that mutating two aspartate amino acids near the end of the cytoplasmic pore, opposite the G-loop, changes inward rectification. We propose a model in which the di-aspartate cluster and the cytoplasmic G-loop act as cytoplasmic regulatory elements for rectification and gating, respectively.

2.3 RESULTS

N- and C-terminal domains fused to form a tetramer in solution. Both N- and C-terminal domains of Kir channels are involved in binding PIP_2 and G proteins (Huang et al., 1998; Huang et al., 1995; Lopes et al., 2002; Schulte et al., 1998; Shyng et al., 2000; Zhou et al., 2001). We therefore first investigated the coexpression of N- and C-terminal domains of Kir3.2 or Kir3.4 channels, which form homo-tetramers unlike hetero-tetrameric Kir3.1 (Corey and Clapham, 1998; Inanobe et al., 1999; Zhou et al., 2001). Expression of the C-terminal domain alone produces insoluble protein. Complexes of N-terminal (residues 1−99 for Kir3.2 and Kir3.4) and C-terminal ($Kir3.2_{198–414}$ and $Kir3.4_{193–419}$) domains were soluble, however, when co-expressed in a dicistronic vector. These non-covalent N- and C-terminal domain complexes of both Kir3.2 and Kir3.4 eluted as dimers upon sizing chromatography (Fig. 2.1). However, the complexes were relatively unstable over time, leading to an unstable C-terminal domain protein with varying amounts of associated N-terminal domain.

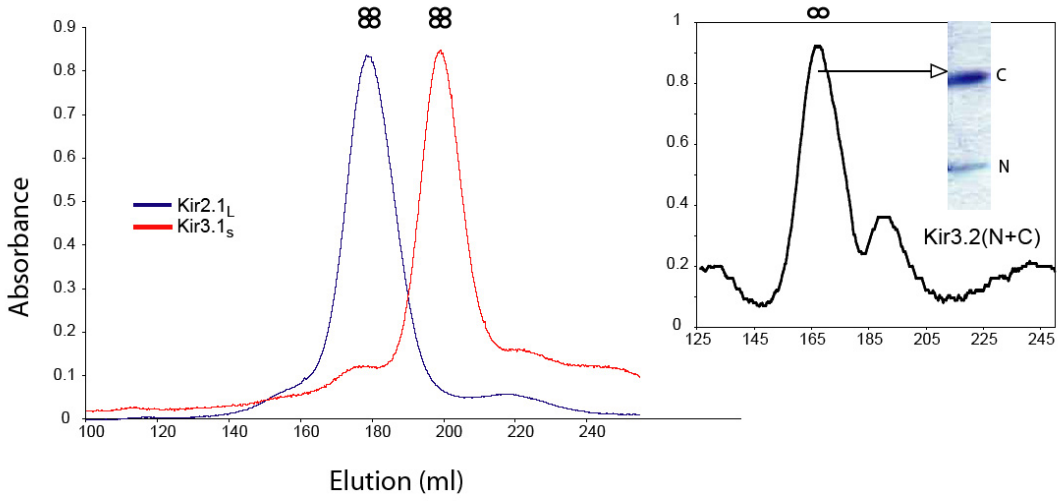

Figure 2.1 Size chromatography of Kir fusion and dicistronically expressed cytoplasmic constructs. Size chromatograms of Kir3.1S (red), Kir2.1L (blue), and Kir3.2's N- and C-terminal domains expressed dicistronically (inset). Elution times for tetrameric Kir3.1S (120 kD) and Kir2.1L (93 kD) based on standard markers are 175 and 185 ml. Noncovalent dimeric complex of Kir3.2 (66 kD) elutes somewhat later than a standard (145 ml) but accurate size measurements of the complexes were confirmed by static light scattering (Wyatt) and by sedimentation analyses on analytical centrifuges (Beckman). Most importantly, the inset shows that the SDS gel of the single-peak dimmer fraction contains both 9 kD N-terminal and 24 kD C-terminal fragments. Circles above spectra denote tetramer or dimer.

To overcome the instability of the complex, we subsequently adopted the fusion strategy used successfully for the Kir3.1 domain structure, the GluR extracellular domain and the KChIP1/Kv4.2 complex (Armstrong et al., 1998; Nishida and MacKinnon, 2002; Zhou et al., 2004). In contrast to the non-covalent complexes, $Kir3.1_S$ contains a smaller N-terminal segment (amino acids 41−63) that is fused directly to a truncated C-terminal domain (amino acids 189−371) of rat Kir3.1 (see Fig. 2.2; (Nishida and MacKinnon, 2002). $Kir2.1_L$, on the other hand, contains the N-

terminal domain (residues 41−64) of mouse Kir2.1 fused to the entire C-terminal domain (residues 189−428), including 57 additional amino acids in the C-terminal end. Both $Kir3.1_S$ and $Kir2.1_L$ were expressed efficiently in bacteria, and they migrated as a stable tetramer in solution (Fig. 2.1) and were successfully crystallized for structural analyses. Notably, fusion complexes of Kir3.2 or Kir3.4 were not successfully produced, unlike the aforementioned non-covalent complexes. It remains to be understood whether the dimeric form of the non-covalent complex reflects an alternate oligomeric state of the cytoplasmic domains resulting from the presence of the entire N-terminal segment (such as residues 1−99).

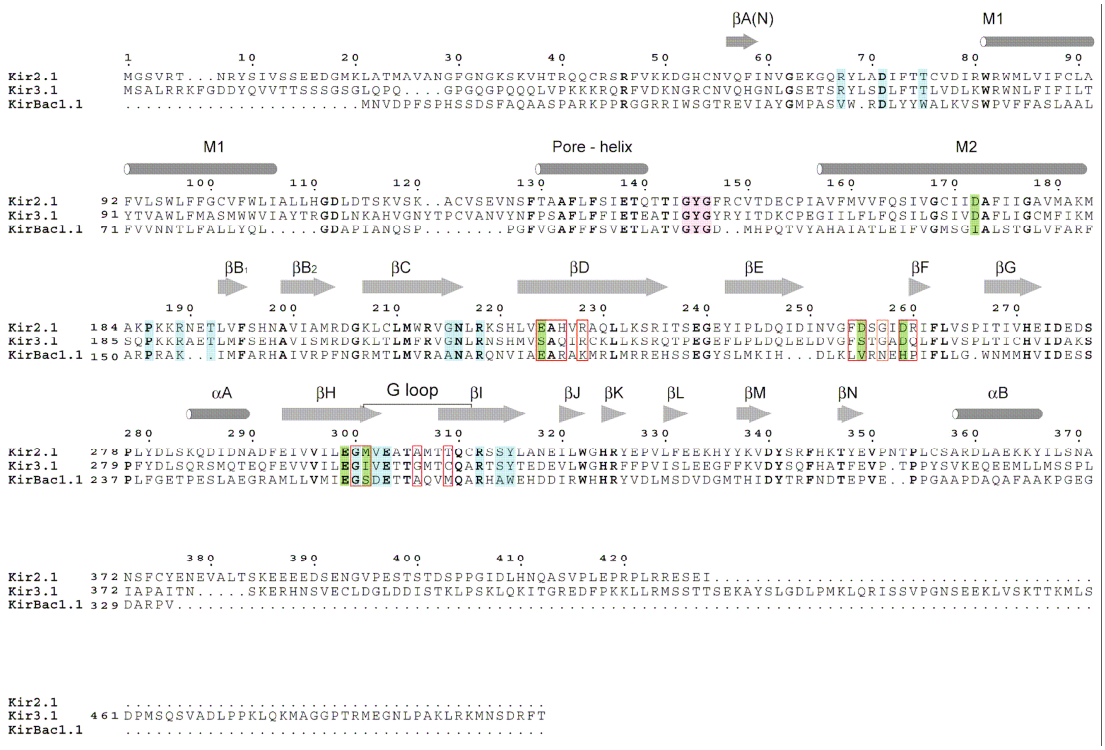

Figure 2.2 Sequence alignment of Kir3.1$_S$, Kir2.1$_L$, and KirBac1.1 with secondary structure elements noted. Pore-facing residues within the cytoplasmic domains based on the structure of Kir2.1$_L$ are boxed in red. The selectivity filter residues GYG are highlighted in pink. Mutations known to be related to Andersen syndrome (blue) and six positions implicated for inward rectification (green) are highlighted.

Structures of Kir2.1$_L$ and Kir3.1$_S$ are similar. We determined the structures of Kir2.1$_L$ and Kir3.1$_S$ by molecular replacement methods (Table 2.1 and Fig. 2.3), using the published rKir3.1 structure as a search model (Nishida and MacKinnon, 2002). We found that Kir2.1$_L$ forms a non-crystallographic homo-tetramer with a long cytoplasmic pore in the space group $C222_1$ (Fig. 2.3a). Kir3.1$_S$ forms a homo-tetrameric assembly in the space group $P42_12$ (Fig. 2.3b). Despite different crystallization conditions, its crystal-packing mode is identical to that for the published rKir3.1 crystals in the same space group, which we refer to as Kir3.1$_{S\text{-}Met}$

(Nishida and MacKinnon, 2002). The core structures of $Kir2.1_L$ and $Kir3.1_S$ are readily superimposed (Fig. 2.3c). Briefly, the core structural elements of three β sheets and two α helices contain the first β sheet (βI, βH, βD and βE) and the second sheet (βJ, βB, βC and βG), forming the protein interior of the monomer subunit. The third β sheet (βA, βM and βL) on the protein exterior faces the inner leaflet of the cell membrane with α helices (αA and αB). Notably, the marked similarity between $Kir3.1_S$ and $Kir2.1_L$ and the full-length KirBac1.1 indicates that the fusion strategy is a reasonable approach for studying these channels.

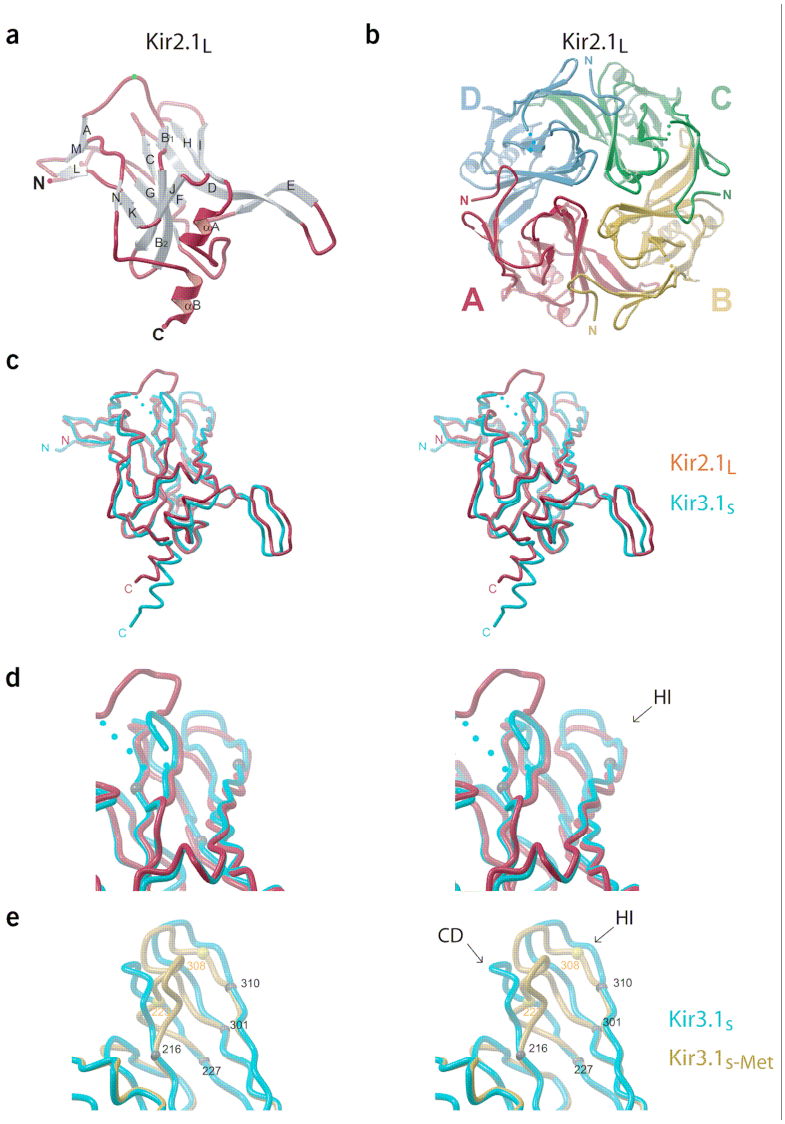

Figure 2.3 Structures of Kir3.1$_S$ and Kir2.1$_L$. (**a**) Standard view of Kir2.1$_L$ ribbon diagram with secondary structure labels consistent with those of Kir3.1$_{S\text{-}Met}$ (Nishida and MacKinnon, 2002). N-terminal domain has been removed for clarity. (**b**) Top-down (membrane-to-cytoplasm) view of Kir2.1$_L$ tetramer with four subunits labeled A (red), B (gold), C (green) and D (blue). Note that the N-terminal segment of the Kir2.1$_L$ interfaces with the C-terminal domain of the neighboring subunit (clockwise). (**c**) Stereo view of Kir2.1$_L$ C_α backbone (red) overlaid onto Kir3.1$_S$ (blue). (**d**) Stereo view of Kir2.1$_L$ C_α (red) and Kir3.1$_S$ (blue) near their G-loops. HI loop is labeled. (**e**) Stereo view of Kir3.1$_S$ C_α (blue) and Kir3.1$_{S\text{-}Met}$ (gold). Gold balls denote two methionine residues at positions 223 and 308 of Kir3. 1$_{S\text{-}Met}$. Black balls highlight four anchoring residues of Kir3.1 (216 and 227 for CD, 301 and 310 for HI loops), including two flexible residues, Gly216 and Gly301. Views in **d** and **e** are very close to that in **a** but are slightly rotated vertically for clarity.

Table 2.1 Crystallographic data for $Kir2.1_L$ and $Kir3.1_S$

Data Collection		
Protein / data set	$Kir2.1_L$	$Kir3.1_S$
Space group	$C222_1$	$P42_12$
Cell constants	a = 112.46	a = 76.36
	b = 138.29	b = 76.37
	c = 138.75	c = 92.16
	$\alpha = \beta = \gamma = 90$	$\alpha = \beta = \gamma = 90$
Wavelength (Å)	1.033	1.080
Source	ALS	SSRL
Resolution (Å)	2.40	2.09
Total observations / total reflections	125,410 / 37,871	109,243 / 16,100
Completeness (highest-resolution shell)	91.7	96.0
I / σ (highest-resolution shell)	16.9 (6.0)	23.0 (2.8)
R_{sym}[a]	.062	.070
Model refinement		
Total reflections (reflections for test)	38,814	15,270 (813)
R_{work}(%) / R_{free}(%)[b]	22.5 / 28.1	19.5 / 23.5
Protein atoms / water atoms	6,332 / 213	1,596 / 132
R.m.s. deviation of bond lengths (Å)	.007	.002
R.m.s. deviation of bond angles (°)	1.3	1.2

[a]$R_{sym}=\sum_h\sum_1|I_1(h) - \langle I(h)|\ \sum_h\sum_I I_1(h)$, where $I_1(h)$ is the i^{th} measurement and $\langle I(h)\rangle$ is weighted mean of all measurements of I(h). [b]$R_{free}=h(|F(h)_{obs}| - |F(h)_{calc}|) / h|F(h)_{obs}|$ for reflections in the working and test sets, respectively. R.m.s., root mean square.

A short β strand, βA (N), of the N-terminal domain interacts extensively with the C-terminal domain of a neighboring subunit (Fig. 2.4a), indicative of its structural role in the subunit assembly by inter-subunit interaction. The additional 57 C-terminal amino acids of $Kir2.1_L$ were disordered in the structure. This suggests that the C-terminal end is highly mobile and may require the full N-terminal domain or other cytoplasmic proteins to gain structural rigidity. All three proteins ($Kir2.1_L$, $Kir3.1_S$ and $Kir3.1_{S\text{-}Met}$) crystallized in the absence of PIP_2; thus, they are most likely to reflect the PIP_2-depleted closed conformation.

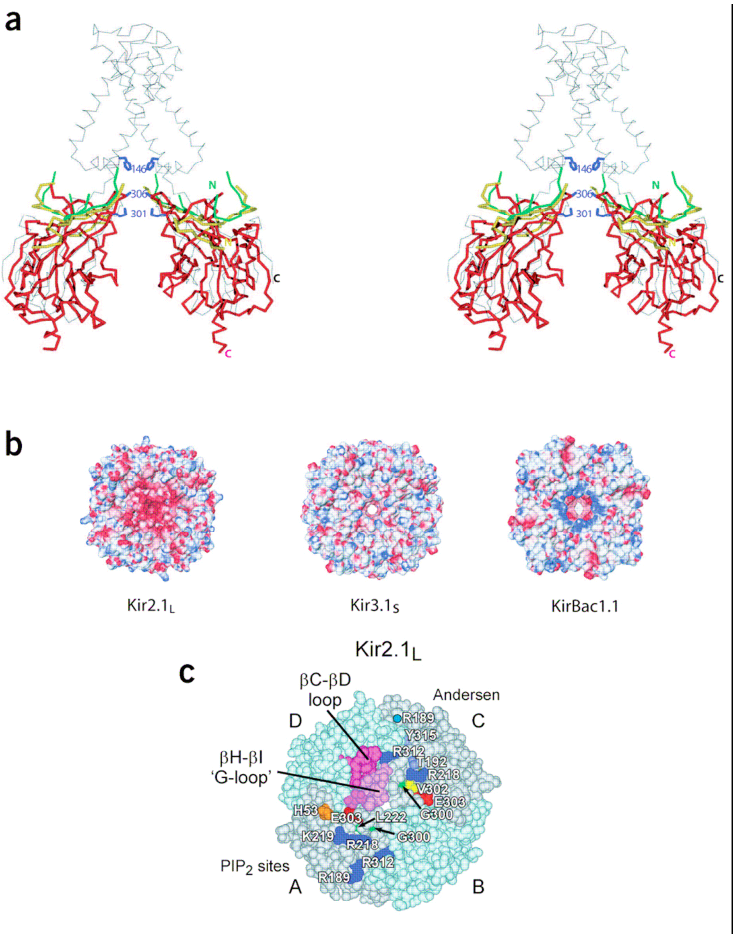

Figure 2.4 Kir3.1$_S$ and Kir2.1$_L$ in comparison to KirBac1.1.
(**a**) Stereo overlay of Kir2.1$_L$ C_α trace (red) overlaid onto KirBac1.1 C_α trace (black). Side-chains of three key residues forming the closest points between M2 (Phe146 of KirBac1.1) and Met301 and Ala306 of Kir2.1$_L$ of the transmembrane and cytoplasmic pores, respectively, are highlighted in blue. (**b**) Electrostatic potential rendered on molecular surface of Kir2.1$_L$ (left), Kir3.1$_S$ (middle), and KirBac1.1 (right) viewed from the cytoplasmic side into the pore. Note highly positive (blue) cytoplasmic vestibule of KirBac1.1 in contrast to highly negative (red) vestibule of Kir2.1$_L$. (**c**) Top-down (membrane-to-cytoplasm) view of molecular surface of Kir2.1$_L$. Andersen syndrome mutations and putative PIP_2-binding sites cluster on surface of Kir2.1$_L$. In 'A' subunit, mutations implicated in changing PIP_2 affinity are highlighted. A PIP_2-binding site Arg228 is buried. In the 'C' subunit, amino acids known for Andersen syndrome are shown for those that are exposed to the surface (Arg189, Thr192, Arg218, Gly300, Val302, Glu303, Tyr315 of Δ314−315). Gly215 and Asn217 are buried in protein interface and invisible from this viewpoint. Also, disordered side-chain atoms of Arg189 of the 'C' subunit are not shown except for its C_α. Amino acids Gly300−Gln310 encompass the βH-βI or 'G-loop' (Met301 is not visible in this view). Gly215−Val227 comprise the βC-βD loop (Gly215, Asn216, Val223−Ala225, Val227 are not visible in this view).

Structural flexibility in the cytoplasmic pore-facing G-loops. Two pore-facing loop regions, located between the βC and βD strands (CD loop) and the βH and βI strands (HI loop), show a high degree of sequence conservation between Kir3.1 and Kir2.1 (red-lined boxes in Fig. 2.2). These loops form the narrowest part of the cytoplasmic structures, forming a girdle around the central pore axis. We refer to this region, in particular the HI loop, as the 'G-loop'. Closer inspection showed that the G-loop in $Kir2.1_L$ (residues 300−315) deviates substantially from that in $Kir3.1_S$ (blue in Fig. 2d) and also from $Kir3.1_{S\text{-}Met}$ (gold in Fig. 2.3e), with a minor shift in the CD loop. A significant conformational difference in the pore-facing HI loop between $Kir2.1_L$, $Kir3.1_{S\text{-}Met}$ and $Kir3.1_S$ indicates that these loops are intrinsically flexible, to possibly accommodate even larger conformational changes during ion conduction or activation with PIP_2. It is noteworthy that these flexible loops are anchored by conserved and backbone-flexible glycines at positions 216 and 301 of Kir3.1, or 215 and 300 of Kir2.1 (Fig. 2.3e). An overlay of the structure of $Kir2.1_L$ tetramer on the C-terminal domain of the KirBac1.1 (Fig. 2.4) suggests that the pore-facing HI-equivalent loop of KirBac1.1 abuts the proposed path-blocking element (Phe 146) of the M2 of KirBac1.1 (Doyle et al., 1998).

Functional role for the G-loop in $Kir2.1_L$ and $Kir3.1_S$. The G-loop contains several small or hydrophobic residues, including Gly300, Met301, Ala306 and Met307 in Kir2.1 (Fig. 4a). In $Kir3.1_S$, I302 forms the narrowest region of the pore with an

opening of 9.0 Å (the diagonal distance between closest atom centers). The G-loop of Kir2.1$_L$ is narrower, with a width of 5.7 Å formed by Ala 306. Given approximately 2.8 Å for van der Waals radii of two opposing atoms, we estimate that the narrowest actual opening is ~2.9 Å (5.7−2.8 Å) between the four C_α atoms of Ala 306 (Fig. 2.4a). Met301 (or Ile302 of Kir3.1) adjacent to Ala306 forms another hydrophobic ring near the G-loop that is comparable to the opening of Kir3.1 of 6.2 Å diameter (9.0−2.8 Å). Thus, the physical opening formed by four opposing hydrophobic G-loops is too narrow to accommodate the passage of a hydrated potassium ion. Examination of the space-filled models for Kir2.1$_L$ and Kir3.1$_S$ viewed from the cytoplasmic side (Fig. 2.4b) makes this readily apparent: the water-filled pore is nearly completely occluded in Kir2.1$_L$. The variation between Kir3.1$_S$ and Kir2.1$_L$ in the size of the opening suggests that the pore-facing G-loop is intrinsically flexible.

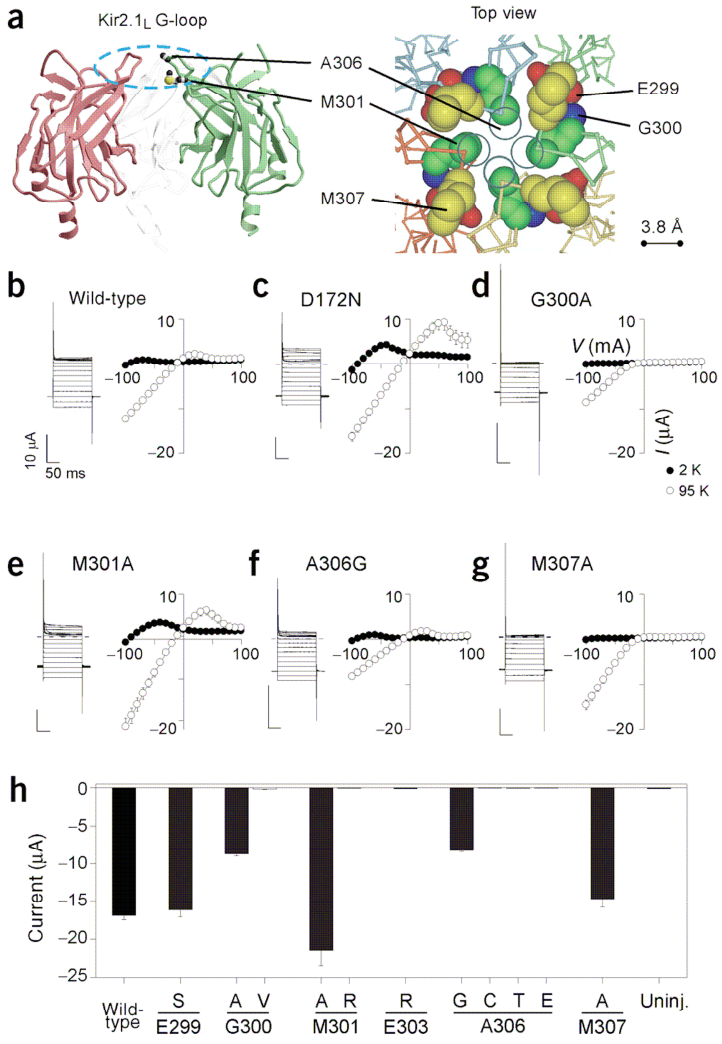

Figure 2.5 Mutations in G-loop disrupt gating and inward rectification. (a) Side (left) and top-down (right; membrane-to-cytoplasm) views of the Kir2.1$_L$ structure. C_β atoms (Ala306) of the G-loop form the narrowest ~3-Å opening of the pore and are shown as open circles for clarity. Other residues near the G-loop are labeled. (b−g) Examples of inwardly rectifying current for wild-type and mutant Kir2.1 channels. Macroscopic current traces show the response to voltage steps from -100 mV to +100 mV in an extracellular containing 95 mM K^+. Dashed line indicates zero current. Current-voltage relation is shown to the right for the currents measured in 2 mM K^+ or 95 mM extracellular K^+. Asp172 is located in the M2 transmembrane domain. (h) Bar graphs shows the average current at -100 mV (6.8 ms after the voltage step) for each mutant (n = 9−51).

To assess whether the G-loop forms an important gating structure in native channels, we studied the effect of mutations in the G-loop of full-length Kir2.1 channels. *Xenopus* oocytes were injected with the cRNA for mutant channels, and macroscopic currents were then recorded in response to a series of voltage steps from -100 mV to +100 mV. To monitor K^+ selectivity and possible changes in rectification, currents were recorded with either 2 or 95 mM extracellular KCl (Fig. 2.5). For wild-type Kir2.1, the zero current potential shifted from ~0 mV in 95 mM KCl to approximately -100 mV in 2 mM KCl and there was little outward current at potentials positive to E_K (Fig. 2.5b). The narrowest opening of the cytoplasmic pore is formed by C_β atoms of Ala306 and to a lesser extent Glu299, Gly300, Met301 and Met307 (Fig. 2.5a). Ala306 is located at the apex of the G-loop. We hypothesized that a side chain larger than alanine would not permit the physical closure of the G-loop without changes in its backbone conformation and would lead to functional disruption. We found that only a glycine substitution (A306G) was well tolerated in Kir2.1 (Fig. 2.5a, Fig. 5). By contrast, glutamate, cysteine and threonine mutations did not produce functional channels (Fig. 2.5h). Similar to A306G, the reverse substitution at Gly300 (G300A) is also tolerated and leads to functional channels, whereas the bulkier G300V does not give rise to appreciable current. These results suggest that the closure of the G-loop (Fig. 2.4b and Fig. 2.5a) reflects a physiologically relevant, closed conformational state during the gating of the channels.

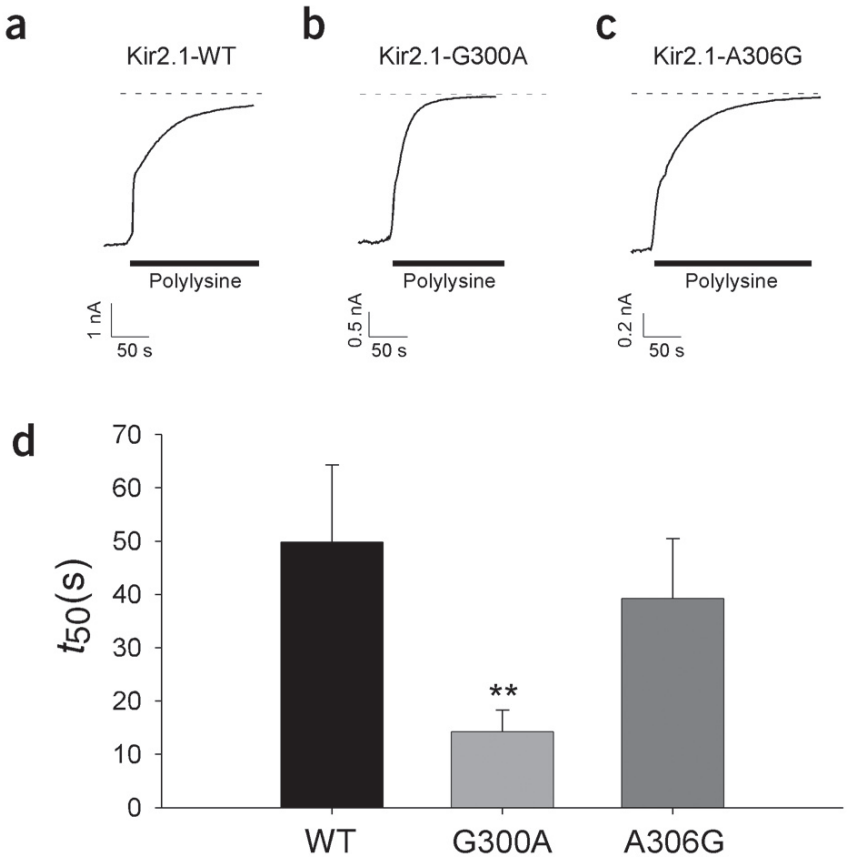

Figure 2.6 Substitution of glycine at Ala306 of Kir2.1 does not alter PIP_2 affinity. Oocytes were injected with the cRNA for mutant Kir2.1 channels and macroscopic patch currents recorded with giant patch technique (Hilgemann, 1995). (**a**−**c**) Inward currents recorded through wild-type (**a**), G300A (**b**) and A306G (**c**) are shown before and during exposure to intracellular polylysine (0.3 mg ml^{-1}). Note the decrease in current occurs with an instantaneous (non-PIP_2: ref. 15) and a slow phase, which represents the removal of PIP_2 from the channel. Intracellular solution ('FVPP') contained 96 mM KCl, 5 mM Na_2EDTA, 10 mM HEPES, 5 mM KF, 3 mM NaO_3V, 10 mM $K_4P_2O_7$ at pH 7.4 (HCl). (**d**) Average t_{50} for wild-type, G300A and A306G channels (n = 5−7). ** indicates statistical difference between G300A and wild-type as determined using one-way ANOVA ($P < 0.05$).

We next examined the effect of mutations at Met301, which points to the cytoplasmic pore. Substituting alanine at Met 301 did not affect functional expression of Kir2.1, although it did alter inward rectification (Fig. 2.5d). A positive charge introduced at Met301 (M301R), however, yields no functional channels. Like the

M301A substitution, substituting alanine at Met307 also did not affect functional expression. Previously, it was found that coexpressing G300V, which is not functional on its own, with wild-type channels produced heteromeric channels with reduced PIP_2 affinity, suggesting this region may be involved in gating by PIP_2 (Lopes et al., 2002). As both A306G and G300A were expressed as functional homomers, we next investigated whether these mutants had altered affinity for PIP_2. Intracellular application of polylysine closes Kir2.1 channels by antagonizing the interaction of endogenous PIP_2 with the channel (Lopes et al., 2002). The time course of current rundown (t_{50}) produced by intracellular polylysine reflects the apparent binding affinity of PIP_2. Whereas G300A showed a t_{50} that was ~80% faster than wild type, the t_{50} for A306G was indistinguishable from that of the wild-type control (Fig. 2.6).

The finding that the affinity for PIP_2 is unchanged in A306G indicates that both the open and closed (PIP_2-depleted) states of the channel tolerate the subtle change from alanine to glycine without disruption of the flexibility in the G-loop. In contrast, the alanine substitution at Gly300 decreases PIP_2 affinity (shorter t_{50}). This affinity change is likely to be the result of an allosteric change in the PIP_2 binding site (Lopes et al., 2002). This difference in PIP_2 affinity with mutations at Gly300 and Ala306 is not entirely unexpected, as the positions of Gly 300 and Ala 306 in the structure are quite distinct. Gly 300 is buried in the closed structure, whereas Ala 306 forms the narrow apex ring around the central pore (see Fig. 2.4c and Fig. 2.5a).

Thus, we conclude that the G-loop is a gating element that is structurally distinct from but functionally coupled to the PIP_2-binding site. PIP_2 binding most likely modulates allosterically the conformational switch of the flexible G-loop for gating.

Di-aspartate cluster is implicated for inward rectification. Using both $Kir3.1_S$ and $Kir2.1_L$ structures, we next performed a side-by-side comparison of the surface charges in the cytoplasmic pore. The $Kir2.1_L$ structure shows a very high degree of electronegative surface potential compared to that of $Kir3.1_S$ (Fig. 2.4b). Notably, the KirBac1.1 cytoplasmic pore shows even less electronegative surface than $Kir3.1_S$ (Fig. 2.4b). Previously, the strong rectification of Kir2.1 has been attributed to two principal electronegative regions: Asp 172 in the M2 domain and Glu 224/Glu 299 in the cytoplasmic domains (Kubo and Murata, 2001; Vanoye et al., 2002; Yang et al., 1995). Using the structure of $Kir2.1_L$ as a guide, we identified four new pore-facing charged amino acids (Arg 228, Asp 255, Asp 259 and Arg260), and examined the effect of charge reversal or neutralization at these residues (Fig. 2.7).

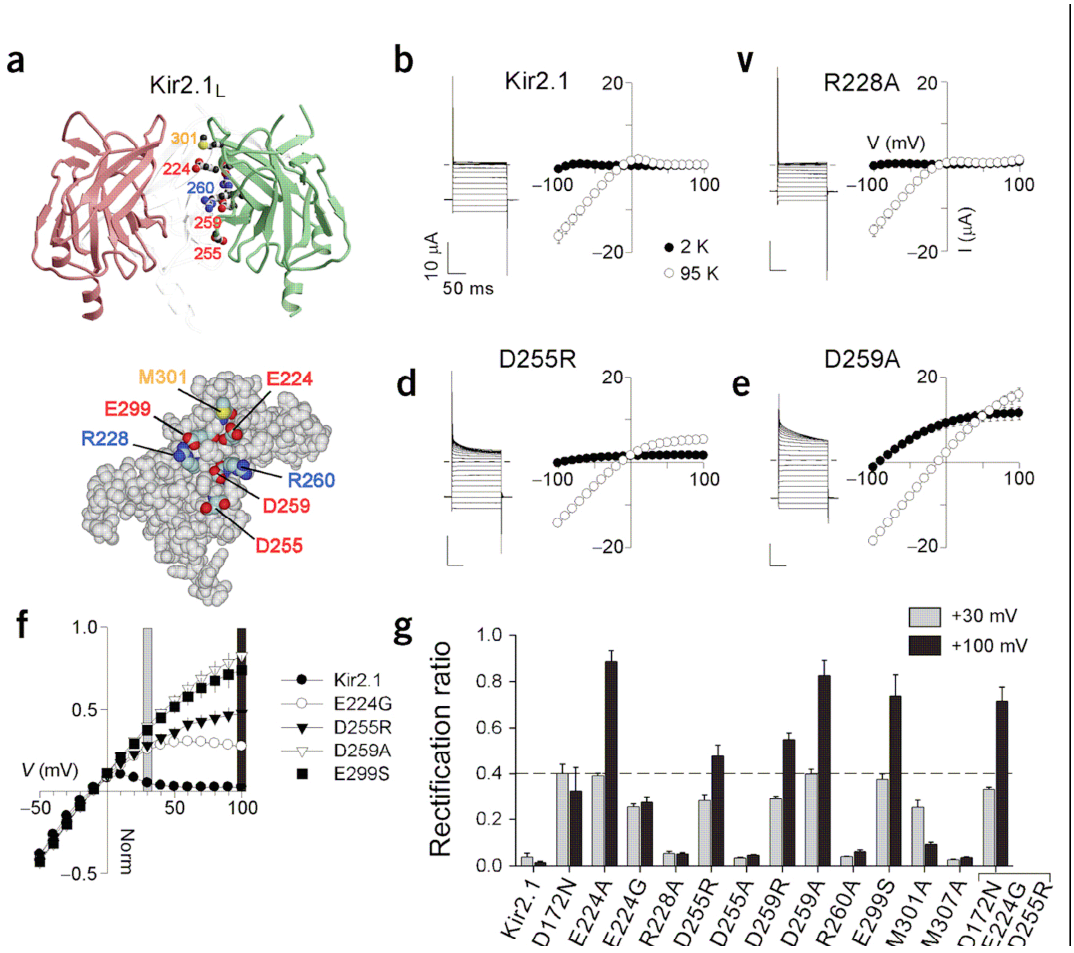

Figure 2.7 Mutation of di-aspartate cluster in Kir2.1 changes inward rectification. Oocytes were injected with the cRNA for mutant Kir2.1 channels and whole-cell macroscopic currents recorded with two-electrode voltage-clamp. (a) Structure of $Kir2.1_L$ (three of four subunits are shown), highlighting amino acids lining permeation pathway. Bottom panel is a view from the axis of the permeation pathway. (b–e) Examples of inwardly rectifying current for wild-type and mutant Kir2.1 channels. Macroscopic current traces show the response to voltage steps from -100 mV to +100 mV in an extracellular solution containing 95 mM K^+. Current-voltage relation is shown to the right for the currents measured in 2 mM K^+ or 95 mM K^+, measured 6.8 ms after the voltage step. Dashed line indicates zero current. (f) Normalized currents show change in rectification for the indicated Kir2.1 mutants. The ratio at +30 mV (gray bar) and +100 mV (black bar) indicate the rectification ratio used in g. (g) Comparison of the rectification ratios at +30 (gray) and +100 mV (black). A value of unity at +100 mV or 0.4 (dashed line) at +30 mV indicates a complete loss of rectification. R228A, D255A, R260A and M307A were not statistically different from Kir2.1 wild-type at +30 or at +100 mV (n = 9–51).

To quantify the differences in rectification among channels with different amplitude currents, we normalized the current measured at +100 mV to that measured at -100 mV (the 'rectification ratio'). We also normalized the current at +30 mV for mutants that might show a change in voltage-dependent rectification, such as D172N. Thus, a value of unity at +100 mV or 0.4 at +30 mV indicates a complete loss of rectification (that is, linear *I-V*), whereas a value close to zero indicates strong rectification. As shown previously, E224G and E299S mutations reduced inward rectification of Kir2.1 (Kubo and Murata, 2001; Yang et al., 1995). Charge reversal at Arg 255 (D255R) or at Arg259 (D259R) also decreased inward rectification (Fig. 2.7d−2.6g). Notably, charge neutralization at Arg 255 (D255A mutation) maintains strong inward rectification whereas that at Arg 259 (D259A mutation) produces a large decrease in rectification. Thus, mutation of each of the four acidic amino acids in the cytoplasmic domain significantly reduces inward rectification (Fig. 2.7f). Mutation of the two pore-facing basic residues (R228A and R260A), on the other hand, produces little change in inward rectification (Fig. 2.7g). Taken together, these results suggest that a di-aspartate cluster (Arg 255/Arg 259) is also important in determining the extent of inward rectification of Kir2.1 channels.

2.4 DISCUSSION

Comparison of Kir3.1 and Kir2.1 structures. Comparison of two different types of cardiac inward rectifiers, Kir2.1 (I_{K1}) and Kir3.1 (I_{KACh}), has shown two new important gating features of Kir channels. First, a narrow girdle formed by G-loops poised near the junction between cytoplasmic and transmembrane pore domains is very flexible, suggesting its conformational change could be a means to modulate gating. Second, a di-aspartate cluster in Kir2.1, located opposite from the G-loop, is important in controlling inward rectification.

Consistent with the conformational change envisioned for G-loops, cysteine-substituted accessibility studies on Kir2.1 using E224C, H226C and R228C mutants, all modified with multiple, large methane thiosulfonate (MTS) reagents (12 X 10 X 6 Å), suggest the inner vestibule must be > 20 Å in the open pore (Vanoye et al., 2002). By contrast, the diagonal distance between Glu224 of Kir2.1$_L$ is 9.2 Å and must therefore widen to accommodate large MTS reagents. Second, intracellular MTS treatment modifies sites buried in the Kir2.1$_L$, as indicated by analysis of G215C, N216C and V223C mutants, as well as sites at the top surface of the cytoplasmic pore (as indicated by analysis of L217C, S220C and H221C mutants) (Vanoye et al., 2002). Third, FRET spectroscopy studies with Kir3 channels have demonstrated that binding of G proteins triggers a conformational change of the cytoplasmic domain (Riven et al., 2003). Finally, the Kir2.1$_L$ and Kir3.1$_S$ structures have been solved in the absence

of PIP_2 and are likely to reflect a closed state of the full-length channel. Taken together, these findings suggest that the cytoplasmic domain undergoes a conformational change in the presence of PIP_2 or G proteins, thereby changing the accessibility of these amino acids and widening the pore.

Whether the additional 60 amino acids in the C-terminal domain of Kir2.1 also are involved in gating remains unclear. The observation that this segment of $Kir2.1_L$ was disordered in our crystals was unexpected; one possible explanation is that the C-terminal end of the channel is flexible because it lacks molecular association with cytoplasmic proteins. For example, the C-terminus of Kir2.1 possesses a sequence motif binding to postsynaptic density proteins (PSD-95; (Doyle et al., 1998) with which structural rigidity may be achieved.

Role for electronegative charge in Kir2 cytoplasmic pore. Inward rectification of Kir channels depends on the binding of intracellular polyamines and Mg^{2+} to the cytoplasmic pore and to the inner vestibule of the channel. Previously, three negatively charged amino acids in Kir2.1 (Asp172, Glu224 and Glu299) were found to be important for the binding of polyamines/Mg^{2+} to the cytoplasmic pore and inner vestibule of the channel for inward rectification (Kubo and Murata, 2001; Vanoye et al., 2002; Yang et al., 1995). Here, we find that a di-aspartate cluster (Arg 255 and Arg 259) is also involved in controlling inward rectification. This brings a

total charge of -5 for the family of Kir2 channels (Table 2.2), which may account for the strong electro-negativity observed in the $Kir2.1_L$ structure. Comparing the different types of Kir channels shows that the total number of acidic residues correlates well with the strength of inward rectification but cannot account completely for strong rectification. For example, Kir4.1 shows strong rectification but only possesses three of the five acidic residues (Fakler et al., 1996). The aspartate in the M2 domain might contribute more than the cytoplasmic domains to controlling the strength of rectification, although Kir7.1 contains a glutamate and does not show strong rectification (Doring et al., 1998). Non-polar interactions are also likely to be important for regulating rectification.

Table 2.2 Summary of cytoplasmic pore mutations involved in rectification

			M2		C-terminal domain[a]						
Kir channel	**Rectification**	**Charge**	172	224	228	255	259	260	299	301	307
Kir2.1	****	–5	D	E	R	D	D	R	E	M	M
Kir2.2	****	–5	D	E	R	D	D	R	E	M	M
Kir2.3	****	–5	D	E	R	D	D	R	E	M	M
Kir4.1	****	–3	E	G	T	D	D	S	S	T	A
Kir3.1	***	–3	D	S	R	S	D	Q	E	I	M
Kir3.2	***	–3	N	E	R	Y	D	R	E	M	M
Kir3.3	N.D.	–4	N	E	R	D	D	R	E	M	M
Kir3.4	**	–4	N	E	R	D	D	R	E	M	M
Kir1.1	*	–3	N	G	Y	D	E	N	D	T	A
Kir6.2	*	–1	N	S	H	G	N	G	E	V	I
Kir7.1	*	–3	E	S	S	D	E	C	S	M	E
KirBac1.1	N.D.	–2	I	E	K	N	H	P	E	S	Q
References			1	2	3	3	3	3	4	3	3

[a]Shaded cells indicate amino acids in Kir2.1 involved in rectification. Number at top indicates amino acid position for Kir2.1. Qualitative difference in rectification among Kir channels ranging from weak (*) to strong (****). N.D. denotes 'not determined'. Note the general correlation of strength of inward rectification with number of acidic amino acids, though there are exceptions (such as Kir7.1). References for mutations demonstrating change in rectification:1: (Fakler et al., 1996; Vanoye et al., 2002) ; 2: (Yang et al., 1995); 3: this study; 4: (Kubo and Murata, 2001).

In the $Kir2.1_L$ structure, the di-aspartate cluster is located farther away from the pore cavity than is the Glu 224-Glu 299 pair (Fig. 2.7). Given the distance from the pore, what mechanistic role could the di-aspartate cluster have in controlling inward rectification? Several different mechanisms for inward rectification have been proposed (John et al., 2004). In general, negative charges can attract cations such as polyamines, Mg^{2+} and K^+. Various studies suggest that the negative charge of Glu 224/Glu 299 serves as a docking site for polyamines and Mg^{2+} such that binding to these sites influences both the entry and exit rates of polyamines in the deep pore formed by M2 domain and selectivity filter (John et al., 2004; Kubo and Murata,

2001). The strong voltage dependence on polyamine inhibition arises from the interaction of amine group both with the Asp 172 in the pore cavity and with the selectivity filter (Pearson and Nichols, 1998). The presence of an additional pair of acidic residues in Kir2.1 could also serve to attract polyamines to the cytoplasmic pore. Consistent with this idea, mutation of Arg 259 showed a slow component of inhibition, which could reflect a slow rate of polyamine entry into the deep pore. Recently, it was proposed that polyamines may regulate high- or low-affinity conformational states (Ishihara and Ehara, 2004). Binding of polyamines to the di-aspartate cluster could be also involved in producing this type of conformational change. Additional studies examining the affinity for polyamines and Mg^{2+} in these mutant channels should provide more insights into the mechanism of inward rectification for Kir channels.

Notably, KirBac1.1 contains only two (Glu 229 and Glu 300) of the five acidic residues implicated in inward rectification of eukaryotic Kir channels (Table 2.2). KirBac1.1 differs in two ways in regards to its cytoplasmic pore. First, the loop between βE and βF residing near the entryway of the cytoplasmic pore bends away from the central pore axis, creating a wider vestibule. Second, the vestibule of the KirBac1.1's cytoplasmic pore is positively charged overall. The less pronounced electronegative surface of KirBac1.1 predicts that KirBac1.1 may not rectify as

strongly as its eukaryotic counterparts. Recent expression studies of purified KirBac1.1 demonstrate much less K^+ selectivity than do Kir channels.

Structural insights into Andersen syndrome mutants. Fourteen of eighteen amino acids that are mutated in Andersen syndrome are found in the cytoplasmic domains of Kir2.1 (mutants known to be associated with Anderson syndrome are R67W, D71V/N, T75R, P186L, R189I, T192A, G215D, N216H, R218W/Q, G300V/D, V302M, E303K, R312C and Δ314−315). These Andersen syndrome−related mutations generally result in a loss of function via dominant negative interactions and heteromeric assembly (Bendahhou et al., 2003; Hosaka et al., 2003; Plaster et al., 2001; Preisig-Muller et al., 2002). Some decreased functions are directly attributed to a change in PIP_2 sensitivity (Lopes et al., 2002). Of the 18 positions affected by mutations, 10 are visualized in the $Kir2.1_L$ structure (Fig. 2.4c), with 8 located on the top surface of the cytoplasmic structure (Arg189, Thr192, Arg218, Gly300, Val302, Glu303, Arg312, Δ314−315), which may be near the PIP_2-binding site, and the other two buried in the protein interface (Gly 215, Asn 216). Four locations, residues Gly 300, Val 302 and Glu 303 and the site of the deletion mutant Δ314−315, are clustered as part of the G-loop region (Fig. 2.4c).

Inspection of the $Kir2.1_L$ structure showed that two particular sites of Andersen-syndrome mutations (Arg 218 and Glu 303) form favorable charged and polar interactions with Thr 309 and Arg312, respectively. This suggested that second-

site mutations might rescue the Andersen mutations. Both single-point mutants Kir2.1$_L$ (R218Q) and Kir2.1$_L$ (E303K) aggregated in aqueous buffer, but Kir2.1$_L$ (R218Q) was rescued by an additional change (T309R). The double mutant Kir2.1$_L$ (R218Q/T309R) formed a stable tetramer, whereas a single-point mutant Kir2.1$_L$ (T309R) aggregates, suggesting that the basis of the Andersen mutation of R218Q is the misfolded cytoplasmic domain (data not shown) that is distinguished by its altered PIP_2 affinity at other sites. Notably, Arg 218 and Thr 309 reside within the CD and HI loops, respectively, thus providing additional evidence that interloop interaction may be important for global conformational coupling of the G-loop.

Functional implications of flexible G-loop in gating control. The movement in the G-loop observed in the different structures of the cytoplasmic domains is notable. From structural perspectives, the different backbone conformations of the G-loops between Kir2.1$_L$ and Kir3.1$_S$ are further highlighted by the contrast between Kir3.1$_S$ and Kir3.1$_{S\text{-}Met}$ (Nishida and MacKinnon, 2002). The narrow opening formed by the G-loop indicates that the G-loops should undergo a conformational change during gating by PIP_2 binding, $G_{\beta\gamma}$ binding, or both. Consistent with this data, mutations at Cys 311 of Kir2.1 alter the kinetics of single-channel activity, Kir3.1/Kir3.2-$_{E315A}$ heteromeric channels show abnormal gating, and mutation of Glu 224 near the G-loop alters single-channel conductance and gating (Chang et al., 2005; Chen et al., 2002; Garneau et al., 2003; Yang et al., 1995). G-

loops may contribute to conductance and gating by triggering allosteric changes in the selectivity filter or PIP_2 affinity of Kir channels (Garneau et al., 2003; Vanoye et al., 2002). Other studies have also substantiated a functional role of the G-loop region. For example, regulation of Kir3 channels by G proteins' G_α subunits involves the region near the G-loop (Glu311-Gly335 of Kir3.2), pH-dependent gating of Kir1.1 channels involves movement of the N terminus and the G-loop in the C terminal domain, and MTS modification of endogenous cysteines within the G-loop of Kir3.1/Kir3.2 channels can completely abolish basal current (Clancy et al., 2005; Guo et al., 2002; Ivanina et al., 2004; Schulte et al., 1998).

An emerging theme is that functional gates are located in different parts of the channel including the selectivity filter (P-loop) and transmembrane helices, and these can in principle operate on different timescales (Phillips et al., 2003; Proks et al., 2003; Xiao et al., 2003). In a broad sense, multiple gates can operate on at least two different timescales: a 'fast' gate in the selectivity filter and a 'slow' gate as a diffusion barrier (Roosild et al., 2004). The fast gate may involve a stochastic switch between different conformational states. The slow gate may involve a larger conformational change similar to that of the octameric gate ring of MthK, the dimer-tetramer conversion of KTN domain, the outwardly sliding helix of KirBac1.1, the twisted S6 helices of Kv channels, or (in the case of Kir channels) the proposed flexible G-loops of the cytoplasmic pore (Doyle et al., 1998; Jiang et al., 2002; Roosild et al., 2004).

2.5 MATERIALS AND METHODS

Molecular biology. N-terminal domains (amino acids 1−99) of mouse Kir3.2 and Kir3.4 and C-terminal domains (amino acids 198−414 and 193−419, respectively) were expressed dicistronically using *pHis8*, a modified *pET28a* vector (Novagen; (Corey and Clapham, 1998; Zhou et al., 2001). For fusion protein constructs, cytoplasmic N-terminal and C-terminal domains of mouse Kir2.1 and rat Kir3.1 were linked directly in frame by PCR to clone into the *pHis8* vector (Kubo et al., 1993; Zhou et al., 2001). BL21 (*DE3*) cells were used to express the proteins. $Kir2.1_L$ mutants were created using the QuikChange Site-Directed Mutagenesis Kit (Stratagene).

For protein purification, cells were grown at 37 °C to 0.6 OD induced by 0.4 mM IPTG, and lysed in 0.5 M NaCl, 5 mM Tris-HCl, pH 8.5, 10% glycerol, 7 mM β-mercaptoethanol (lysis buffer) and 1 mg lysozyme per 100 ml lysate. The supernatant from the lysate was loaded on a nickel-affinity column (Qiagen) and eluted with 200 mM imidazole. Thrombin-cleaved protein samples were separated by S200 and S75 Sepharose chromatography, and concentrated to 15 mg ml^{-1} $Kir2.1_L$ and 12 mg ml^{-1} $Kir3.1_S$ in the presence of 10 mM DTT for analyses.

Crystallography. $Kir2.1_L$ was crystallized in the space group $C222_1$ at 4 °C with vapor diffusion hanging drops of 30% isopropanol, 0.1 M Tris-HCl, pH 8.5, and

0.2 M $MgCl_2$. Crystals were treated with 10% glycerol before flash freezing. $Kir3.1_S$ crystallized in the space group $P42_12$, the same as for $Kir3.1_{S\text{-}Met}$, but under different conditions (15% ethanol, 0.1 M HEPES, pH 7.5, and 0.2 M $MgCl_2$; (Nishida and MacKinnon, 2002). $Kir3.1_S$ crystals were treated with 20% glycerol before flash freezing. Data were collected for $Kir2.1_L$ and $Kir3.1_S$ at Advanced Light Source (ALS), Berkeley, and Stanford Linear Accelerator Center (SSRL), respectively. Molecular replacement solutions were derived using models of $Kir3.1_{S\text{-}Met}$ and $Kir3.1_S$ for $Kir3.1_S$ and $Kir2.1_L$, respectively, by AMORE and MOLREP and refinement by Crystallography and NMR System (CNS).

Electrophysiology. Kir2.1 and its mutants were constructed in *pBSK* using PCR. *In vitro*, methyl-capped cRNA was made from linear cDNA and T3 or T7 RNA polymerase (Stratagene; (Kubo et al., 1993) . The quality of cRNA was estimated using an ethidium-stained formaldehyde gel. *Xenopus* oocytes were isolated as described previously[12]. Oocytes were injected with a 46 nl Kir2.1 cRNA solution (0.5−5 ng) and incubated in ND96 (96 mM NaCl, 2 mM KCl, 1 mM $CaCl_2$, 1 mM $MgCl_2$, 5 mM HEPES, pH adjusted to 7.6 with NaOH) for 1−4 days at 16 °C. Macroscopic currents were recorded with a two-electrode voltage-clamp amplifier as described previously (ref. 12). Mutants were studied in two or three different batches of oocytes and produced similar changes in rectification. In one case, M301A

consistently showed less rectification at +30 mV, but the extent of rectification was more variable at +100 mV in different batches of oocytes.

To study PIP_2 affinity, Kir2.1 currents were recorded in 'giant' membrane patches from *Xenopus* oocytes (Hilgemann, 1995). Patch pipettes had inner tip diameters of 10−20 μm. Inside-out patches were perfused through a manifold connected to solution reservoirs by polyethylene tubes and switching perfusion solutions controlled by a valve system (ALA Scientific). The electrodes, recording chamber and perfusion lines were filled with 'FVPP' solution: (in mM) 96 KCl, 5 Na_2EDTA, 10 HEPES, 5 KF, 3 NaO_3V, 10 $K_4P_2O_7$, pH 7.4 (HCl; (Lopes et al., 2002). Polylysine (average molecular weight 7 kDa, 50 mg ml^{-1}; P6403, Sigma) was added to the FVPP perfusion solution to 0.3 mg ml^{-1}. The patch-clamp amplifier was an Axopatch 200B (Axon Instruments). Currents were filtered at 1 kHz, and data acquired at 5 kHz with a Digidata 1320A computer interface and pClamp 8 (Axon Instruments) for analyses. Membrane voltage was held at 0 mV and stepped every 1 or 5 s to 50 mV for 400 ms and then to -50 mV for 400 ms. Current was averaged over the last 10 ms of the -50 mV step.

Data analysis. Macroscopic currents were elicited with voltage steps from -100 mV to +100 mV. The current amplitude was measured at the beginning (6.8 ms) or end (146.8 ms) of a 150-ms step pulse. The 6.8-ms time point was selected to

ensure that the oocyte membrane capacitative current did not contribute to the current measurement and was used for calculating the mean current and rectification ratio. For quantifying change in PIP_2 affinity, t_{50} was calculated by measuring the time taken for the current to decrease by one-half, after the instantaneous change in current produced with intracellular polylysine. The instantaneous decrease in current is not due to loss of PIP_2 (ref. 15). All values are given as mean ±s.e.m. Statistical differences were determined using one-way ANOVA, followed by Bonferroni *post hoc* using Kir2.1 as control.

2.6 ACKNOWLEDGMENTS

We thank D. Clapham, M. Lazdunski and S. Hebert for *GIRK4*, *GIRK2* and *ROMK1* cDNAs, respectively. We also thank D. Kaiser for analytical ultracentrifugation, C. Park for mass spectroscopy, and the staff at ALS and SSRL for X-ray data collection. This work was supported by grants from the National Institutes of Health (P.A.S & S.C.) and the McKnight Endowment for Neuroscience (P.A.S). S.C. acknowledges the support from the American Heart Association.

Chapter 2 is in part a reprint of the material as it appears in Pegan, S., Arrabit, C., Zhou W., Kwiatkowski W., Collins A., Slesinger PA., Choe, S. (2005) *Cytoplasmic domain structures of Kir2.1 and Kir3.1 shows sites for modulating gating and rectification.* Nat Neurosci. **8**: 279-287. The dissertation author was the primary researcher and author of this publication.

2.7 REFERENCES

Armstrong, N., Sun, Y., Chen, G. Q., and Gouaux, E. (1998). Structure of a glutamate-receptor ligand-binding core in complex with kainate. Nature *395*, 913-917.

Bendahhou, S., Donaldson, M. R., Plaster, N. M., Tristani-Firouzi, M., Fu, Y. H., and Ptacek, L. J. (2003). Defective potassium channel Kir2.1 trafficking underlies Andersen-Tawil syndrome. J Biol Chem *278*, 51779-51785.

Chang, H. K., Yeh, S. H., and Shieh, R. C. (2005). A ring of negative charges in the intracellular vestibule of Kir2.1 channel modulates K+ permeation. Biophys J *88*, 243-254.

Chen, L., Kawano, T., Bajic, S., Kaziro, Y., Itoh, H., Art, J. J., Nakajima, Y., and Nakajima, S. (2002). A glutamate residue at the C terminus regulates activity of inward rectifier K+ channels: implication for Andersen's syndrome. Proc Natl Acad Sci U S A *99*, 8430-8435.

Clancy, S. M., Fowler, C. E., Finley, M., Suen, K. F., Arrabit, C., Berton, F., Kosaza, T., Casey, P. J., and Slesinger, P. A. (2005). Pertussis-toxin-sensitive Galpha subunits selectively bind to C-terminal domain of neuronal GIRK channels: evidence for a heterotrimeric G-protein-channel complex. Mol Cell Neurosci *28*, 375-389.

Corey, S., and Clapham, D. E. (1998). Identification of native atrial G-protein-regulated inwardly rectifying K+ (GIRK4) channel homomultimers. J Biol Chem *273*, 27499-27504.

Derst, C., Konrad, M., Kockerling, A., Karolyi, L., Deschenes, G., Daut, J., Karschin, A., and Seyberth, H. W. (1997). Mutations in the ROMK gene in antenatal Bartter syndrome are associated with impaired K+ channel function. Biochem Biophys Res Commun *230*, 641-645.

Doring, F., Derst, C., Wischmeyer, E., Karschin, C., Schneggenburger, R., Daut, J., and Karschin, A. (1998). The epithelial inward rectifier channel Kir7.1 displays unusual K+ permeation properties. J Neurosci *18*, 8625-8636.

Doyle, D. A., Morais Cabral, J., Pfuetzner, R. A., Kuo, A., Gulbis, J. M., Cohen, S. L., Chait, B. T., and MacKinnon, R. (1998). The structure of the potassium channel: molecular basis of K+ conduction and selectivity. Science *280*, 69-77.

Enkvetchakul, D., Jeliazkova, I., and Nichols, C. G. (2005). Direct modulation of Kir channel gating by membrane phosphatidylinositol 4,5-bisphosphate. J Biol Chem *280*, 35785-35788.

Fakler, B., Bond, C. T., Adelman, J. P., and Ruppersberg, J. P. (1996). Heterooligomeric assembly of inward-rectifier K+ channels from subunits of different subfamilies: Kir2.1 (IRK1) and Kir4.1 (BIR10). Pflugers Arch *433*, 77-83.

Garneau, L., Klein, H., Parent, L., and Sauve, R. (2003). Contribution of cytosolic cysteine residues to the gating properties of the Kir2.1 inward rectifier. Biophys J *84*, 3717-3729.

Guo, Y., Waldron, G. J., and Murrell-Lagnado, R. (2002). A role for the middle C terminus of G-protein-activated inward rectifier potassium channels in regulating gating. J Biol Chem *277*, 48289-48294.

Hilgemann, D. (1995). The giant membrane patch (Plenum, New York).

Hosaka, Y., Hanawa, H., Washizuka, T., Chinushi, M., Yamashita, F., Yoshida, T., Komura, S., Watanabe, H., and Aizawa, Y. (2003). Function, subcellular localization and assembly of a novel mutation of KCNJ2 in Andersen's syndrome. J Mol Cell Cardiol *35*, 409-415.

Huang, C. L., Feng, S., and Hilgemann, D. W. (1998). Direct activation of inward rectifier potassium channels by PIP2 and its stabilization by Gbetagamma. Nature *391*, 803-806.

Huang, C. L., Slesinger, P. A., Casey, P. J., Jan, Y. N., and Jan, L. Y. (1995). Evidence that direct binding of G beta gamma to the GIRK1 G protein-gated inwardly rectifying K+ channel is important for channel activation. Neuron *15*, 1133-1143.

Inanobe, A., Yoshimoto, Y., Horio, Y., Morishige, K. I., Hibino, H., Matsumoto, S., Tokunaga, Y., Maeda, T., Hata, Y., Takai, Y., and Kurachi, Y. (1999). Characterization of G-protein-gated K+ channels composed of Kir3.2 subunits in dopaminergic neurons of the substantia nigra. J Neurosci *19*, 1006-1017.

Ishihara, K., and Ehara, T. (2004). Two modes of polyamine block regulating the cardiac inward rectifier K+ current IK1 as revealed by a study of the Kir2.1 channel expressed in a human cell line. J Physiol *556*, 61-78.

Ivanina, T., Varon, D., Peleg, S., Rishal, I., Porozov, Y., Dessauer, C. W., Keren-Raifman, T., and Dascal, N. (2004). Galphai1 and Galphai3 differentially interact with, and regulate, the G protein-activated K+ channel. J Biol Chem *279*, 17260-17268.

Jiang, Y., Lee, A., Chen, J., Cadene, M., Chait, B. T., and MacKinnon, R. (2002). The open pore conformation of potassium channels. Nature *417*, 523-526.

John, S. A., Xie, L. H., and Weiss, J. N. (2004). Mechanism of inward rectification in Kir channels. J Gen Physiol *123*, 623-625.

Kubo, Y., Baldwin, T. J., Jan, Y. N., and Jan, L. Y. (1993). Primary structure and functional expression of a mouse inward rectifier potassium channel. Nature *362*, 127-133.

Kubo, Y., and Murata, Y. (2001). Control of rectification and permeation by two distinct sites after the second transmembrane region in Kir2.1 K+ channel. J Physiol *531*, 645-660.

Lopatin, A. N., Makhina, E. N., and Nichols, C. G. (1994). Potassium channel block by cytoplasmic polyamines as the mechanism of intrinsic rectification. Nature *372*, 366-369.

Lopes, C. M., Zhang, H., Rohacs, T., Jin, T., Yang, J., and Logothetis, D. E. (2002). Alterations in conserved Kir channel-PIP2 interactions underlie channelopathies. Neuron *34*, 933-944.

Matsuda, H., Saigusa, A., and Irisawa, H. (1987). Ohmic conductance through the inwardly rectifying K channel and blocking by internal Mg2+. Nature *325*, 156-159.

Miyazawa, A., Fujiyoshi, Y., and Unwin, N. (2003). Structure and gating mechanism of the acetylcholine receptor pore. Nature *423*, 949-955.

Nishida, M., and MacKinnon, R. (2002). Structural basis of inward rectification: cytoplasmic pore of the G protein-gated inward rectifier GIRK1 at 1.8 A resolution. Cell *111*, 957-965.

Pearson, W. L., and Nichols, C. G. (1998). Block of the Kir2.1 channel pore by alkylamine analogues of endogenous polyamines. J Gen Physiol *112*, 351-363.

Phillips, L. R., Enkvetchakul, D., and Nichols, C. G. (2003). Gating dependence of inner pore access in inward rectifier K(+) channels. Neuron *37*, 953-962.

Plaster, N. M., Tawil, R., Tristani-Firouzi, M., Canun, S., Bendahhou, S., Tsunoda, A., Donaldson, M. R., Iannaccone, S. T., Brunt, E., Barohn, R.*, et al.* (2001). Mutations in Kir2.1 cause the developmental and episodic electrical phenotypes of Andersen's syndrome. Cell *105*, 511-519.

Preisig-Muller, R., Schlichthorl, G., Goerge, T., Heinen, S., Bruggemann, A., Rajan, S., Derst, C., Veh, R. W., and Daut, J. (2002). Heteromerization of Kir2.x potassium channels contributes to the phenotype of Andersen's syndrome. Proc Natl Acad Sci U S A *99*, 7774-7779.

Proks, P., Antcliff, J. F., and Ashcroft, F. M. (2003). The ligand-sensitive gate of a potassium channel lies close to the selectivity filter. EMBO Rep *4*, 70-75.

Riven, I., Kalmanzon, E., Segev, L., and Reuveny, E. (2003). Conformational rearrangements associated with the gating of the G protein-coupled potassium channel revealed by FRET microscopy. Neuron *38*, 225-235.

Roosild, T. P., Le, K. T., and Choe, S. (2004). Cytoplasmic gatekeepers of K+-channel flux: a structural perspective. Trends Biochem Sci *29*, 39-45.

Schulte, U., Hahn, H., Wiesinger, H., Ruppersberg, J. P., and Fakler, B. (1998). pH-dependent gating of ROMK (Kir1.1) channels involves conformational changes in both N and C termini. J Biol Chem *273*, 34575-34579.

Shyng, S. L., Cukras, C. A., Harwood, J., and Nichols, C. G. (2000). Structural determinants of PIP(2) regulation of inward rectifier K(ATP) channels. J Gen Physiol *116*, 599-608.

Signorini, S., Liao, Y. J., Duncan, S. A., Jan, L. Y., and Stoffel, M. (1997). Normal cerebellar development but susceptibility to seizures in mice lacking G protein-coupled, inwardly rectifying K+ channel GIRK2. Proc Natl Acad Sci U S A *94*, 923-927.

Vanoye, C. G., MacGregor, G. G., Dong, K., Tang, L., Buschmann, A. S., Hall, A. E., Lu, M., Giebisch, G., and Hebert, S. C. (2002). The carboxyl termini of K(ATP) channels bind nucleotides. J Biol Chem *277*, 23260-23270.

Wickman, K., Nemec, J., Gendler, S. J., and Clapham, D. E. (1998). Abnormal heart rate regulation in GIRK4 knockout mice. Neuron *20*, 103-114.

Xiao, J., Zhen, X. G., and Yang, J. (2003). Localization of PIP2 activation gate in inward rectifier K+ channels. Nat Neurosci *6*, 811-818.

Yang, J., Jan, Y. N., and Jan, L. Y. (1995). Control of rectification and permeation by residues in two distinct domains in an inward rectifier K+ channel. Neuron *14*, 1047-1054.

Zhou, W., Arrabit, C., Choe, S., and Slesinger, P. A. (2001). Mechanism underlying bupivacaine inhibition of G protein-gated inwardly rectifying K+ channels. Proc Natl Acad Sci U S A *98*, 6482-6487.

Zhou, W., Qian, Y., Kunjilwar, K., Pfaffinger, P. J., and Choe, S. (2004). Structural insights into the functional interaction of KChIP1 with Shal-type K(+) channels. Neuron *41*, 573-586.

CHAPTER THREE

Andersen's Syndrome Mutation Effects on the Structure and Assembly of the Cytoplasmic Domains of Kir2.1

3.1 ABSTRACT

Andersen's Syndrome is caused by defects in the inwardly rectifying potassium channel 2.1 (Kir2.1). These channels play a key role in maintaining the correct resting potential in eukaryotic cells. We have characterized individual Andersen's Syndrome mutants R218Q, G300V, E303K, and Δ314-315 and have shown that they have multiple effects on the ability of the cytoplasmic domains in Kir2.1 channels to form proper tetrameric assemblies. The 2.0 Å x-ray crystal structure of the N- and C-terminal cytoplasmic domains of Kir2.1 R218Q combined with T309K reveals multiple conformations of the G-loop and CD loop in AS-affected Kir2.1 channels. We also show that E303 plays an important role in gating. Finally, we demonstrate that the DE loop is involved in stabilizing a 2-methyl-2,4-pentanediol binding site found near the putative $G_{\beta\gamma}$-binding site, and illustrate the first identified potassium ion bound to a cytoplasmic domain for this class of K^+ channels.

3.2 INTRODUCTION

Andersen's Syndrome (AS) is a rare autosomal disorder caused by the non-functional inwardly rectifying potassium (Kir) channels (Lopes et al., 2002; Plaster et al., 2001). Individuals affected with AS exhibit electrophysiological symptoms of periodic paralysis, a prolonged QT interval, and ventricular arrhythmias. Also present in AS individuals are distinct physical abnormalities that include low-set ears, clinodactyly, scoliosis, hypertelorism, and micrognathia (Donaldson et al., 2003; Plaster et al., 2001). AS has been directly linked to the potassium inwardly rectifying channel 2.1 (Kir2.1)(Preisig-Muller et al., 2002; Tristani-Firouzi et al., 2002). Over the past decade and a half, point mutations occurring at one of 15 sites and two internal deletions in Kir2.1 channels have been found in patients with AS (Fig. 3.1) (Chen et al., 2002; Donaldson et al., 2003; Hosaka et al., 2003; Lopes et al., 2002; Plaster et al., 2001; Tristani-Firouzi et al., 2002).

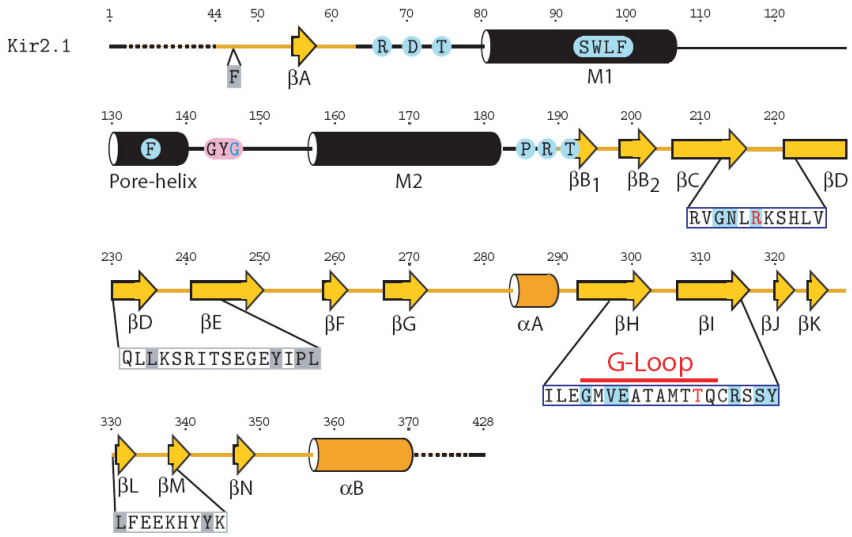

Figure 3.1 Secondary structure elements of Kir2.1 with key Andersen's Syndrome and MPD binding site locations (β sheets in arrows and α helices in cylinders). Those in gold are from the $Kir2.1_S$ R218Q/T309K, added by those in black from the KirBac1.1. Shaded residues in pink denote the K^+ selectivity filter. Andersen's Syndrome sites are shaded in light blue. MPD binding sites are shaded in gray. $Kir2.1_S$ R218Q/T309K mutation sites are in red. Red underline represents the G-loop region.

The Kir2.1 channel is a strong inward rectifier that belongs to the classic Kir group (Hille, 2001). In contrast to the voltage-gated potassium channels that allow large fluxes of ions to flow passively either in or out of the cell when opened, Kir2.1 channels allow large fluxes of K^+ ions into the cell but only small fluxes of K^+ out of the cell (Hille, 2001). This behavior, known as inward rectification, occurs when cytosolic polyamines and Mg^{2+} occlude the ion conductance pathway as K^+ ions are flowing outward (Kubo and Murata, 2001; Lopatin et al., 1994; Vanoye et al., 2002). These positively charged particles are then washed off when K^+ ions flow into the cell (Enkvetchakul et al., 2005). The rate of rectification by these positively charged polyamine and Mg^{2+} block varies between different members of the Kir family

depending on the presence of key hydrophilic residues located at two major locations. The strongest binding site of these blockers resides within the trans-membrane site defined by Asp 172 in Kir2.1 and weaker, recruiting sites are comprised of several positive and negative charged residues in the cytoplasmic domain (Enkvetchakul et al., 2005; Fujiwara and Kubo, 2006; Pegan et al., 2005). The overall effect of rectification allows Kir2.1 to play a key role in eukaryotic cells by driving the resting membrane potential to E_K when the cell is at rest (Hille, 2001). Among Kir channels, Kir3.1 channels require binding of G-proteins and phosphylinositol-4,5-bisphosphate (PIP_2) in order to open, whereas Kir2.1 channels require only PIP_2 (Huang et al., 1998; Lopes et al., 2002). All Kir channels and a bacterial homolog, KirBac1.1, share the structural scaffold of a K+ selectivity filter, two trans-membrane spanning helices, a pore filter helix, a slider helix, and the N- and C-terminal cytoplasmic domain structures comprised of fifteen β-sheet fold with two helices (Doyle et al., 1998; Nishida and MacKinnon, 2002; Pegan et al., 2005).

Biochemical data indicate that eukaryotic Kir channels form either hetero- or homo-tetramers (Preisig-Muller et al., 2002; Silverman et al., 1996). Some $G_{\beta\gamma}$-gated Kir3 family members form primarily hetero-tetramers. For instance, Kir3.1 subunits assemble with other Kir3.2-4 subunits, but homo-tetrameric Kir3.2 and Kir3.4 are also present in certain cell types (Corey and Clapham, 1998; Inanobe et al., 1999; Silverman et al., 1996; Zhou et al., 2001). In comparison, the Kir2.1 channels readily

form homo-tetramers, as well as hetero-tetramers with other Kir2 family members such as Kir2.2 and Kir2.3 (Fink et al., 1996; Preisig-Muller et al., 2002). The ability of Kir2 subunits assembled with AS-affected Kir2.1 subunits to restore surface expression without ion-conducting function has been a subject of recent discussion. Non-conducting hetero-tetramers containing AS-affected Kir2.1 subunits indicate that the AS-affected Kir2.1 subunits provide a dominant negative effect on the channels (Preisig-Muller et al., 2002). Furthermore, a recent report showed that AS-affected Kir2.1 channels carrying mutants: D71V, Δ95-98, S136F, G144S, N216H, R218Q, G300V, V302M, E303K, and Δ314-315, were largely incapable of reaching the membrane by themselves; but G144S, N216H, G300V, and E303K could be transported successfully if co-expressed with wild-type (wt) Kir2.1 (Bendahhou et al., 2003). Nevertheless, these channels were all non-conducting like the hetero-tetrameric Kir2.x channels containing AS-affected Kir2.1 subunits (Preisig-Muller et al., 2002).

It has been reported that the ability of wt Kir2.1 and Kir2.3 channels to recover surface expression with some AS-affected Kir2.1 channel subunits do not necessarily restore channel activity. Based on the structure of the N-terminal and C-terminal domains of wt Kir2.1 at 2.4 Å, we previously have proposed that AS mutations could interfere with the flexibility of the pore-facing G-loop to gate the channel properly (Pegan et al., 2005). Alternatively, we suggested that some of these AS mutations

such as R218Q may interfere with the ability of the channel to form a tetrameric membrane-bound assembly in the first place. In the present study, we characterized Kir2.1 cytoplasmic domain in order to probe how four cytoplasmic AS mutations, R218Q, G300V, E303K, and Δ314-315, impact the maintenance of a functional tetrameric assembly. We also describe the structure of the Kir2.1 cytoplasmic domain containing two AS mutations; R218Q and T309K, in order to understand the roles of R218, E303, and T309 in both gating and the tetrameric assembly of functional channels. In the course of this study, we found a novel ligand bound to a biologically relevant site in the C-terminal domain. Finally, we discuss how the presence of the first potassium ion trapped in the cytoplasmic domain of the ion-permeation pathway may affect K^+ permeation.

2.3 RESULTS

Effects of AS Mutations on the assembly of the cytoplasmic domains of Kir2.1. To investigate the effect of specific AS mutation on the tetrameric assembly of the channel, AS mutations, R218Q, G300V, E303K, and Δ314-315, were introduced individually into the $Kir2.1_L$ construct (N-terminal 44-64 fused to C-terminal 189-428; Fig. 3.1). Of these mutants, R218Q, G300V, and E303K were selected on their ability to traffic to the cell membrane when co-expressed with wt Kir2.1 and their proposed roles in gating (G300V), forming intra- (R218Q) and inter-subunit (E303K) interactions (Bendahhou et al., 2003; Pegan et al., 2005). The Δ314-315 was chosen because it does not allow proper trafficking when co-expressed with wt. Each of these mutations has a distinct effect on the quaternary state of the channel's cytoplasmic domains. Δ314-315 in $Kir2.1_L$ ($\Delta 314\text{-}315_L$) resulted mostly in mis-folded protein. R218Q ($R218Q_L$) produced mildly-larger aggregates (Fig. 3.2a). Unlike $\Delta 314\text{-}315_L$ and $R218Q_L$, $E303K_L$ produced significant amounts of soluble tetrameric protein. Interestingly, $E303K_L$ eluted earlier than wt on S200 Sepharose size chromatography (designated as profile 2 in Fig. 3.2a). The $G300V_L$ also eluted to the left of the wt reproducibly, but not to the same extent as the E303K, and was designated as profile 1. G300V and E303K without the flexible tail (truncated at position 372 named as $Kir2.1_S$ (Pegan et al., 2005)), showed a similar left shift in their elution, indicating that these changes were not caused by the flexible C-terminal tail of $Kir2.1_L$ (residues 373-428). Attempts to crystallize G300V and E303K were

unsuccessful. However, these results already demonstrate the two Kir2.1 AS mutations cause the cytoplasmic domain to adopt conformations that are distinct from that of the wt species.

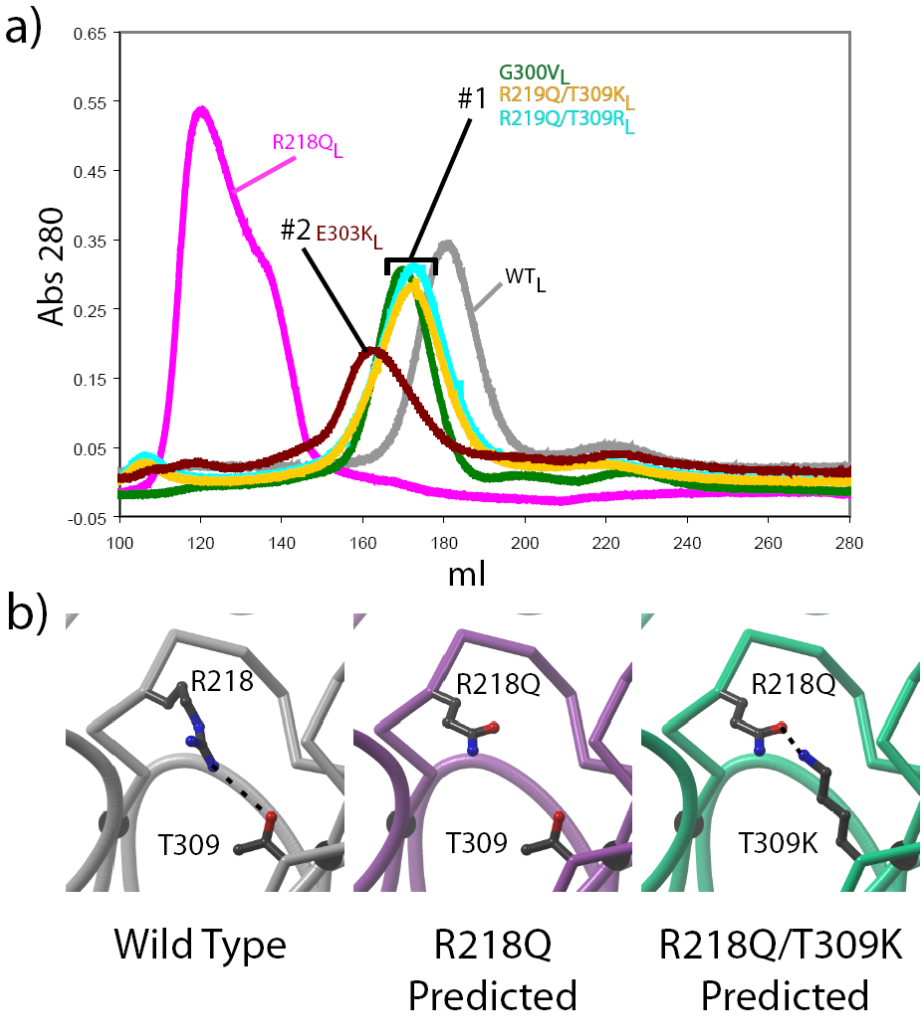

Figure 3.2 Sizing chromatograms of various mutants of Kir2.1$_L$ by S200 Sepharose column (void volume at 105 ml). (a) wt Kir2.1$_L$ (gray), E303K$_L$ (red), R218Q$_L$ (magenta), G300V$_L$ (green), R218Q/T309R$_L$ (teal), and R218Q/T309K$_L$ (gold). **(b)** Close up of positions Arg 218, Thr 309 in the wt Kir2.1$_L$ structure (gray), predicted models of Kir2.1$_L$ R218Q (violet) and Kir2.1$_L$ R218Q/T309K (teal). Dashed lines represent polar interactions.

To understand the nature of the mildly-aggregating R218Q, we reasoned that changing the Thr 309 to a positive charge residue would restore a polar interaction similar to the native one present in Kir2.1 between Arg 218 and Thr 309 (Fig. 3.2b). Here, we examined the electrophysiological properties of these mutants. Two-electrode voltage clamp was used to record macroscopic currents in oocytes injected with cRNA for Kir2.1 or Kir2.1 mutants. We previously showed that additional change to Lys or Arg at Thr 309 could restore the tetrameric assembly of the $Kir2.1_L$ (Pegan et al., 2005). Interestingly, however, both R218Q/T309R and R218Q/T309K did not restore the wt current of the channel (Fig. 3.3). Furthermore, it was apparent from the sizing column that the extent of conformational change in $R218Q/T309K_L$ or $R218Q/T309R_L$ is similar to $G300V_L$, profile 1, as they both eluted nearly at the same position. These results lead to the idea that these two double mutants share an altered non-functional conformation, as with G300V, that disrupts channel function.

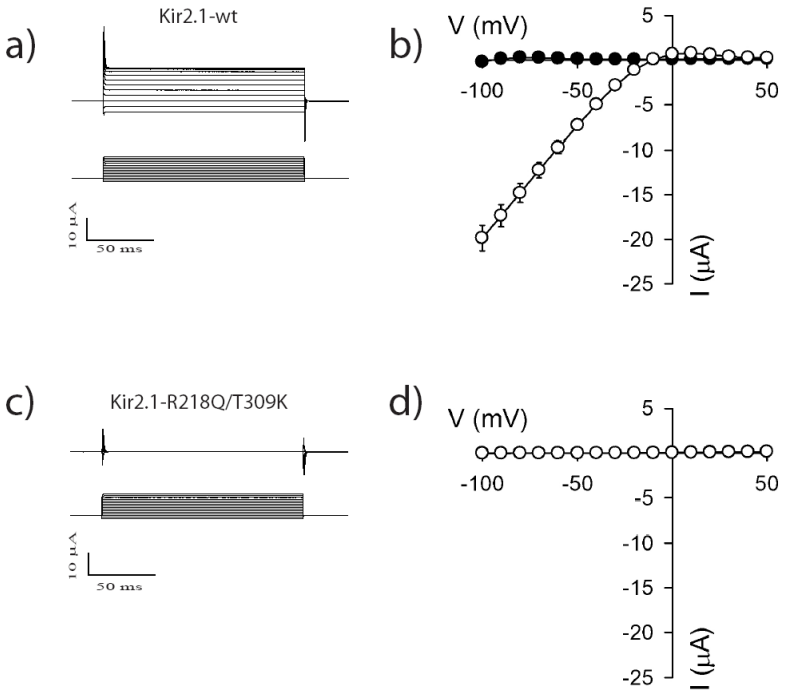

Figure 3.3 Inwardly rectifying K^+ currents of Kir2.1 and the R218Q/T309K mutant expressed in Xenopus oocytes. Oocytes were injected with cRNA for **(a, b)** Kir2.1 wild-type, or **(c, d)** Kir2.1 R218Q/T309K. Macroscopic currents were elicited with voltage steps from -100 mV to +50 mV. The average current is plotted in the current-voltage relations. Average currents at -100 mV were -0.21 ± 0.01 µA in 2K and -19.87 ± 1.43 µA in 95K for wild-type (n=5), -0.011 ± 0.002 µA in 2K and -0.036 ± 0.002 µA in 95K for R218Q (n=10), -0.009 ± 0.002 µA in 2K and -0.036 ± 0.003 µA in 95K for T309K (n=10), and -0.011 ± 0.003 µA in 2K and -0.039 ± 0.020 µA in 95K for R218Q/T309K (n=10).

G-loop conformation of a double mutant R218Q/T309K. The ability of the R218Q/T309K and R218Q/T309R to restore the native tetrameric state of the cytoplasmic domains, but be trapped in an altered conformation (profile 1; Fig. 3.2a) and fail to rescue channel function suggests that Arg 218 may play a more complex role than just forming a stable tetramer. Furthermore, the $G300V_L$-like profile and proximity of Arg 218 to the G-loop structure suggested that mutation of R218Q may

be affecting the flexible G-loops in the same way as the G300V mutation. In order to resolve the molecular impact of the R218Q mutation, we sought to obtain x-ray crystal structure of the isolated, R218Q/T309K_L and R218Q/T309R_L. Both R218Q/T309K_L and R218Q/T309R_L produced crystals in 35% t-butanol; (0.1 M citrate, pH 5.2, 0.2 M $MgCl_2$), in the I4 space group, which diffracted to 6.0 Å in one direction and 4.0 Å in the other. Subsequently, crystals of the R218Q/T309K_S lacking the 56 C-terminal residues of Kir2.1_L grew in a 35% MPD, 50 mM NaCl, 0.1 M Na/KPO_4 condition in the C2 space group, diffracting to 2.0 Å resolution (a=140.67 Å, b= 98.82 Å, c=98.09 Å; $\alpha=90^o$, $\beta=130.68^o$, $\gamma=90^o$). We have determined the structure of Kir2.1_S R218Q/T309K. There is one tetramer per asymmetric unit containing 818 residues, 713 waters, four MPD molecules, and one K^+ ion (Table 1).

Table 1. Crystallographic data for R218Q/T309K$_S$

Data Collection	
Protein / data set	R218Q/T309K$_S$
Space group	C2
Cell constants	a=140.67
	b=98.87
	c=98.09
	$\alpha=\gamma=90$
	$\beta=130.68$
Wavelength (Å)	1.000
Source	ALS
Resolution (Å)	2.0
Total observations / total reflections	238256 / 66107
Completeness (highest-resolution shell)	99.45 (94.17)
I / σ (highest-resolution shell)	13.4 (2.7)
R_{sym}[a]	0.086
Model refinement	
Total reflections (reflections for test)	62743 (3363)
R_{work}(%) / R_{free}(%)[b]	17.8 / 23.0
Protein atoms / water atoms	6546 / 713
R.m.s. deviation of bond lengths (Å)	0.018
R.m.s. deviation of bond angles (°)	1.65

[a]$R_{sym}=\sum_h\sum_1|I_1(h) - \langle I(h)|\ \sum_h\sum_I I_1(h)$, where $I_1(h)$ is the i^{th} measurement and $\langle I(h)\rangle$ is weighted mean of all measurements of I(h). [b]$R_{free}=h(|F(h)_{obs}| - |F(h)_{calc}|) / h|F(h)_{obs}|$ for reflections in the working and test sets, respectively. R.m.s., root mean square.

The overall scaffold of R218Q/T309K$_S$ is similar to that of the wt Kir2.1$_L$ (Fig. 3.4 a,b). Closer inspection of the two structures show five regions that differ significantly (Fig. 3.4c,d). One of these regions was the linker between N- and C-terminal domains; the electron density supported only the main chain placement with high temperature factors, suggesting higher flexibility of the region. Two other regions included the loop between β sheet D and β sheet E (DE loop) and the region

from the beginning of the β sheet L to β sheet M (LM loop) (Figure4c; see below). The two most intriguing sections are located at the G-loop and CD loop (Fig. 3.4c).

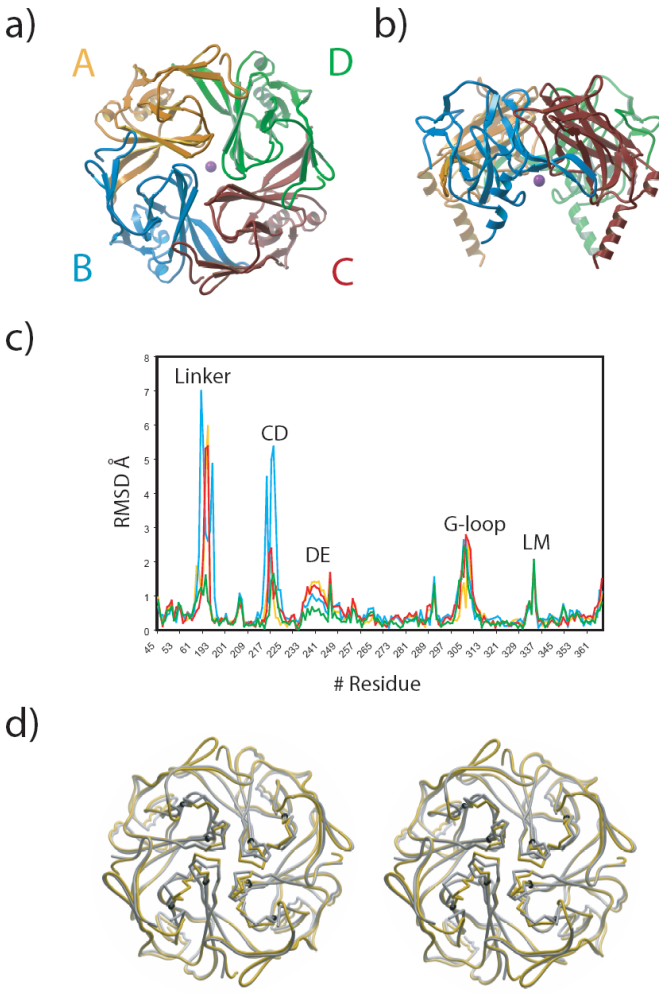

Figure 3.4 R218Q/T309K$_S$ structure. **(a)** Top view of Kir2.1$_S$ R218Q/T309K tetramer; monomers A(gold), B(blue), C(red), D(green); K^+ ion is represented in purple. **(b)** Side view of Kir2.1$_S$ R218Q/T309K tetramer. K^+ ion is represented in purple. **(c)** Root-mean-square deviations between Kir2.1$_L$ to Kir2.1$_S$ R218Q/T309K monomers A (gold), B (blue), C (red), D (green). **(d)** Stereo-view of Kir2.1$_L$ (gray) and R218Q/T309K$_S$ (gold) to highlight the G-loop conformation variations near the pore. Pore comparison stereo top view of Kir2.1$_L$(gray) and Kir2.1$_S$ R218Q/T309K (gold).

Intriguingly, these structural changes are non-uniform in each subunit. G-loops of monomers B and D collapsed toward the center of the pore reducing the pore size of channel from 5.7 Å to 3.6 Å between the carboxyl oxygen of Ala 304 of monomer B and C_β of Ala 304 in the monomer D (Fig. 3.4d). In contrast to the monomers B and D collapsing in, the monomers A and C are displaced away from the center of the channel to a more open conformation resulting in a 9.41 Å distance between their C_β of Ala 304. G-loops of all four subunits have relatively low temperature factors than those in the wt structure. Closer inspection of the G-loop and CD loop regions shows that β sheet I backbone containing T309K is unperturbed, and the conformational change is restricted to the CD loop containing R218Q and the G-loop (Fig. 3.5a,b). Monomer D subunit regains the polar interaction between R218Q and T309K as predicted in Fig. 3.2b (Fig. 3.5b). Surprisingly, the other three monomers have a mix of conformations, with monomers A and B having relatively high temperature factors than the wt. These non-uniform conformational changes of the CD loop and the reduced temperature factors of the displaced G-loops observed in the R218Q/T309K_S structure result in asymmetrical displacement of the G-loop with a smaller opening than that of the wt Kir2.1_L channel.

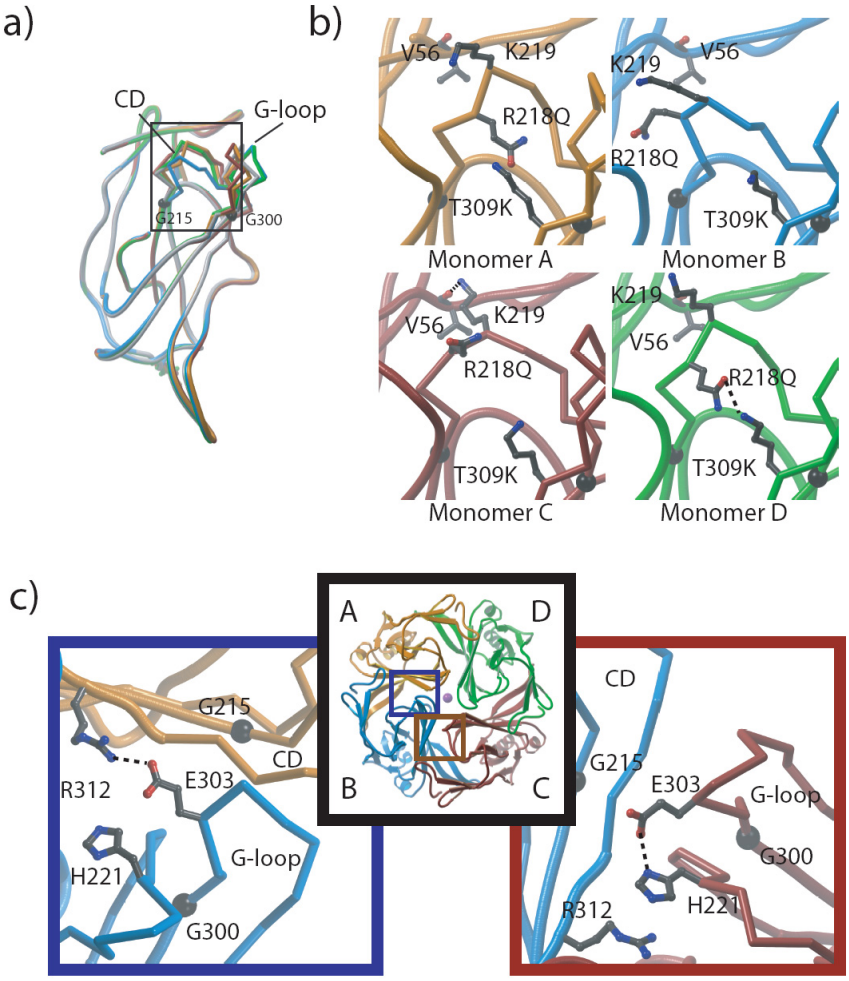

Figure 3.5 **Close-up near Arg 218 an Thr 309.** **(a)** Kir2.1$_S$ R218Q/T309K monomers A (gold), B (blue), C (red), & D (green). **(b)** Close-up views of the boxed area in (a) near Arg 218 and Thr 309 positions. Dashed lines represent polar interactions. **(c)** Close-up view near Glu 303 between monomers, A and B (left), or B and C (right). Dashed lines represent salt bridges.

Disruption of K219 by R218Q creates different salt bridge partners for E303K. In the wild-type structure, Lys 219 side chain points into a void that is expected to be a putative PIP_2 binding site and Arg 218 points also out of the site (Lopes et al., 2002; Pegan et al., 2005). In the R218Q/T309K$_S$ structure, Lys 219 in

monomers A, B, and D are highly flexible (Fig. 3.5a,b). In contrast, the Lys 219 in the monomer C has a low temperature factor (electron density peak at 1.7 σ) and interacts with the carboxyl oxygen of intra-subunit Val 56, rotated 180^{o} from its wt orientation. Like Lys 219, Glu 303 also shows a non-uniform difference in position. As a result, we observe two different conformations of the G-loop near the Glu 303. In the wt, as with monomers A and B of R218Q/T309K_S, Glu 303 forms a salt bridge to Arg 312 across monomer to monomer. The other conformation shows that E303K of monomer C interacts with His 221 of the C subunit forming the intra-subunit charge pair (Fig. 3.5c). These local disparities contribute to the formation of the asymmetric disposition of the G-loops (Fig. 3.4d).

2-methyl-2,4-pentanediol (MPD). As stated earlier, the DE and LM loops are two of the regions that are divergent between the wt Kir2.1$_L$ and R218Q/T309$_L$ structures (Fig. 3.4c,d). Both regions form key interactions between adjacent monomers. Examination of the DE and LM loops identified electron density attributed to MPD. The distinct C2 tetrahedral coordination of MPD coupled with the resulting stereochemistry of the C4 atom allows easy placement within the density with agreeable (F_o-F_c) density (Fig. 3.6b). Extensive interactions of MPD with the solvent-accessible site show H-bonding and hydrophobic interactions pull the DE and LM loops closer together (Fig. 3.6b). O2 atom of MPD contacts Tyr 337. The other oxygen atom O4 of MPD forms H-bond interactions with the carbonyl oxygen of Pro

244 and Tyr 242 via water. Phe 47, Leu 232, Leu 245, and Leu 330 provide the hydrophobic interactions with the methyl groups of MPD.

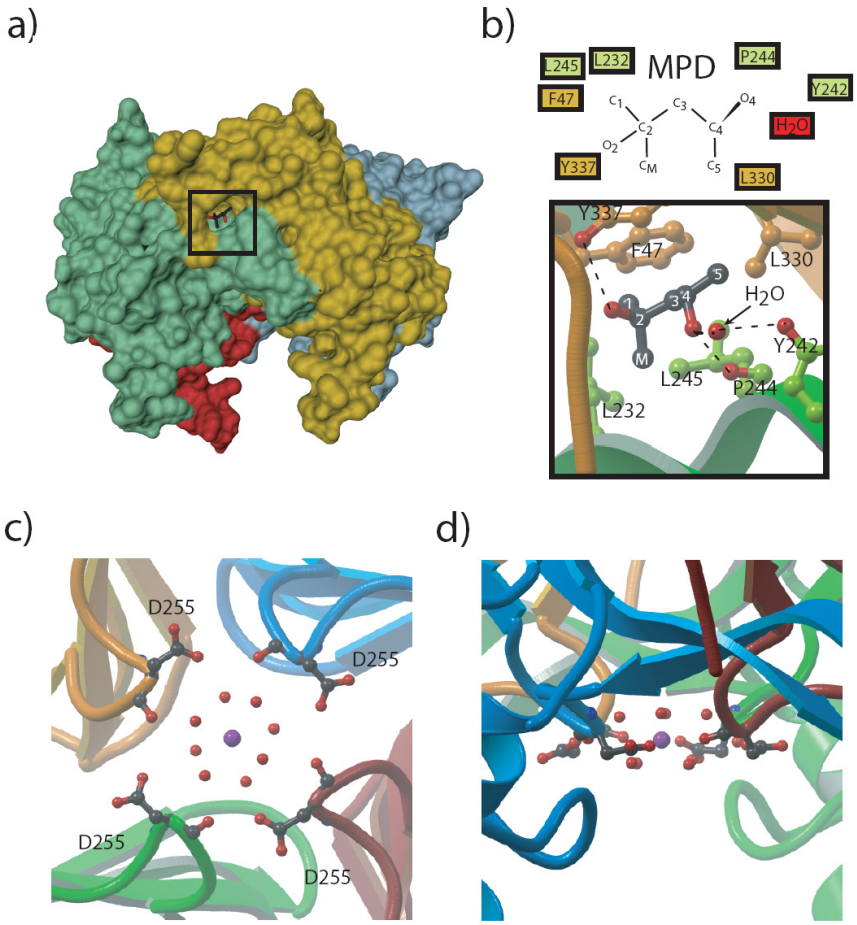

Figure 3.6. **MPD and water caged K^+ binding sites. (a)** Standard side view of R218Q/T309K_S as in Fig. 3.4b. **(b)** MPD binding site residues in box of (a). Dashed lines represent polar interactions. **(c)** Bottom-up view of K^+ binding site showing eight waters and Asp 255 in ball and stick. Waters starting from the top clockwise are 75, 421, 89, 427, 121, 266, 80, and 498. **(d)** Side view of (c).

K^+ binding at the cytoplasmic pore entrance. Analysis of the electron density present in the pore of R218Q/T309K_S, revealed a single K^+ at the cytoplasmic

end of the pore (Fig. 3.4b). Surprisingly, the coordination of the K^+ is not formed by anionic residues in the pore, but is mediated through eight caging waters (Fig. 3.6c, d). The electron density in F_o-F_c maps is consistent with K^+ present during purification and crystallization. Placement of Na^+, the only other cation in the crystallization buffer, in the position of K^+ would not account for electron density in the F_o-F_c maps, nor the 2.8 Å bond distance to the water molecules typical of K+ coordination. Four of the waters are located on the cytoplasmic side of the site and the other four internally to the pore. All of these waters are coordinated via H-bonds to the anionic side chain and backbone carboxyl oxygen of Asp 255. The presence of the water-caged K^+ completely occluding the pore establishes this site as the first binding site in the K^+ permeation pathway toward the selectivity filter.

3.4 DISCUSSION

Sizing chromatography analysis and structure of the R218Q/T309$_S$ have revealed the presence of a significant asymmetrical conformation at a critical region (G-loop) in the permeation pathway. This may explain why the tetrameric assembly of the Kir2.1 channel's cytoplasmic domains is insufficient to restore ion-conducting functionality. Furthermore, the mutant structure suggests how Arg 218 and Glu 303 may affect PIP_2 binding and alter conformational states. These findings clearly imply multiple conformations of the cytoplasmic domain in functional channels. This result is consistent with our prediction that the Δ314-315 Kir2.1 is mis-folded and cannot form a tetramer prior to leaving the endoplasmic reticulum. Similarly, both G300V and E303K, which can form stable homo-tetramers with their cytoplasmic domains, have been shown to be successfully trafficked to the membrane when co-expressed wt channel subunits but do not function (Bendahhou et al., 2003). The R218Q/T309K$_L$ structure suggests that the ability to attain the symmetry of Kir2.1 cytoplasmic domains near the G-loop gate is required for the proper function of the channel. This would explain how heteromeric channels carrying AS-affected subunits can be trafficked properly to the cell surface but remain non-conducting (Bendahhou et al., 2003; Preisig-Muller et al., 2002).

We have described stereochemical details of small molecules MPD bound to the cytoplasmic domain. MPD in the Kir2.1$_L$ structure brings both the DE and LM

loop regions closer toward each other. Whether the binding of MPD or analogs to this site will trigger or block Kir channel opening is unknown. However, these loops have been shown to be part of putative $G_{\beta\gamma}$ activation site in Kir3 channels (Finley et al., 2004). Interestingly, hydrophobic residues that interact with MPD are conserved between the Kir2 and Kir3 families. Most importantly, Tyr 337 and Pro 244, the key residues that form the H-bonds to the hydroxyl groups of MPD, are conserved as well, with the exception of Kir3.1 (Fig. 3.1). Because Kir3 channels form hetero-tetramers with Kir3.1 and homo-tetramers with non-Kir3.1 subunits, we predict that two to four MPD binding sites can be present in any given Kir3 channel. With this site being conservatively present in both Kir2 and Kir3 channels and its central location at the putative G-protein activation site, MPD could be exploited as a framework to design a novel drug to modulate Kir2 and/or Kir3 channels.

Previous x-ray structural studies of KirBac1.1 have uncovered K^+ ions in the selectivity filter. No K^+ ions were resolved in the cytoplasmic domains of KirBac1.1, Kir3.1, or Kir2.1 (Doyle et al., 1998; Nishida and MacKinnon, 2002; Pegan et al., 2005). Most likely, the lack of K^+ ions in the crystallization buffer of Kir3.1 and Kir2.1 can explain the absence of this ion in the structure (Doyle et al., 1998; Nishida and MacKinnon, 2002; Pegan et al., 2005). For KirBac1.1, two residues are absent in the loop that form the cytoplasmic end of the pore, resulting in a wider opening that may not coordinate a hydrated K+ ion through the waters of the first hydration shell

(Doyle et al., 1998). Finding a single hydrated potassium ion in the inner vestibule of Kir2.1 along the permeation pathway is intriguing because of the known conduction properties of K^+ channels. Potassium ions and polyamines are focused on the central water-filled canal leading to the selectivity filter. The central location and exact coordination of the K^+ suggest the ion permeation pathway of the cytoplasmic domain is more like a set of stops mediated by both waters and anionic side chains, not a hydrophilic wall that only recruits K+ ions at random sites along its wall (Enkvetchakul et al., 2005; Fujiwara and Kubo, 2006; Kubo and Murata, 2001). Asp 255 represents one of the first positions along this permeation pathway for both polyamines and potassium ions. Although the 'long-pore' effect of K channels is attributed to the multiple potassium ions located in the selectivity filter, the presence of the hydrated potassium ion along the central canal demonstrates that the long pore indeed extends quite far into the cytoplasm.

3.5 MATERIALS AND METHODS

Molecular biology and protein purification. Fusion constructs $Kir2.1_S$, N-terminal (44-64) and C-terminal (189-371), and $Kir2.1_L$, N-terminal (44-64) and C-terminal (189-428), were generated from mouse Kir2.1 (Fig. 3.1) and linked through 2-step PCR prior to being cloned into an octa-histidine expression vector modified from pet28a (Invitrogen). Andersen's Syndrome mutations were incorporated via QuikChange Site-directed Mutagenesis Kit (Stratagene).

Kir2.1 mutants were grown in Terrific Broth at 37 ^{o}C to the OD_{600} of 0.6, then induced with 0.5 mM IPTG for 3 hours prior to harvesting. Cells were lysed in 0.5M NaCl, 20 mM Tris-HCl pH 8.5, 10% glycerol, 7 mM β-mercaptoethanol, 0.1 mM PMSF, 10 mM imidazole and 0.5 mg lysozyme per 100 ml of lysate. The lysate was sonicated and spun at 94,000 G for 45 minutes. The supernatant was loaded on a 2 ml-packed nickel affinity column (Qiagen), washed with 5 ml of lysis buffer without PMSF, and then eluted with lysis buffer with 250 mM imidazole. Thrombin was added to the eluted fraction and it was dialyzed against the sizing column buffer, 150 mM NaCl, 5 mM Tris-HCl pH 8.5, 2 mM DTT. Kir2.1 was then purified by S200 Sepharose chromatography and concentrated to 10 mg/ml with 10mM DTT. Kir2.1 proteins were loaded on a G4000PWXL HPLC column (TOSOH) equilibrated in 150 mM NaCl, 5 mM Tris-HCl 8.5, 2 mM DTT. Molecular weights (MW) were

calculated using an extinction coefficient based on the primary sequence of the protein.

Crystallography. Kir2.1$_S$ mutant R218Q/T309K was crystallized in the space group C2 at 4 ^oC by vapor diffusion with hanging drops mixed 1:1 with 35% 2-methyl-2,4,pentanediol (MPD), 0.1 M Na/KPO_4 pH 6.2, 50 mM NaCl. Crystals were placed in a precipitation solution for 15 seconds prior to flash freezing in liquid nitrogen. Data sets were collected for Kir2.1$_S$ R218Q/T309K and Kir2.1$_L$ R218Q/T309K at Advanced Light Source (ALS), Berekeley, and Stanford Linear Accelerator Center (SSRL), respectively. Molecular replacement solutions were derived using the model of wt Kir2.1$_L$ by Phaser. The final model was refined with the 2.0 Å data from R218Q/T309K$_S$ by the software CCP4 suite.

Electrophysiology. Full-length wt Kir2.1 and the following point mutants, R218Q, T309K, T309R, R218Q/T309R and R218Q/T309K, were constructed in pBSK using PCR (Kubo et al., 1993). All constructs were confirmed by DNA sequencing. *In vitro* methyl-capped cRNAs were synthesized from linearized cDNA and transcribed with T3 RNA polymerase (Stratagene). The quality of cRNA was estimated using an ethidium-stained formaldehyde gel. Oocytes were isolated from *Xenopus laevis* frogs as described previously (Finley et al., 2004). The experimental procedure was approved by the IACUC at The Salk Institute. Oocytes were injected

with a 46 nl solution containing cRNA for the Kir2.1 channels (0.5 to 5 ng) and incubated in ND96 (96 mM NaCl, 2 mM KCl, 1 mM $CaCl_2$, 1 mM $MgCl_2$, 5 mM HEPES, pH 7.6 with NaOH) for 1-4 days at 16° C.

Macroscopic currents were recorded using the two-electrode voltage-clamp method as described previously (Finley et al., 2004). Briefly, currents were recorded from oocytes with Geneclamp 500 amplifier (Axon Instruments), filtered at 0.05-2 kHz, digitized (0.1-2 kHz) with a Digidata 1200 A/D interface (Axon Instruments) and stored on a laboratory computer. Electrodes were filled with 3 M KCl and had resistances of 0.6-1 MΩ. Oocytes were perfused continuously with an extracellular "95K" solution (90 mM KCl, 2 mM $MgCl_2$ and 10 mM HEPES; pH 7.5 with ~5 mM KOH), "2K" solution (2 mM KCl, 88 mM NaCl, 2 mM $MgCl_2$ and 10 mM HEPES; pH 7.5 with ~5 mM NaOH) or "95Na" solution (90 mM NaCl, 2 mM $MgCl_2$ and 10 mM HEPES; pH 7.5 with ~5 mM NaOH). The 95Na was used to determine the leakage current and subtracted directly from the currents measured in 95K and 2K. A small chamber (0.125 x 0.600 in) with fast perfusion was used to exchange the extracellular solution and was connected to ground via a 3 M KCl agarose bridge. Macroscopic currents were elicited with 150 ms voltage-steps from -100 mV to +50 mV. Mutants were studied in 2-3 different batches of oocytes. The current amplitude was measured at the end of a 150 ms step pulse. All values are given as mean ± SEM.

3.6 ACKNOWLEDGMENTS

We thank ALS and SSRL for X-ray data collection. This work was supported by grants from the National Institutes of Health (P.A.S & S.C.), National Institutes of Health Molecular Biophysics Training Grant (S.P.; GM08326) and the McKnight Endowment for Neuroscience (P.A.S).

Chapter 3 is in part a reprint of the material that has been submitted for publication as Pegan, S., Arrabit, C., Slesinger, P. A., and Choe, S. (2006). *Andersen's Syndrome Mutation Effects on the Structure and Assembly of the Cytoplasmic Domains of Kir2.1.* Submitted. The dissertation author was the primary researcher and author of this publication.

3.7 REFERENCES

Bendahhou, S., Donaldson, M. R., Plaster, N. M., Tristani-Firouzi, M., Fu, Y. H., and Ptacek, L. J. (2003). Defective potassium channel Kir2.1 trafficking underlies Andersen-Tawil syndrome. J Biol Chem *278*, 51779-51785.

Chen, L., Kawano, T., Bajic, S., Kaziro, Y., Itoh, H., Art, J. J., Nakajima, Y., and Nakajima, S. (2002). A glutamate residue at the C terminus regulates activity of inward rectifier K+ channels: implication for Andersen's syndrome. Proc Natl Acad Sci U S A *99*, 8430-8435.

Corey, S., and Clapham, D. E. (1998). Identification of native atrial G-protein-regulated inwardly rectifying K+ (GIRK4) channel homomultimers. J Biol Chem *273*, 27499-27504.

Donaldson, M. R., Jensen, J. L., Tristani-Firouzi, M., Tawil, R., Bendahhou, S., Suarez, W. A., Cobo, A. M., Poza, J. J., Behr, E., Wagstaff, J.*, et al.* (2003). PIP2 binding residues of Kir2.1 are common targets of mutations causing Andersen syndrome. Neurology *60*, 1811-1816.

Doyle, D. A., Morais Cabral, J., Pfuetzner, R. A., Kuo, A., Gulbis, J. M., Cohen, S. L., Chait, B. T., and MacKinnon, R. (1998). The structure of the potassium channel: molecular basis of K+ conduction and selectivity. Science *280*, 69-77.

Enkvetchakul, D., Jeliazkova, I., and Nichols, C. G. (2005). Direct modulation of Kir channel gating by membrane phosphatidylinositol 4,5-bisphosphate. J Biol Chem *280*, 35785-35788.

Fink, M., Duprat, F., Heurteaux, C., Lesage, F., Romey, G., Barhanin, J., and Lazdunski, M. (1996). Dominant negative chimeras provide evidence for homo and heteromultimeric assembly of inward rectifier K+ channel proteins via their N-terminal end. FEBS Lett *378*, 64-68.

Finley, M., Arrabit, C., Fowler, C., Suen, K. F., and Slesinger, P. A. (2004). betaL-betaM loop in the C-terminal domain of G protein-activated inwardly rectifying K(+) channels is important for G(betagamma) subunit activation. J Physiol *555*, 643-657.

Fujiwara, Y., and Kubo, Y. (2006). Functional Roles of Charged Amino Acid Residues on the Wall of the Cytoplasmic Pore of Kir2.1. J Gen Physiol.

Hille, B. (2001). Ion Channels of Excitable Membranes, Third edn (Sunderland, MA: Sinauer Associates, Inc.).

Hosaka, Y., Hanawa, H., Washizuka, T., Chinushi, M., Yamashita, F., Yoshida, T., Komura, S., Watanabe, H., and Aizawa, Y. (2003). Function, subcellular localization and assembly of a novel mutation of KCNJ2 in Andersen's syndrome. J Mol Cell Cardiol *35*, 409-415.

Huang, C. L., Feng, S., and Hilgemann, D. W. (1998). Direct activation of inward rectifier potassium channels by PIP2 and its stabilization by Gbetagamma. Nature *391*, 803-806.

Inanobe, A., Yoshimoto, Y., Horio, Y., Morishige, K. I., Hibino, H., Matsumoto, S., Tokunaga, Y., Maeda, T., Hata, Y., Takai, Y., and Kurachi, Y. (1999). Characterization of G-protein-gated K+ channels composed of Kir3.2 subunits in dopaminergic neurons of the substantia nigra. J Neurosci *19*, 1006-1017.

Kubo, Y., Baldwin, T. J., Jan, Y. N., and Jan, L. Y. (1993). Primary structure and functional expression of a mouse inward rectifier potassium channel. Nature *362*, 127-133.

Kubo, Y., and Murata, Y. (2001). Control of rectification and permeation by two distinct sites after the second transmembrane region in Kir2.1 K+ channel. J Physiol *531*, 645-660.

Lopatin, A. N., Makhina, E. N., and Nichols, C. G. (1994). Potassium channel block by cytoplasmic polyamines as the mechanism of intrinsic rectification. Nature *372*, 366-369.

Lopes, C. M., Zhang, H., Rohacs, T., Jin, T., Yang, J., and Logothetis, D. E. (2002). Alterations in conserved Kir channel-PIP2 interactions underlie channelopathies. Neuron *34*, 933-944.

Nishida, M., and MacKinnon, R. (2002). Structural basis of inward rectification: cytoplasmic pore of the G protein-gated inward rectifier GIRK1 at 1.8 A resolution. Cell *111*, 957-965.

Pegan, S., Arrabit, C., Zhou, W., Kwiatkowski, W., Collins, A., Slesinger, P. A., and Choe, S. (2005). Cytoplasmic domain structures of Kir2.1 and Kir3.1 show sites for modulating gating and rectification. Nat Neurosci *8*, 279-287.

Plaster, N. M., Tawil, R., Tristani-Firouzi, M., Canun, S., Bendahhou, S., Tsunoda, A., Donaldson, M. R., Iannaccone, S. T., Brunt, E., Barohn, R.*, et al.* (2001). Mutations in Kir2.1 cause the developmental and episodic electrical phenotypes of Andersen's syndrome. Cell *105*, 511-519.

Preisig-Muller, R., Schlichthorl, G., Goerge, T., Heinen, S., Bruggemann, A., Rajan, S., Derst, C., Veh, R. W., and Daut, J. (2002). Heteromerization of Kir2.x potassium channels contributes to the phenotype of Andersen's syndrome. Proc Natl Acad Sci U S A *99*, 7774-7779.

Silverman, S. K., Lester, H. A., and Dougherty, D. A. (1996). Subunit stoichiometry of a heteromultimeric G protein-coupled inward-rectifier K+ channel. J Biol Chem *271*, 30524-30528.

Tristani-Firouzi, M., Jensen, J. L., Donaldson, M. R., Sansone, V., Meola, G., Hahn, A., Bendahhou, S., Kwiecinski, H., Fidzianska, A., Plaster, N.*, et al.* (2002). Functional and clinical characterization of KCNJ2 mutations associated with LQT7 (Andersen syndrome). J Clin Invest *110*, 381-388.

Vanoye, C. G., MacGregor, G. G., Dong, K., Tang, L., Buschmann, A. S., Hall, A. E., Lu, M., Giebisch, G., and Hebert, S. C. (2002). The carboxyl termini of K(ATP) channels bind nucleotides. J Biol Chem *277*, 23260-23270.

Zhou, W., Arrabit, C., Choe, S., and Slesinger, P. A. (2001). Mechanism underlying bupivacaine inhibition of G protein-gated inwardly rectifying K+ channels. Proc Natl Acad Sci U S A *98*, 6482-6487.

CHAPTER FOUR

Structure Dynamics and Binding of Kir2.1 C-terminal Tail with PSD95 PDZ 1 & 2

4.1 ABSTRACT

Potassium inwardly rectifying (Kir) channel function and localized surface expression are essential to maintaining post synaptic areas of excitable cells at a resting potential close to E_K. The scaffold protein, PSD95, localizes these channels via the PDZ domain mediated protein to protein binding of the Kir2.1 C-terminus. By utilizing a multi-probe solution NMR approach we show the structural dynamics of the previously unresolved Kir2.1 tail (residues 372-428 of Kir2.1). Furthermore, we directly observe the extent the tail interacts with the PDZ1 and PDZ2 tandem region of PSD95.

4.2 INTRODUCTION

The potassium inwardly rectifying (Kir) channel is essential for excitable cells to retain their resting potentials. These channels allow large amount of potassium ions to flow into the cell, while only allowing small amounts to flow out. As a result they drive the cell's resting potential to the E_K of potassium (Nichols and Lopatin, 1997). Although there are several types of Kir channels ranging from G-protein gated Kir3 and pH gated Kir1 to the ATP inhibited Kir6, the primary channel family responsible for this activity is the Kir2 family of channels, also known as the classic inward rectifiers (Hille, 2001). These channels only bind phosphylinositol 4, 5 bisphosphate (PIP_2) in order to open unlike other Kir subfamilies (Nichols and Lopatin, 1997). Once these channels are open, potassium passively flows along the electrochemical gradient of the cell. If that gradient pushes potassium out of the cell, the channel quickly becomes blocked by cytosolic polyamines and Mg^+ ions (John et al., 2004; Lopatin et al., 1994; Matsuda et al., 1987). The importance of these channels is underlined by a non-conducting Kir2.1 channel mutation disease, known as Andersen's Syndrome (AS). AS-affected Kir2.1 channels are known to be dominate negative as homotetramers of Kir2.1 and heterotetramers of Kir2.1 / Kir2.3 containing AS-affected channels fail to function (Lopes et al., 2002; Pegan et al., 2005; Plaster et al., 2001; Preisig-Muller et al., 2002). As a result of AS, a host of ailments that includes but is not limited to developmental physical disfigurements, periodic paralysis, and cardiac arrhythmias can occur.

Although gating the channel is a primary mechanism of controlling the amount of current that flows in or out of the cell, the availability of these channels in the trans-membrane at given time or location can also affect the ability of these channels to properly govern the resting potential in certain cellular areas (Cohen et al., 1996). One of these areas where the resting potential needs to be carefully managed, and as a result Kir2 channels need to be present in high concentration, is the post synaptic density (PSD) area. This area contains a complex localization of receptors and ion channel proteins that are responsible for synapse transmission along the dendritic spine. High concentrations of receptors and ion channels in the PSD is caused primarily by a class of scaffold proteins (Kim and Sheng, 2004). Although there are four different types of these PSD or synapse-associated proteins (SAP), SAP97, SAP102, PSD93 (chapsyn-110), and PSD95 (SAP90), Kir2.1 and Kir2.3 preferentially bind to PSD95 where as Kir2.2 binds preferentially to SAP97 (Leonoudakis et al., 2004; Nehring et al., 2000).

Each of these three highly homologous Kir2 channels have a sizable cytoplasmic C-terminal domain, in which a small percentage of residues at the C-terminus end interact with the scaffold proteins. Most of the structure of this domain is known from the Kir2.1 N-C terminal fusion of $Kir2.1_L$ (44-64 and 189-428) and $Kir2.1_S$ R218Q/T309K (44-64 and 189-371) protein crystal structures (Pegan et al.,

2006; Pegan et al., 2005). The resolved portion of the cytoplamic domain shows a tetrameric β sheet fold forming a long (~27 Å) pore in the center of the channel closed at the membrane end by the G-loop. In addition there are four α helices that point a further ~20 Å into the cytoplasm (Fig. 4.1a,b). Although the fusion included the entire C-terminal residues, no density or structure was observed beyond position 370 (Pegan et al., 2006). This unresolved part, contains 58 amino acids and is where the ER forwarding tag and a PDZ binding motif reside (Fig. 4.1c). As with all receptors and channels that interact with PSD proteins they do so through a PDZ binding motif recognizable through the last four amino acids of the proteins conforming to T/S-X(D/E/A)-V/I (Doyle et al., 1996; Kim and Sheng, 2004). Most PDZ binding motif containing proteins have been shown to bind PDZ domains in a singular or tandem fashion (Long et al., 2003).

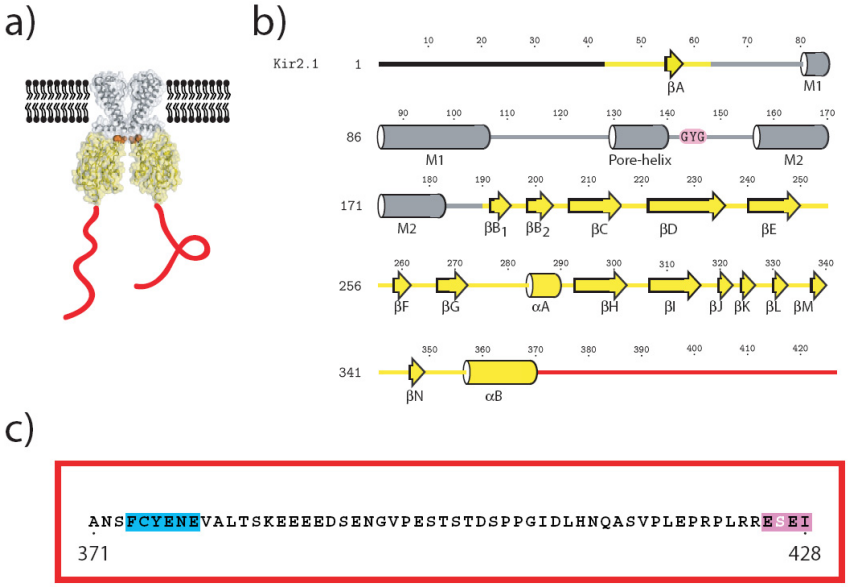

Figure 4.1 **Known structure regions of Kir like channels.** **(a)** Model consisting of known Kir like structures with two of the chains removed for clarity of the pore. Gray represents portions comprised of KirBac1.1; Gold structure is derived from the $Kir2.1_L$ structure; Red represents the unknown structural region of the C-terminal tail of Kir2.1. **(b)** Secondary structure representation of (a). The GYG potassium selectivity filter is represented in pink. The red region corresponds to the structurally undetermined region in Kir2.1's C-terminal domain. **(c)** The amino acid sequence of the red regions of (b) and (c). The known PDZ binding motif is colored in magenta and the ER forwarding tag is in teal. Serine 426 that is involved in phosphorylation is in white .

The 90 residues that comprise a PDZ domain, to which channels bind, are highly conserved throughout the four different types of PSD proteins; however, as previously mentioned some of the PSD proteins preferentially bind to different receptors and ion channels then others, as is the case Kir channels (Kim and Sheng, 2004; Nehring et al., 2000). Kir2.2 has been shown in GST pull down assays to bind preferentially to SAP97 but can also bind to PSD95. Kir2.1 on the other hand can only bind to PSD95 (Nehring et al., 2000). The Kir2.1's specificity for PSD95

compared to its Kir2.2 family member is perplexing because both these channels share 100% identity in the last four residues (ESEI) which also doubles as part of a Protein Kinase A (PKA) phosphorylation regulation site (Cohen et al., 1996). Although observed, the molecular mechanism for the preference of one channel over the other is has not been elucidated.

In order to fully resolve Kir2.1's affinity for PSD95 we have chosen to look at PSD95 and its interaction with the C-terminal tail of Kir2.1. PSD95 is a 95 KD protein that forms head to head N-terminal interactions and utilizes palmitylation on Cys 3 and Cys 5 to anchor the resulting "C" shaped scaffold to the membrane (Kim and Sheng, 2004). PSD95 itself is comprised of three PDZ domains, an SH3 domain, and guanlylate kinase-like domain (Fig 4.2a). The first two PDZ domains both have been shown to effectively bind ion channels and are highly conserved (Fig. 4.2b). Each of the PDZ domains is comprised of a six β sheet type fold with two α helices (Fig4.2c; (Tochio et al., 2000). Based on previous complex studies on similar PDZ domains and other PDZ binding motifs, the ion channel's four residue PDZ motif should form an anti β sheet interaction with βF resulting in the C-terminal hydrophobic residue being buried in a hydrophobic pocket with it's terminal carboxyl group forming an interaction with a backbone amide group (Doyle et al., 1996). Additionally, other groups believe that recognition of the PDZ domain to the Kir2.1

channel involves the last six residues, RRESEI, and possibly further residues upstream of the four residue motif (Cohen et al., 1996; Nehring et al., 2000).

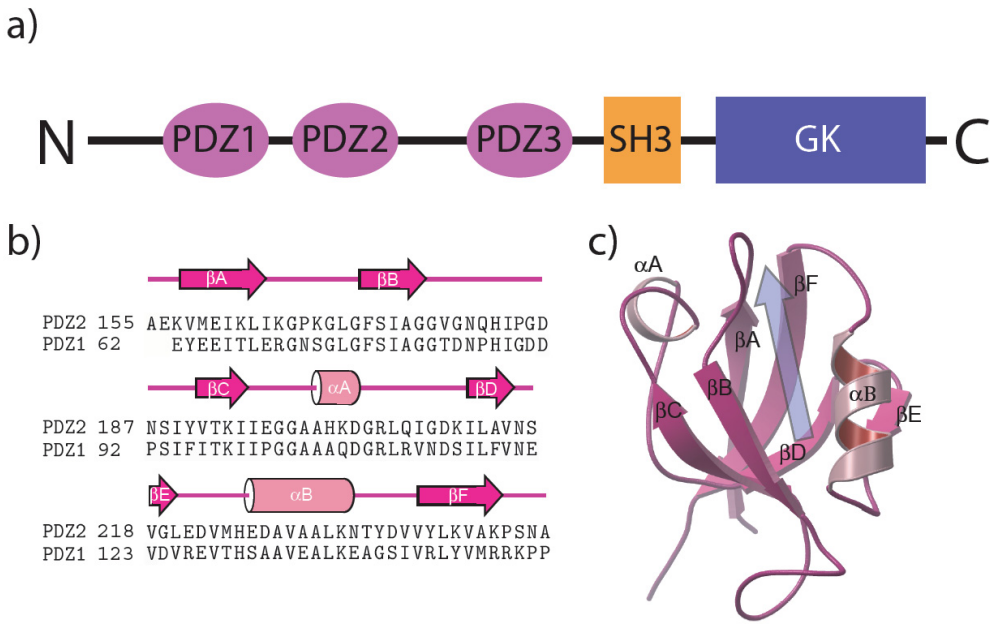

Figure 4.2 PDZ 95 sub-domains. **(a)** Cartoon depiction of PSD95. **(b)** sequence alignment with secondary structure of PDZ1 and PDZ2 of PSD95. **(c)** Structure of PSD95 PDZ2 with translucent blue arrow representing the expected primary binding site for peptide ligands.

In our paper, we utilize NMR techniques in a muilti-probe structural study approach to address the structural nature of the unresolved C-terminal domain structure of Kir2.1. Furthermore, we show through direct observation that although the four C-terminal residue motif is necessary for binding PDZ domains, that the binding footprint is substantially larger, increasing the possibility that residues further upstream of the last four or six are involved in the binding of PDZ1 and PDZ2 of PSD95 to Kir2.1.

4.3 RESULTS

Assignment of the Kir2.1$_L$ cytoplasmic C-terminal tail 371-428. To achieve the most natural system possible, we used the Kir2.1$_L$ fusion construct that was used for the crystallization of the domain (Pegan et al., 2005). Normally performing solution NMR on the 130 KD homo-tetrameric moiety would be difficult, as the larger the protein under study, the slower it tumbles in solution resulting in weaker signal strength.

From the tail's (371-428) absence in crystal structure we proposed that the tail may be flexible. If true, the tail's extra degrees of freedom would compensate for being a component of a larger slower tumbling moiety. The resulting signal from the tail's residue's N-H moiety would be considerably stronger then the rest of the domain and measurable through solution NMR. To test our hypothesis we made ^{15}N labeled Kir2.1$_L$, intentionally not using deuterium label in an effort to suppress any signal from the known structural components of the cytoplasmic domains. We then performed a 3 hr [^{15}N, ^{1}H] TROSY at 298 K experiment to visualize the N-H moieties of the protein (Pervushin et al., 1997). The [^{15}N, ^{1}H] TROSY showed two glycine residues being present (Fig. 4.3). This matched exactly with the number of glycines present in the structurally unresolved tail of Kir2.1$_L$. Furthermore, we preformed the same technique on the Kir2.1$_L$ truncated at 372 where no signal from any residues was observed.

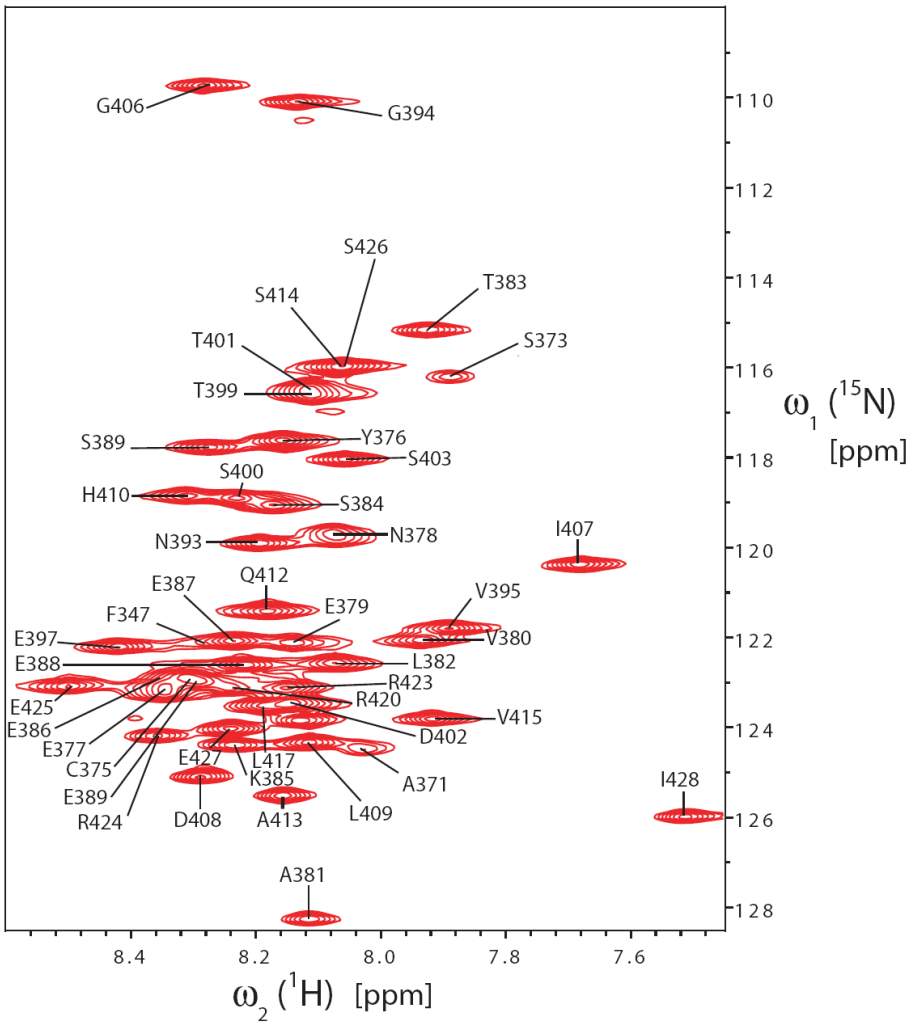

Figure 4.3 Assignment of Kir2.1$_L$ cytoplasmic C-terminal Region 371-428. [^{15}N, ^{1}H] TROSY spectrum of residues 371-428 in Kir2.1$_L$.

With the [^{15}N, ^{1}H] TROSY results confirming our hypothesis, we moved on to assigning the peaks to their corresponding residues. With six prolines present in the Kir2.1$_L$ tail region only 51 out of 57 residues have an N-H moiety possible of generating signal. Through the use of [^{15}N, ^{13}C] HNCA and [^{15}N, ^{1}H] NOESY experiments to confirm connectivity coupled with [^{15}N, ^{1}H] TOCSY experiments to

confirm side chain identity, we were able to locate and assign 44 distinct peaks of the 51 possible residues in the tail, 86% coverage of the possible N-H moieties. (Fig. 4.3).

C-terminal tail of Kir2.1 is highly flexible with no secondary structure.

Analysis of the N-H moiety shifts observed from the [^{15}N, ^{13}C] HNCA across the tail region on the average showed low divergence from the values of a random coil indicating a lack of secondary structure for this region (Fig. 4.4a). As expected the C-terminal residue had a positive shift due to the influence of the additional carboxyl group of the C-terminus. Furthermore, there were some small negative shifts near the C-terminus; however, most of these due to the proximity of prolines. Two other residues, Phe 375 and Tyr 376 showed small shifts, but again no substantial and sustained (α helical), or negative (β sheet) deviation, could be observed from neighboring residues.

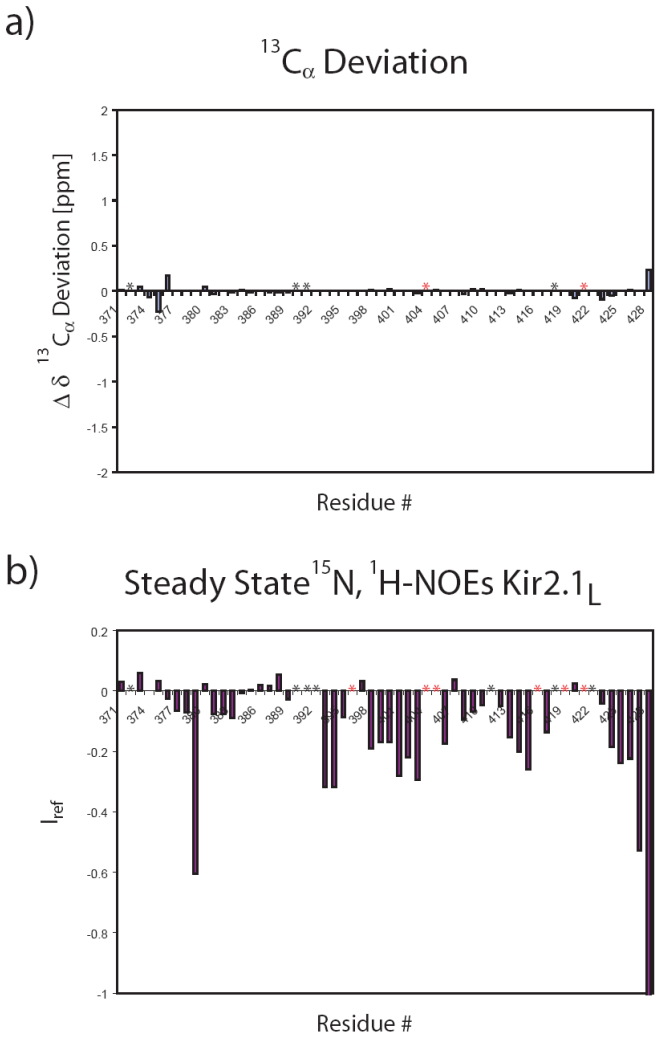

Figure 4.4 Flexibility of the C-terminal residues 371-428. a) Chart of [^{15}N, ^{13}C] HNCA deviations of $^{13}C_\alpha$ shift from random coil values. Red asterisks denote Proline positions that values could not be determined because the preceding residue was also a proline of no sequanial shift was observed. Black asterisks represent N/A positions due unassigned residues. b) Chart of Steady State ^{15}N, ^{1}H-NOEs experiment results. I_{ref} is derived from dividing the ^{15}N, ^{1}H-NOEs experiment by the Reference experiment. Red asterisks denote Proline positions. Black asterisks represent N/A positions due unassigned residues.

In order confirm the flexibility and lack of secondary structure; we conducted a Steady State ^{15}N, ^{1}H-NOEs experiment to test the relaxation rate of energized N-H moieties in the tail regions. Positive values would have indicated structured regions

that were unable to shed the energy as quickly as the flexible regions. As Figure 4.4b shows, most of the residues either were negligibly positive or substantially negative confirming the [^{15}N, ^{13}C] HNCA results that the tail of the Kir2.1 channel is flexible and does not possess any secondary structure.

PSD95 PDZ 1 & 2 Binding Region on Kir2.1$_L$ tail. With the structural dynamics of the tail now understood, we shifted our attention to the binding of PDZ domains to the Kir2.1$_L$ construct. To probe the most natural model system possible, we employed a PDZ1 and PDZ2 tandem PSD95 construct (62-249) to probe the tail region of Kir2.1$_L$. We expected tail residues that interact with the tandem PDZ domains would have their [^{15}N, ^{1}H] TROSY signal quenched due to the reduction of their flexibility.

Upon addition of the PDZ tandem protein in a 1:1 molar ration with the ^{15}N labeled channel (2 PDZs per Kir2.1$_L$ monomer), we observed that several residues beyond the four residue PDZ motif were quenched (Fig 4.5a). Taking into account the general signal quenching of a 90 KD protein being added to a 130 KD, we observed that the region from S414 to the C-terminal residue I428 showed significant interactions with the PDZ domain. Nine out of ten possible signal generating residues showed significant quenching, exhibiting signal change values of greater then 64%. The exception was V415 that appears to only suffer general weakening. Interestingly, the C-terminus was not the only area we observed noticeable shifts. Residues Ala 371

and Ser 373 showed shifts of 60% and 73% respectively. Three others also were slightly elevated, Glu 379, Val 380, and Leu 382, but all below 60%. The elevation of residues that are close to the structured cytoplasmic domain is not too surprising. The resulting profile suggests, like a jump rope, that when bound at one end these tail residues enjoys incredible freedom. The subsequent binding of the far end of the tail can result in the middle residues maintaining high degree of flexibility but reducing the degrees of freedom the residues close to the structured region.

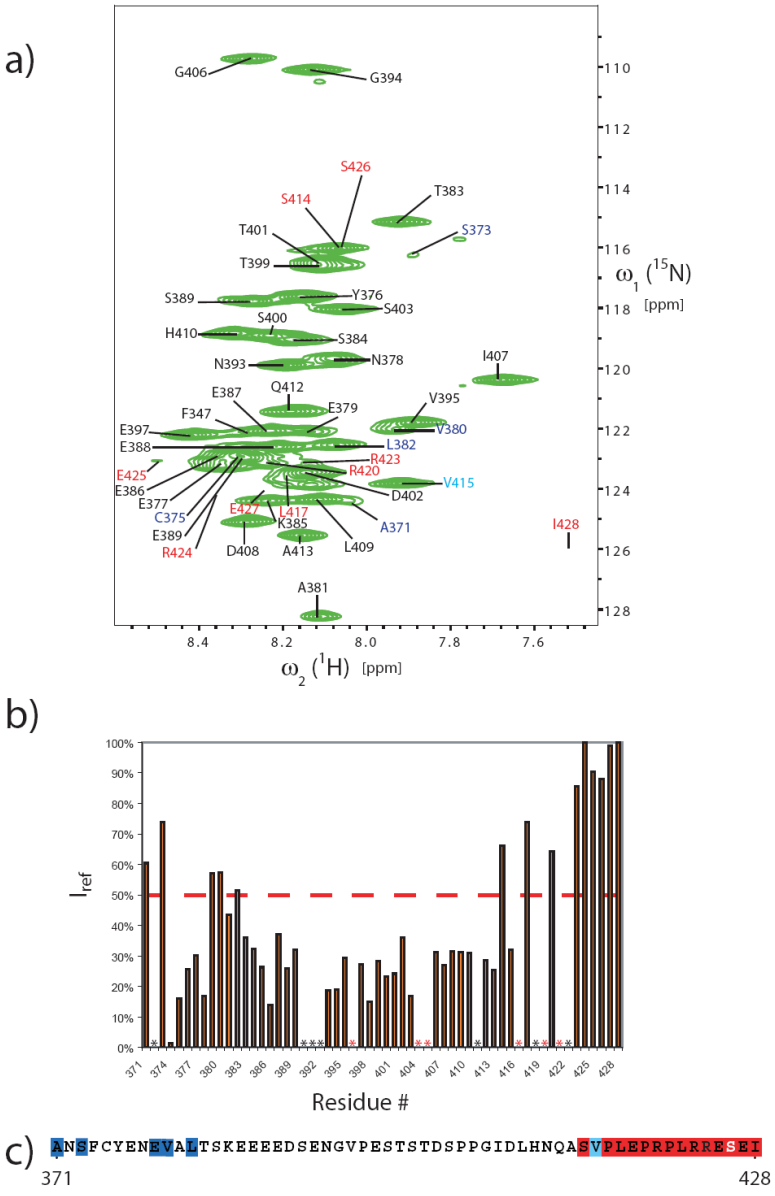

Figure 4.5 Binding Footprint of PSD95 PDZ 1 & 2. (a) [^{15}N, ^{1}H] TROSY of Kir2.1$_L$ when combined with a 1:1 molar ration of Kir2.1$_L$ to PSD95 PDZ 1 & 2. Residues involved in binding are labeled in red. **(b)** Percent of Change per residue between the bound and unbound [^{15}N, ^{1}H] TROSY spectrums. I_{ref} is calculated by [(unbound signal)-(bound signal)]/(unbound signal). Red line indicates magnitude of change necessary to be considered significant. **(c)** Amino acid sequence 371-428 Kir2.1$_L$ with binding region highlighted in red, Serine 426 that is involved in phosphorylation is in white. Blue residues represent upstream residues that are affected by binding. Valine 415 is highlighted in light blue.

4.4 DISCUSSION

A flexible region of proteins performing critical functions is not a new concept. The potassium voltage (Kv) gated channel for instance has a naturally occurring flexible region on its N-terminal cytoplasmic tip that performs a biologically important function of quickly closing the channel (Baker et al., 2006). However, the lack of secondary structure in the Kir2.1 C-terminal tail is still intriguing given the number of residues present. Conservatively assuming the distance on the backbone from one C_α to the next mirrors amino acids arrange in a β sheet, 3.5 Å, the tail could elongate up to 199 Å from the C-terminus to the αB of Kir2.1. The tail coupled with the structured region of the cytoplasmic domains of Kir2.1, 48 Å, is roughly double the distance observed thru cryo EM studies, 120 Å, between the membrane and PSD95 scaffold (Fig. 4.6a). Part of the reason for the extra length could be to allow the cells to endure mechanical stresses without severing the anchor that both stabilizes and localizes the channel. Another explanation, in conjunction with allowing the flexibility, is that a significant amount of the tail could be involved with binding the PDZ domains as observed in this study. As the binding experiments of $Kir2.1_L$ to tandem PDZ1 and PDZ2 shows, up to 15 residues (52.5 Å) could be involved with binding. In order to accommodate all the 15 residues the amino acids binding with the PDZ domains, they could wrap around the PDZ domains, like DNA does with histone proteins in the nucleus (Luger et al., 1997). Also, the resulting model would increase

the recognition site of C-terminal tails beyond the currently proposed six and four amino acid models.

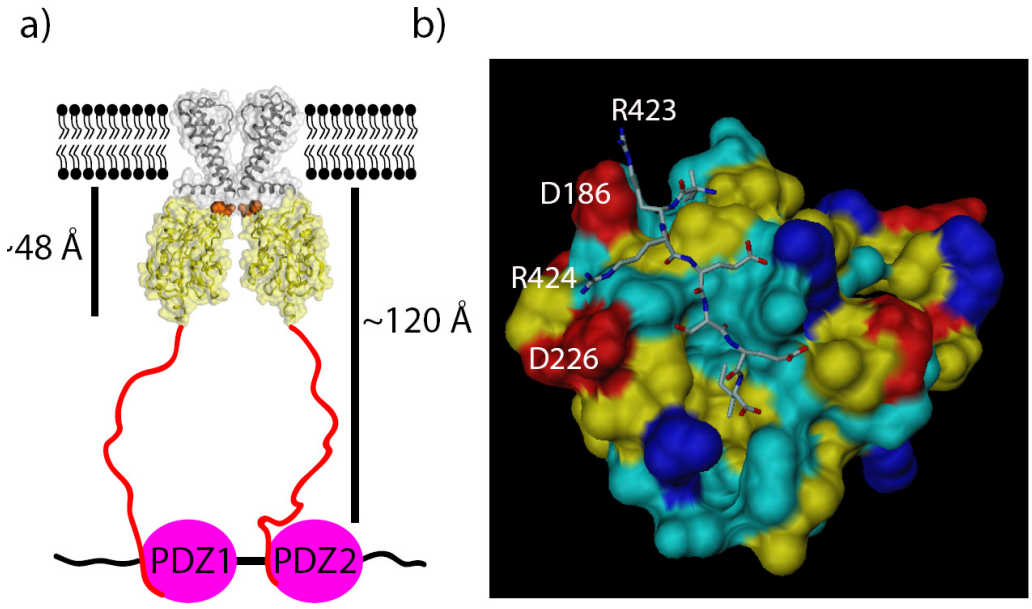

Figure 4.6 Proposed model for 1 & 2 PDZ PSD95 binding to Kir2.1 tail. (a) cartoon model of Kir2.1's interaction with PDZ 1 and PDZ 2 domains of PSD95. **(b)** Model of PDZ2 PSD95 binding and Kir2.1's last seven amino acids (VRRESEI) based on PDZ3 PSD95 bound structure.

Based on previous structure of PDZ3 bound to a PDZ binding motif peptide, the homology model of PDZ2 PSD95 with a seven residue Kir2.1's C-terminal peptide allows us a glimpse of the proposed model. Although the template of the model only includes the four full residues of the PDZ motif, we can utilize the known size of the PDZ binding footprint to extend the peptide by three residues, Arg 223, Arg 224, and Leu 222. As seen in figure 4.6b, the Arginines potentially form favorable bonds with D226 and D186 respectively. These residual interactions could provide the discrimination factor between Kir and other PDZ targeted proteins, but does not

shed light on the Kir2.1's specificity for PDZ95. The last residue that could be placed was Leu 222. Although this residue was not assigned, its interaction with a hydrophobic patch on PDZ2 makes it a probable interacting residue. Interestingly, position 222 Kir2.1's cousin, Kir2.2, has a polar tyrosine in that position instead of the hydrophobic leucine. We propose that this leucine is the beginning of the affinity determining region on the Kir2.1 tail. Further studies that would confirm this finding and rule out other models, such as large binding footprint of PDZ 1 and PDZ 2 PSD 95 being caused by the tandem domain binding to one tail, would be to replicate the binding experiments with single PDZ domains. Additionally, [^{15}N, ^{1}H] TROSY conducted on ^{15}N labeled PDZ2 complexed to a Kir2.1 15 C-terminal tail peptide allow the visualization of N-H moieties shifts on PDZ2 residues away from the β sheet binding pocket.

4.5 MATERIALS AND METHODS

Molecular biology. PDZ1 and PDZ2 PSD95 tandem domain construct was cloned from human PSD95 into *pHis8* vector. For Kir2.1 fusion protein constructs, cytoplasmic N-terminal and C-terminal domains of mouse Kir2.1 was linked directly in frame by PCR to clone into the *pHis8* vector (Kubo et al., 1993; Slesinger et al., 1996). BL21 (*DE3*) cells were used to express the proteins.

Expression of proteins. ^{15}N and ^{13}C labeled protein was expressed in cells that were grown at 37 °C to 0.6 OD in LB media then spun down, washed with PBS, spun again and re-suspended in minimal media containing appropriate labels (Marley et al., 2001). Half of an hour after of growing at 37 °C post media exchange, the cells were induced by 0.5 mM IPTG and grown for three hours at 30 °C. Non-labeled proteins were expressed in cells grown in TB at 37 °C to 0.6 OD and induced with 0.5 M IPTG for three hours. For protein purification, once pelleted, all cells were lysed in 0.5 M NaCl, 5 mM Tris-HCl, pH 8.5, 10% glycerol, 7 mM β-mercaptoethanol (lysis buffer) and 1 mg lysozyme per 100 ml lysate. The supernatant from the lysate was loaded on a nickel-affinity column (Qiagen) and eluted with 200 mM imidazole. Thrombin-cleaved protein samples were separated by S200 and S75 Sepharose chromatography, and concentrated to 10 mg ml^{-1} $Kir2.1_L$.

NMR. The NMR experiments were carried out on a Bruker DRX700 spectrometer at 25°C by using protein in solutions of 85% H2O / 15% D_2O containing 150mM NaCl, 2 mM DTT, and 20 mM K PO_4 / $NaPO_4$ at pH 6.5. [^{15}N, ^{1}H] TROSY spectrum (Pervushin et al., 1997) of free ^{15}N-labeled $Kir2.1_L$ was measured at a protein concentration of 0.25 mM, with *t*1,max = 88 ms, *t*2,max = 98 ms, a data size of 512 X 1,024 complex points, and an overall recording time of 3 h. TROSY based steady-state ^{15}N {1H}-NOEs of the backbone amide groups were measured in a 0.25 mM solution of $Kir2.1_L$. Binding experiment [^{15}N, ^{1}H] TROSY spectrum of a solution of 0.25 mM ^{15}N labeled $Kir2.1_L$ and .25 mM unlabeled PDZ1 and PDZ2 PSD95 (62-249) for 24 hrs. The NMR data were processed with the program PROSA (Güntert et al., 1995) and analyzed with the program CARA (Keller, 2004).

4.6 ACKNOWLEDGMENTS

This work was supported by grants from the National Institutes of Health (P.A.S. & S.C.), National Institutes of Health Molecular Biophysics Training Grant (S.P.; GM08326) and the Mcknight Endowment for Neuroscince (P.A.S).

Chapter 4 would not have been completed without the assistance of Roland Riek and the use of his NMR facilities at the Salk Institute.

4.7 REFERENCES

Baker, K. A., Hilty, C., Peti, W., Prince, A., Pfaffinger, P. J., Wider, G., Wuthrich, K., and Choe, S. (2006). NMR-Derived Dynamic Aspects of N-Type Inactivation of a Kv Channel Suggest a Transient Interaction with the T1 Domain. Biochemistry *45*, 1663-1672.

Cohen, N. A., Brenman, J. E., Snyder, S. H., and Bredt, D. S. (1996). Binding of the inward rectifier K+ channel Kir 2.3 to PSD-95 is regulated by protein kinase A phosphorylation. Neuron *17*, 759-767.

Doyle, D. A., Lee, A., Lewis, J., Kim, E., Sheng, M., and MacKinnon, R. (1996). Crystal structures of a complexed and peptide-free membrane protein-binding domain: molecular basis of peptide recognition by PDZ. Cell *85*, 1067-1076.

Güntert, P., Dötsch, V., Wider, G., and Wüthrich, K. (1995). Processing of multi-dimensional NMR data with the new software PROSA J Biomol NMR *2*, 619-629.

Hille, B. (2001). Ion Channels of Excitable Membranes, Third edn (Sunderland, MA: Sinauer Associates, Inc.).

John, S. A., Xie, L. H., and Weiss, J. N. (2004). Mechanism of inward rectification in Kir channels. J Gen Physiol *123*, 623-625.

Keller, R. (2004). The Computer Aided Resonance Assignment Tutorial, 1 edn (Goldau: Cantina Verlag).

Kim, E., and Sheng, M. (2004). PDZ domain proteins of synapses. Nat Rev Neurosci *5*, 771-781.

Kubo, Y., Baldwin, T. J., Jan, Y. N., and Jan, L. Y. (1993). Primary structure and functional expression of a mouse inward rectifier potassium channel. Nature *362*, 127-133.

Leonoudakis, D., Conti, L. R., Anderson, S., Radeke, C. M., McGuire, L. M., Adams, M. E., Froehner, S. C., Yates, J. R., 3rd, and Vandenberg, C. A. (2004). Protein trafficking and anchoring complexes revealed by proteomic analysis of inward rectifier potassium channel (Kir2.x)-associated proteins. J Biol Chem *279*, 22331-22346.

Long, J. F., Tochio, H., Wang, P., Fan, J. S., Sala, C., Niethammer, M., Sheng, M., and Zhang, M. (2003). Supramodular structure and synergistic target binding of the N-terminal tandem PDZ domains of PSD-95. J Mol Biol *327*, 203-214.

Lopatin, A. N., Makhina, E. N., and Nichols, C. G. (1994). Potassium channel block by cytoplasmic polyamines as the mechanism of intrinsic rectification. Nature *372*, 366-369.

Lopes, C. M., Zhang, H., Rohacs, T., Jin, T., Yang, J., and Logothetis, D. E. (2002). Alterations in conserved Kir channel-PIP2 interactions underlie channelopathies. Neuron *34*, 933-944.

Luger, K., Mader, A. W., Richmond, R. K., Sargent, D. F., and Richmond, T. J. (1997). Crystal structure of the nucleosome core particle at 2.8 A resolution. Nature *389*, 251-260.

Marley, J., Lu, M., and Bracken, C. (2001). A method for efficient isotopic labeling of recombinant proteins. J Biomol NMR *20*, 71-75.

Matsuda, H., Saigusa, A., and Irisawa, H. (1987). Ohmic conductance through the inwardly rectifying K channel and blocking by internal Mg2+. Nature *325*, 156-159.

Nehring, R. B., Wischmeyer, E., Doring, F., Veh, R. W., Sheng, M., and Karschin, A. (2000). Neuronal inwardly rectifying K(+) channels differentially couple to PDZ proteins of the PSD-95/SAP90 family. J Neurosci *20*, 156-162.

Nichols, C. G., and Lopatin, A. N. (1997). Inward rectifier potassium channels. Annu Rev Physiol *59*, 171-191.

Pegan, S., Arrabit, C., Slesinger, P. A., and Choe, S. (2006). Andersen's Syndrome Mutation Effects on the Structure and Assembly of the Cytoplasmic Domains of Kir2.1. Submitted.

Pegan, S., Arrabit, C., Zhou, W., Kwiatkowski, W., Collins, A., Slesinger, P. A., and Choe, S. (2005). Cytoplasmic domain structures of Kir2.1 and Kir3.1 show sites for modulating gating and rectification. Nat Neurosci *8*, 279-287.

Pervushin, K., Riek, R., Wider, G., and Wuthrich, K. (1997). Attenuated T2 relaxation by mutual cancellation of dipole-dipole coupling and chemical shift anisotropy indicates an avenue to NMR structures of very large biological macromolecules in solution. Proc Natl Acad Sci U S A *94*, 12366-12371.

Plaster, N. M., Tawil, R., Tristani-Firouzi, M., Canun, S., Bendahhou, S., Tsunoda, A., Donaldson, M. R., Iannaccone, S. T., Brunt, E., Barohn, R.*, et al.* (2001). Mutations in Kir2.1 cause the developmental and episodic electrical phenotypes of Andersen's syndrome. Cell *105*, 511-519.

Preisig-Muller, R., Schlichthorl, G., Goerge, T., Heinen, S., Bruggemann, A., Rajan, S., Derst, C., Veh, R. W., and Daut, J. (2002). Heteromerization of Kir2.x potassium channels contributes to the phenotype of Andersen's syndrome. Proc Natl Acad Sci U S A *99*, 7774-7779.

Slesinger, P. A., Patil, N., Liao, Y. J., Jan, Y. N., Jan, L. Y., and Cox, D. R. (1996). Functional effects of the mouse weaver mutation on G protein-gated inwardly rectifying K+ channels. Neuron *16*, 321-331.

Tochio, H., Hung, F., Li, M., Bredt, D. S., and Zhang, M. (2000). Solution structure and backbone dynamics of the second PDZ domain of postsynaptic density-95. J Mol Biol *295*, 225-237.

CHAPTER FIVE

Discussion

5.1 DISCUSSION

In the previous four chapters I have covered my recent findings concerning rectification, gating mechanism, and PDZ domain interactions in the cytoplasmic domains of the potassium inwardly rectifying channel 2.1 (Kir2.1). Here I will discuss these findings and other more recent electrophysiology studies in the context of our current understanding of K^+ ion permeation, rectification and gating from a molecular prospective.

K+ ion permeation. Potassium channels in general have been long known to be able to allow K^+ ions to flow through the cellular membrane at high rates while being highly selective for K^+ ions (Hille, 2001). Utilizing the data gained in the KirBac1.1 structure and a recent electrophysiology studies coupled with information in Chapters 2 and 3, we have a glimpse of the flow of K+ ions through the channel from the extracellular side of the channel to the cytoplasmic side occurs (Kuo et al., 2003; Pegan et al., 2006; Pegan et al., 2005).

Through the KirBac1.1 structure, we know that the Kir channel selectivity filter is similar to other K channels such as KcsA and the recently solved rat Kv1.2 (Kuo et al., 2003; Long et al., 2005; Zhou and MacKinnon, 2003). A homology model of Kir2.1's trans-membrane domain, based on KirBac1.1, shows that a K+ entering the channel, driven by the electrochemical gradient, would occupy four sites

in the selectivity filter (Fig. 5.1). This stacking is proposed to contribute the long pore effect for all K^+ channels. Once the K^+ ion passes the selectivity filter and travels into the inner vestibule it rehydrates. The next residues that could coordinate the ion in the Kir2.1 channels would be from the partial negative charge of the side chain of Cys 169 and the negative side chain of Asp 172. The latter of which is located in box 1 (Fig. 5.1). In the absence of an open conformation trans-membrane Kir structure, the hydration state of the K^+ ions within gate 1 can only be speculated (Fig. 5.1). However, the accessibility of the inner vestibule to Mg^{2+} and other Cysteine modifying agents suggests that the opening is large enough for hydrated K+ ions to pass (Guo et al., 2002; Lu et al., 1999a; Lu et al., 1999b; Lu and MacKinnon, 1994). The partial negative charge on Met 180, which comprises gate 1, also potentially assists in coordinating the hydrated ion as it passes through gate 1.

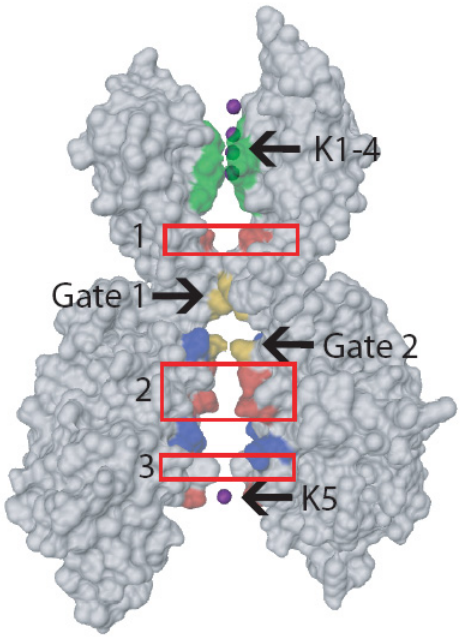

Figure 5.1. K^+ Proposed Permeation Pathway Model of Kir2.1. Structure Surface is rendered from mounting the A and B subunits from the Kir2.1 cytoplasmic domain structure with the B and D trans-membrane subunits based on a homology model derived from KirBac1.1 utilizing Modeller v8. Green: shaded areas represent the K^+ selectivity filter (144-148); Red: anion pore lining residues; Blue: cation pore lining residues; Yellow: residues forming the narrowest part of the pore. Purple: K^+.

The proposed model for K^+ permeation through the trans-membrane domain has changed little since the KcsA structure was first resolved. In contrast, the model for K^+ permeation through the cytoplasmic domain has changed. Prior to the structure of $Kir2.1_L$ (residues 44-64 fused to 189-428) in Chapter 2 and elucidation of the caged K^+ ion at the end of the cytoplasmic pore in Chapter 3, the lining of the cytoplamic domain was proposed to be a negatively charged region that binds ions and polyamines in a disordered manner as they awaited movement through the trans-membrane region (Fujiwara and Kubo, 2006; Kubo and Murata, 2001; Lu et al., 1999a).

The Kir2.1$_L$ structure in chapter 2 contrasts this model suggesting that the ion is presented with a cytoplasmic pore that contains both positively and negatively charged residues, which will be addressed in the rectification section below (Pegan et al., 2005). The presence of a well ordered water caged K^+ ion (position K5) and further structured waters in the structure of R218Q/T309K$_S$ suggests that K^+ ion will travel in a single file line through the cytoplasmic domains (Pegan et al., 2006). Interestingly, the K^+ ion was not directly interacting with negatively charged side chains, but mediated through waters bound to Asp 255. Looking across the whole Kir family of channels this mediation of K+ ions through water is an important concept. Although the Asp 255 is highly conserved in the Kir family, some hetero-tetrameric Kir channels have two serines at this location. As the K+ ion is hydrated it could still be coordinated with the serine. A recent electrophysiology study based on the Kir2.1 structure found that an absence of negatively charged residues located in the cytoplasmic pore (box 2 and box 3) reduces single channel conduction. When observed from a perspective of the channel having discreet sites for hydrated inline potassium to occupy, this result was not surprising. The absence of one occupied state would inhibit the movement of K+ from the pre-mutated site to the next site. In the end, the results in Chapter 2 and Chapter 3 coupled with more in-depth electrophysiology experiments carried out recently, suggests that the K+ ions

permeate through the cytoplasmic domains as inline hydrated ions via discreet binding sites.

Rectification. As mentioned previously in Chapter 1, the flow of K^+ ions from the cytoplasm to the extracellular environment through Kir2.1 channels is impeded by the property of rectification. Over the past two decades, several electrophysiology studies have provided data on the residues responsible for rectification. The resulting consensus is that rectification occurs when polyamines and Mg^{2+} ions bind to a strong site in the trans-membrane region, coordinated by Asp 172, and a weaker site in the cytoplasmic domain (Kubo and Murata, 2001; Nichols and Lopatin, 1997; Yang et al., 1995).

Prior to the Kir2.1$_L$ structure, exactly which residues in the cytoplasmic domains influenced binding of the blockers was not yet fully determined (Chen et al., 2002; Kubo and Murata, 2001; Lu and MacKinnon, 1994; Yang et al., 1995). In Chapter 2 we visualized all residues that are pore-lining revealing the complexity of the weaker site (Pegan et al., 2005). As expected we see multiple negatively charged side chains facing the pore. Surprisingly, we also see positively charged residues that form either full or partial salt bridges with these negative residues. The presence of these positive residues suggests that they fine tune the binding of positively charged particles to the weaker site and serve as another way that nature can adjust the inward

rectification strength without eliminating the negatively charged residues. These findings are reinforced by recent in-depth electrophysiology studies based on the work presented in Chapter 2 (Fujiwara and Kubo, 2006). Many attempts have been subsequently made to visualize the binding of polyamines directly to the weak site via x-ray crystallography; however, they have been inconclusive. Based on the hypothesis that the K^+ may travel through the pore single file by interacting with negative residues via its hydrated shell, polyamines acting in a similar matter can not be ruled out.

Gating of the Cytoplasmic domain. All of the structures of Kir channels to this date have been solved without phosphylinositol-4,5-bisphosphate (PIP_2) or other ligands required for them to be in an open state (Kuo et al., 2003; Nishida and MacKinnon, 2002; Pegan et al., 2006; Pegan et al., 2005). One of the major obstacles in directly determining the gating mechanism of the Kir2.1 channel and Kir channels at large was the absence of direct observation of this state. With the PIP_2 containing long fatty side chains, direct application of PIP_2 to a non-micelle bound cytoplasmic domain was impractical. However, several attempts were made to co-crystallize $Kir2.1_L$ with a PIP_2 analog, which contained only the head-group and a four carbon fatty side chain, failed. The addition at low concentrations resulted in no PIP_2 analog being observed and at higher concentrations it inhibited crystal growth.

In the absence of a definitive open state, we were able to compare in Chapter 2 the Kir2.1 and Kir3.1 structures and observe the G-loops flexibility (Pegan et al., 2005). By indirectly observing the role of the G-loop via electrophysiology we were able to determine that this loop forms Gate 2 (Fig. 5.1). Based of the structure of $Kir2.1_L$, the G-loop gating mechanism is coupled at its base to the CD loop via a Glu 303/Arg 312 salt bridge and the polar interactions of Arg 218 with Thr 309. The CD loop contains Lys 219, which is believed to comprise part of the putative PIP_2 binding site. The $R218Q/T309_S$ (44-64 fused to 189-371) structure in Chapter 3 supports several elements of this proposed mechanism (Pegan et al., 2006). Disruption of the Arg 218/Thr 309 site results in each monomer's G-loops adopting a different conformation and Glu 303 is seen in differing states that could provide a glimpse of its open state conformation. The $R218Q/T309_S$ structure also allowed us to observe the flexibility of the G-loop within the same channel, instead of across family lines. By utilizing the different states of the monomers in the $R218Q/T309_S$ structure, multiple cytoplasmic states can be constructed (Fig 5.2). The different states suggest that the G-loop can bend up and away exposing the Ala 306 main chain carboxylic oxygen atom and Met 301 side chain to the cytoplasmic pore. In conjunction with providing coordinating pore facing atoms, bending of the G-loop also opens the pore from the ~2.9 Å to ~5.8 Å. The increase in pore size and availability of coordinating atoms allows hydrated K^+ ions through gate 2 (Fig. 5.2).

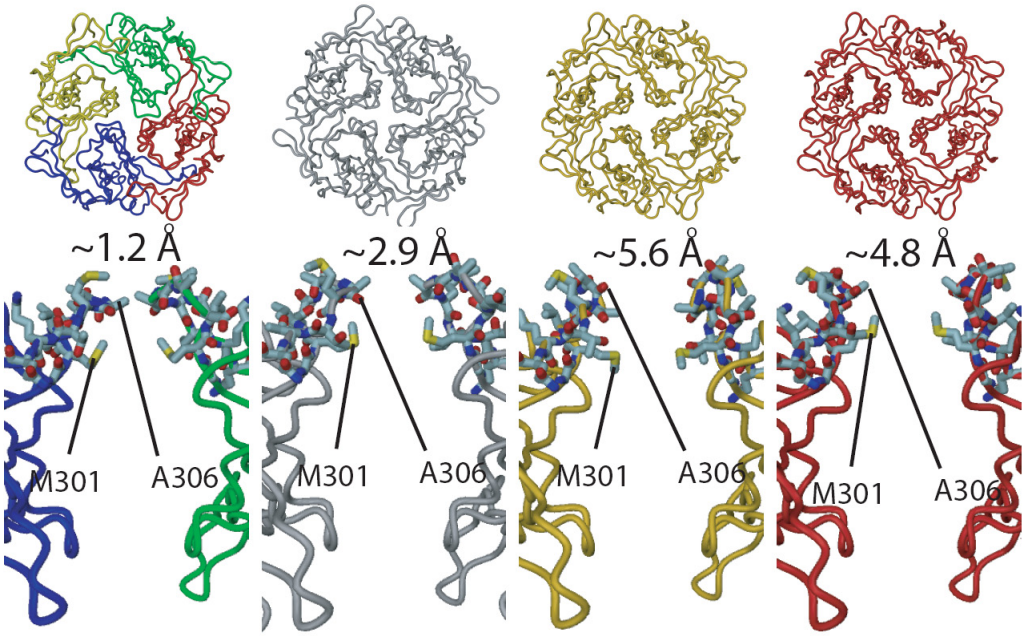

Figure 5.2. Different Confirmations of the G-loop. From left to right. In the first frame on top is the R218Q/T309K$_S$ structure. Below is monomers B and D from the R218Q/T309K$_S$ structure. Frame 2 top is of the wild type Kir2.1$_L$ structure with the monomers A and C below. Frame 3 top is of a tetramer comprised of R218Q/T309K$_S$ structure's A monomer with side view below of two subunits. Frame 4 top is of a tetramer comprised of R218Q/T309K$_S$ structure's C monomer with side view below of two subunits.

Conclusion. Throughout the past four chapters I have described the structural characterization of the entire cytoplasmic domain of the Kir2.1 channel. Findings stemming from these structures and structurally guided electrophysiology studies have uncovered the roles that the Kir2.1 cytoplasmic domain plays in gating, rectification, and K+ permeation. In the course of this research I have also uncovered a chemical that binds to a biologically relevant site, which can be used as a drug frame work to potentially modulate different types of Kir channels. Furthermore, I have revealed possible molecular mechanisms for certain Andersen's Syndrome cytoplasmic mutations result in non-conducting channels. Taken together, these advances allow us

a greater understanding of the role that cytoplamic domains play not just in Kir2.1 channels but Kir channels as a whole.

5.2 REFERENCES

Chen, L., Kawano, T., Bajic, S., Kaziro, Y., Itoh, H., Art, J. J., Nakajima, Y., and Nakajima, S. (2002). A glutamate residue at the C terminus regulates activity of inward rectifier K+ channels: implication for Andersen's syndrome. Proc Natl Acad Sci U S A *99*, 8430-8435.

Fujiwara, Y., and Kubo, Y. (2006). Functional Roles of Charged Amino Acid Residues on the Wall of the Cytoplasmic Pore of Kir2.1. J Gen Physiol.

Guo, Y., Waldron, G. J., and Murrell-Lagnado, R. (2002). A role for the middle C terminus of G-protein-activated inward rectifier potassium channels in regulating gating. J Biol Chem *277*, 48289-48294.

Hille, B. (2001). Ion Channels of Excitable Membranes, Third edn (Sunderland, MA: Sinauer Associates, Inc.).

Kubo, Y., and Murata, Y. (2001). Control of rectification and permeation by two distinct sites after the second transmembrane region in Kir2.1 K+ channel. J Physiol *531*, 645-660.

Kuo, A., Gulbis, J. M., Antcliff, J. F., Rahman, T., Lowe, E. D., Zimmer, J., Cuthbertson, J., Ashcroft, F. M., Ezaki, T., and Doyle, D. A. (2003). Crystal structure of the potassium channel KirBac1.1 in the closed state. Science *300*, 1922-1926.

Long, S. B., Campbell, E. B., and Mackinnon, R. (2005). Crystal structure of a mammalian voltage-dependent Shaker family K+ channel. Science *309*, 897-903.

Lu, T., Nguyen, B., Zhang, X., and Yang, J. (1999a). Architecture of a K+ channel inner pore revealed by stoichiometric covalent modification. Neuron *22*, 571-580.

Lu, T., Zhu, Y. G., and Yang, J. (1999b). Cytoplasmic amino and carboxyl domains form a wide intracellular vestibule in an inwardly rectifying potassium channel. Proc Natl Acad Sci U S A *96*, 9926-9931.

Lu, Z., and MacKinnon, R. (1994). Electrostatic tuning of Mg2+ affinity in an inward-rectifier K+ channel. Nature *371*, 243-246.

Nichols, C. G., and Lopatin, A. N. (1997). Inward rectifier potassium channels. Annu Rev Physiol *59*, 171-191.

Nishida, M., and MacKinnon, R. (2002). Structural basis of inward rectification: cytoplasmic pore of the G protein-gated inward rectifier GIRK1 at 1.8 A resolution. Cell *111*, 957-965.

Pegan, S., Arrabit, C., Slesinger, P. A., and Choe, S. (2006). Andersen's Syndrome Mutation Effects on the Structure and Assembly of the Cytoplasmic Domains of Kir2.1. Submitted.

Pegan, S., Arrabit, C., Zhou, W., Kwiatkowski, W., Collins, A., Slesinger, P. A., and Choe, S. (2005). Cytoplasmic domain structures of Kir2.1 and Kir3.1 show sites for modulating gating and rectification. Nat Neurosci *8*, 279-287.

Yang, J., Jan, Y. N., and Jan, L. Y. (1995). Control of rectification and permeation by residues in two distinct domains in an inward rectifier K+ channel. Neuron *14*, 1047-1054.

Zhou, Y., and MacKinnon, R. (2003). The occupancy of ions in the K+ selectivity filter: charge balance and coupling of ion binding to a protein conformational change underlie high conduction rates. J Mol Biol *333*, 965-975.

SECTION II

CHAPTER SIX

High-throughput backbone resonance assignment of small ^{13}C, ^{15}N labeled proteins by a triple resonance experiment with four sequential connectivity pathways: HNCACB$^{\text{coded HAHB}}$

6.1 ABSTRACT

The proposed three-dimensional triple resonance experiment HNCACB^{coded}HAHB correlates sequential ^{15}N,^{1}H moieties *via* the chemical shifts of $^{13}C^{\alpha}$, $^{13}C^{\beta}$, $^{1}H^{\alpha}$ and $^{1}H^{\beta}$. The four sequential correlation pathways are achieved by the incorporation of the concept of chemical shift-coding to the TROSY-HNCACB experiment (Kwiatkowski and Riek, 2003). The monitored $^{1}H^{\alpha}$ and $^{1}H^{\beta}$chemical shifts are then coded in the line-shape of the cross-peaks of $^{13}C^{\alpha}$, $^{13}C^{\beta}$ along the ^{13}C dimension through an apparent residual scalar coupling, the size of which depends on the attached hydrogen chemical shift. The information of four sequential correlation pathways enables a rapid backbone assignment. The HNCACB^{coded}HAHB experiment was applied to ~85% labeled ^{13}C,^{15}N-labeled amino-terminal fragment of Vaccinia virus DNA topoisomerase I comprising residues 1-77. After one day of measurement on a Bruker Avance 700 MHz spectrometer and one day of manual analysis of the spectrum 93% of the backbone assignment was achieved.

6.2 INTRODUCTION

Rapid chemical shift assignment of proteins combined with a reduction of NMR measuring time are instrumental for high-throughput structure activity relationship by NMR and structural genomics (Montelione et al., 2000; Zuiderweg, 2002). In the so-called "non-sensitivity-limited" data collection regime, the combination of both requirements can be fulfilled by limiting the number of dimensions to less than 4, but increasing the number of (sequential) correlations per data set (footnote: in the "non-sensitivity-limited" data collection regime the sampling of the multidimensional NMR experiment determines the minimally achievable measurement time and not the sensitivity of the experiment) (Szyperski et al., 2002). One approach to achieve this is the concept of reduced dimensionality introduced by Szyperski et al. (1993) and successively expanded to a variety of experiments including G-matrix Fourier transform NMR spectroscopy (Ding and Gronenborn, 2002; Kim and Szyperski, 2003; Szyperski et al., 1993; Szyperski et al., 2002). Reduced dimensionality NMR is based on simultaneous evolutions of two or more different chemical shifts reducing a n+1 dimensional triple resonance experiment to n dimensions. Indeed, the measurement of 5 3D reduced dimensionality triple-resonance experiments and one 3D HNCACB experiment with a total measuring time of 42.5 hours enabled an automatic backbone assignment (including beta carbon and beta hydrogens) of a 71 residue $^{13}C,^{15}N$-labeled protein (concentration 1 mM, pH 6.5, 298 K; (Szyperski et al., 2002). An additional approach to increase the quality of

correlation in triple-resonance experiments was proposed by Zweckstetter and Bax using splitting of cross-peaks by residual dipolar coupling (Zweckstetter and Bax, 2001).

We proposed an alternative approach to increase the number of correlations without the increase of the number of dimensions (Kwiatkowski and Riek, 2003). The strength of the so-called concept of chemical shift-coding is the ease of implementation and the addition of chemical shift information without major losses of signal, since no additional chemical shift evolution and polarization transfers are required, whereas both are required in the reduced dimensionality experiments. In return, the resolution of the additional chemical shifts is limited (Kwiatkowski and Riek, 2003). The minimal sensitivity loss enables the incorporation of the concept of chemical shift-coding to the low-sensitive TROSY-HNCACB experiment (Bax and Grzesiek, 1993; Pervushin et al., 1997; Riek et al., 2000; Salzmann et al., 1999; Sattler et al., 1999; Witekind and Muller, 1993). As a result, this implementation enhances the sequential correlations between $^{15}N,^{1}H$-moieties from two ($^{13}C^{\alpha}$ and $^{13}C^{\beta}$ chemical shifts) to four ($^{13}C^{\alpha},^{13}C^{\beta}$ $^{1}H^{\alpha},^{1}H^{\beta}$ chemical shifts). By employing this method, we demonstrate four sequential correlation pathways enables a high-throughput manual backbone assignment for a small $^{13}C,^{15}N$-labeled protein.

6.3 METHODS AND RESULTS

Technically, the proposed HNCACB^{coded}HAHB experiment is essentially based on the 3D TROSY-HNCACB experiment, but obtains additional information of the chemical shift of $^{1}H^{\alpha}$ and $^{1}H^{\beta}$ through the concept of chemical shift-coding (Kwiatkowski and Riek, 2003). This pulse sequence is depicted in the experimental scheme of Figure 6.1. Between time points *a* and *c*, magnetization is transferred from ^{1}H via ^{15}N to $^{13}C^{\alpha/\beta}$, using three successive INEPT steps (Morris and Freeman, 1979; Wider, 1998). During the frequency labeling period t_2 the $^{13}C^{\alpha/\beta}$ chemical shifts evolve. Simultaneously, the $^{1}J(^{13}C,^{1}H)$ scalar coupling of ~140-155 Hz begins to evolve. However, the apparent extent of the evolution of the $^{1}J(^{13}C,^{1}H)$ coupling is under the control of the 180° soft pulse on $^{1}H^{\alpha/\beta}$. The soft pulse is on-resonance at 3.5 ppm and contains a Gaussian inversion profile, which decreases to ~5% at 2 ppm and 5 ppm. Thus, the multiplet splitting of the cross-peak along the ^{13}C dimension and concomitantly the extent of the apparent $^{1}J(^{13}C,^{1}H)$ coupling depend on the position of the attached $^{1}H^{\alpha/\beta}$ chemical shifts. In other words, the $^{1}H^{\alpha/\beta}$ chemical shifts are encoded in the pattern of the cross-peak along ^{13}C dimension through an apparent residual scalar coupling $^{residual}J(^{13}C,^{1}H)$ (Kwiatkowski and Riek, 2003). After chemical shift evolution modulated by the chemical shift-dependent scalar coupling, magnetization is transferred back to ^{15}N at time point *d*. Between *d* and *e* the ^{15}N nuclei evolve with their chemical shifts during a constant time period. From time point

e onward magnetization is transferred back to ^{1}H. The flow coherence can thus be described as follows:

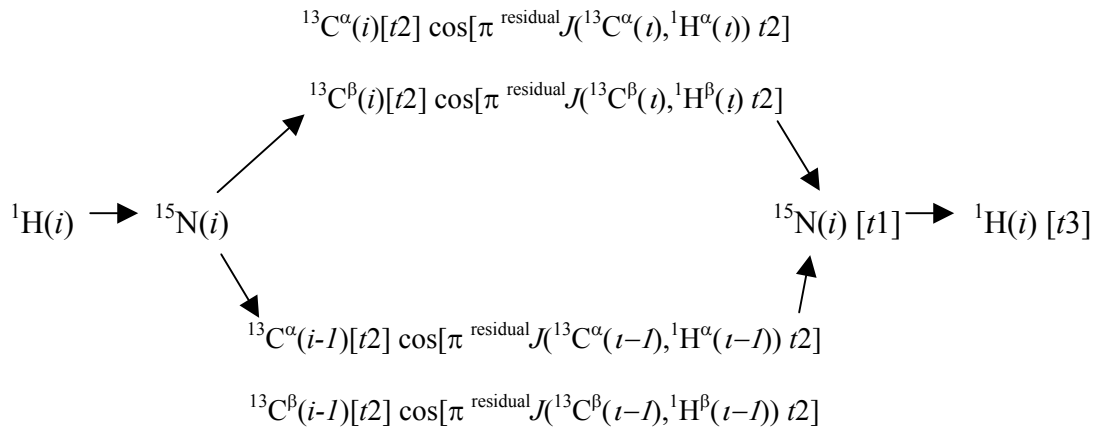

where t_1 and t_2 are the ^{15}N and ^{13}C evolution times and t_3 is the ^{1}H acquisition time. Indices *i* and *i*-1 indicate that coherence is transferred from $^{15}N(i)$-$^{1}H(i)$ to both the sequentially and the intra-residually adjoining carbons. The coded ^{1}H chemical shift is designated with the cosine modulation of its apparent residual scalar coupling, $^{residual}J(^{13}C^{\alpha},^{1}H^{\alpha})$, or $^{residual}J(^{13}C^{\beta},^{1}H^{\beta})$active during *t*2.

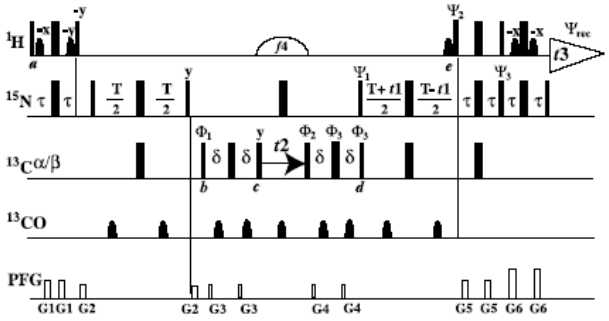

Figure 6.1 Pulse Sequences. Experimental scheme for the HNCACB^{coded}HAHB experiment for ^{13}C,^{15}N-labeled proteins. The radio-frequency pulses on ^{1}H, ^{15}N, ^{13}C$^\alpha$ or ^{13}C$^\beta$ were applied at 4.8, 119, 45, and 174 ppm, respectively. The narrow and wide black bars indicate non-selective 90° and 180° pulses, respectively. On the line marked ^{1}H a large sine-bell shaped pulse labeled with *f4* indicates a selective 180° pulse with a Gaussian shape truncated at 5% and the duration of 1.3 ms. The soft pulse is on resonance at 3.5 ppm and its length has been optimized for the magnetic field strength of 700 MHz ^{1}H frequency. The inversion profile is described in Kwiatkowski et al. (2003). On the line marked ^{13}C$^\beta$, black sine bell shapes indicate selective 180° pulses with the duration of 0.08 ms and a Gaussian shape truncated at 5%. The line marked PFG indicates durations and amplitudes of sine shaped pulse magnetic field gradients applied along the z-axis. : G1: 0.8 ms, 15 G/cm, G2: 0.8 ms, 9 G/cm; G3: 0.5 ms, 18 G/cm; G4: 0.5 ms, 18 G/cm; G5: 0.8 ms, 12 G/cm; G4: 0.8 ms, 22 G/cm. The delays τ, T, ανδ δ are 2.7 ms, 24 ms and 3.6 ms, respectively. The phase cycle is Ψ_1 = {y,-y,x,-x}, Ψ_2 = {-y}, Ψ_3 = {-y}, Φ_1 = {x, x, x, x,-x,-x,-x,-x}, Φ_2 = {-y}, Φ_3= {x}, and Φ_{rec} = {y,-y,-x,x,-y,y,x,-x}. All other radio frequency pulses are applied either with phase x or as indicated above the pulses. In the ^{15}N(*t*1) dimension a phase-sensitive spectrum is obtained by recording a second FID for each increment of *t*1, with Ψ_1 = {y, -y, -x, x}, Ψ_2 = {y}, Ψ_3 = {y} and the data are processed as described by (Kay et al., 1992). Quadrature detection in the ^{13}C$^\alpha$(*t*2) dimension is achieved by the States-TPPI method (Marion et al., 1989) applied to phase Φ_1, Φ_2 and Φ_3. Between time points *c* and *d* the timing of the radio frequency pulses of the different nuclei have been implemented in a parallel manner to achieve an initial $t_2 = 0$. On the line marked ^{1}H, black sine-bell shapes indicate water-selective 90° pulses with the duration of 1 ms and a Gaussian shape truncated at 5%. With these pulses, the water magnetization stays aligned along the +z-axis throughout the experiment (Grzesiek and Bax, 1993). Alternatively, we replaced the water-selective pulses with a superposition of two Gaussian pulses (truncated at 5% and length 1 ms) on resonance at the water-frequency and at 1.7 ppm, respectively. This procedure aligns the water magnetization and part of the aliphatic hydrogens along the +z axis throughout the experiment yielding longitudinal relaxation-optimized spectroscopy (Pervushin et al., 2002). The measured gain in signal-to-noise was about 10% (data not shown). In our hands, the performance of the superposition of two Gaussian pulses is superior to the E-BURP pulse proposed by (Pervushin et al., 2002) since the extent of the water-flip back can be controlled better and an incomplete alignment of the water magnetization along the +z axis results in severe losses in signal-to-noise when applied to our high pH sample (pH 7). The soft pulse *f4* is chosen to perturb the water resonance frequency minimally.

Fig. 6.2 shows strips from a 3D HNCACB^{coded}HAHB spectrum of uniformly 85% $^{13}C,^{15}N$-labeled N-terminal domain of Vaccinia virus DNA topoisomerase I comprising residues 1-77 (Sharma et al., 1994). In addition, the protein sample contains a six residues-long histidine-tag residual with the sequence GSHGGS. The relatively low incorporation of stable isotopes is due to the cost-effective, effienct, and rapid approach of protein preparation that was used (Marley et al., 2001). As in the conventional HNCACB experiment, two positive cross-peaks for the sequential and intra-residual $^{13}C^{\alpha}$s two negative cross-peaks for the sequential and intra-residual $^{13}C^{\beta}$s are observed for each spin system. The stronger cross-peaks correspond to intra-residue correlations between the carbons and the ^{15}N-^{1}H moiety, and the weaker cross-peak represents the sequential correlations. These cross-peaks are split due to the active $^{residual}J(^{13}C,^{1}H)$-coupling, the size of which is related to the attached hydrogen chemical shift. The cross-peak is not split if the attached $^{1}H^{\alpha}$ chemical shift is 3.5 ppm, whereas the cross-peak is a doublet of 144 Hz if the corresponding $^{1}H^{\alpha}$ chemical shift is ≥ 5.3 ppm. An apparent residual scalar coupling of 0-144 Hz corresponds to a $^{1}H^{\alpha}$chemical shift between 3.5-5.3 ppm with a resolution of ~ 0.2 ppm (Kwiatkowski and Riek, 2003). Similarly, the $^{13}C^{\beta}$- cross-peaks are split due to the $^{1}H^{\beta}$ chemical shifts. Thus, sequential correlations can be traced with four probes: the $^{13}C^{\alpha}$, $^{13}C^{\beta}$ $^{1}H^{\alpha}$, and $^{1}H^{\beta}$ chemical shifts. Although the resolution of the coded chemical shifts in the line shape of the cross-peak is low, it enhances the sequential correlation quality by

more than one order in magnitude (Kwiatkowski and Riek, 2003). Indeed, with the HNCACB^{coded}HAHB experiment a straight-forward sequential walk can be traced through the multiplets of the ^{13}C cross-peaks including the overall position of the $^{13}C^{\alpha}$ and $^{13}C^{\beta}$ cross-peaks as a point of departure (Fig. 6.2). Only when the multiplet pattern of the sequential $^{13}C^{\alpha}$ and $^{13}C^{\beta}$ cross-peaks coincides with the multiplet of the intra-residual cross-peaks, the sequential connectivity can be traced. When the patterns do not fit, the two involved ^{15}N-^{1}H moieties are not neighbors. With this procedure the sequential assignment is ensured by four independent correlations, the alpha-carbon and beta-carbon chemical shifts and indirectly the alpha-hydrogen and beta-hydrogen chemical shifts by the residual scalar couplings. Since this high quality of information generates practically no ambiguities, sequential assignment is also possible in rare cases where the sequential and intra-residual cross-peaks have similar intensities and can not be classified straightforwardly. In the conventional experiments additional spectra, i.e. HN(CO)CA or CBCA(CO)NH, are collected to classify the crosspeak into a sequential or intraresidual correlation.

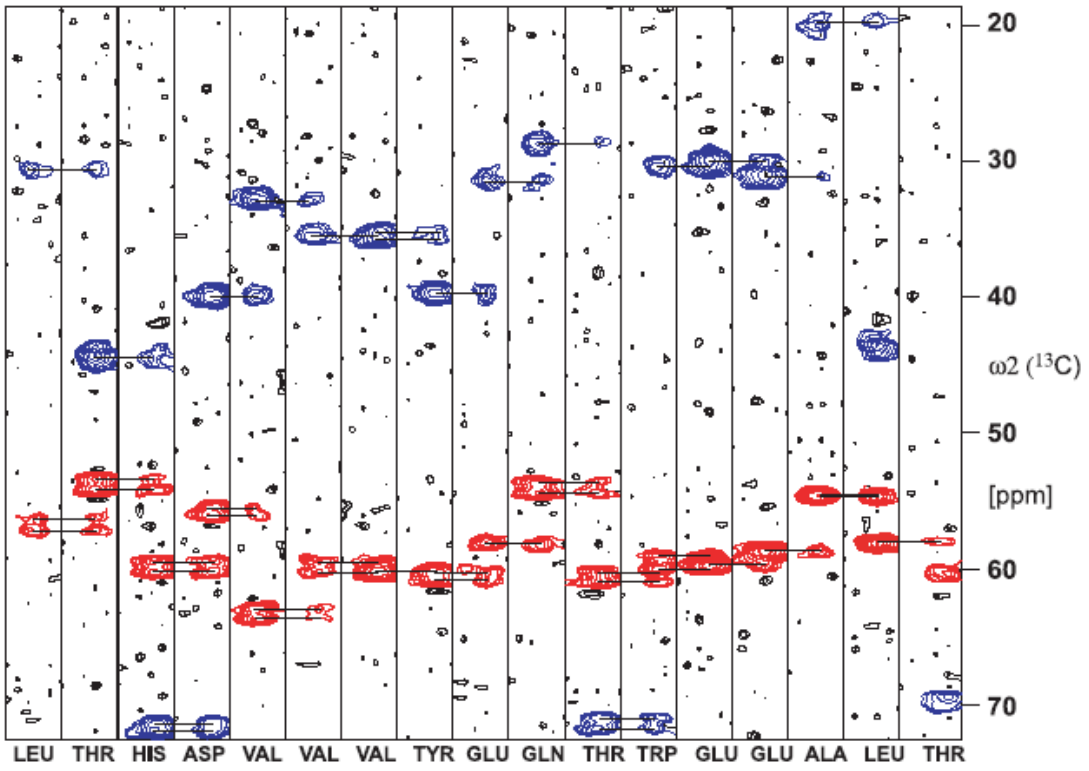

Figure 6.2 Sample of TOPO(-77) Assignment. Strips along the $\omega_2(^{13}C)$ dimension of the 3D HNCACB^{coded}HAHB spectrum of $^{13}C,^{15}N$-labeled TOPO(1-77). The sequence-specific backbone assignment of residues 39-55, which corresponds to 20% of the protein, is shown. The strips are centered about the corresponding $^{1}H^{N}$ chemical shifts. The sequential connectivities are indicated by horizonal lines. Positive contour lines are red, negative contour lines blue, respectively. The experiment was recorded at 20° C with a 0.8 mM sample of $^{13}C,^{15}N$-labeled TOPO(1-77) in a mixed solvent of 95% H_2O/5% D_2O at pH 7, using a Bruker Avance 700 MHz spectrometer equipped with five radio-frequency channels, a pulsed field gradient unit and a triple resonance probe with an actively shielded z-gradient coil. The following parameter settings were used: data size = 50($t1$)* 85($t2$)*1024($t3$) complex points; $t1_{max}$ (^{15}N)= 23 ms, $t2_{max}$ ($^{13}C^{\alpha}$) = 7.5 ms, $t3_{max}$(^{1}H) = 100 ms. The data set was zero-filled to 128*1024*2048 complex points; 8 scans per increment were acquired, resulting in 22 hours of measuring time. Prior to Fourier transformation the data were multiplied with a 75° shifted sine-bell window in all dimensions.

6.4 DISCUSSION

The HNCACB^{coded}HAHB experiment of Figure 2 was measured in 24 hours on our Bruker Avance 700 MHz spectrometer, which corresponds to about 3 hours measurement time with a cryoprobe. Manual analysis of the spectrum during one 8 hour working day yielded 93% of the backbone assignment of 80%-labeled $^{13}C,^{15}N$-labeled TOPO(1-77). The remaining five ^{15}N-^{1}H moieties were not assigned due to the lack of sequential correlations in the HNCACB^{coded}HAHB experiment. The absence of sequential peaks is probably because of local relaxation properties attributed to slow conformational exchange. In combination with a $^{13}C,^{15}N$-resolved [$^{1}H,^{1}H$]-NOESY experiment, these residual moieties were easily assigned. Alternatively, a HN(CO)CA experiment (Salzmann et al., 1999) with inherently higher sensitivity for sequential cross-peaks than the HNCACB^{coded}HAHB would give complementary information.

As demonstrated with TOPO(1-77) (Fig. 6.2 shows 20% of the sequential backbone assignment) the proposed HNCACB^{coded}HAHB is a very powerful experiment in the "non-sensitivity-limited" data collection regime and therefore highly recommended for small $^{13}C,^{15}N$-labeled proteins. However, for a 20 kDa ^{13}C, ^{15}N labeled protein the HNCACB^{coded}HAHB experiment is a factor of 1.5-2 less sensitive than a conventional TROSY-HNCACB experiment, which itself is a factor of 10 less sensitive than a TROSY-HNCA experiment (Sattler et al., 1999). Therefore, for large target systems we propose the use of the sensitivity-driven HNCA^{coded}CB and

HNCA^{coded}CO experiments combined with ~70% deuteration and uniformly ^{13}C and ^{15}N labeling (Ritter et al., 2003).

In conclusion, the proposed HNCACB^{coded}HAHB reduces dramatically ambiguities in linking the spin systems of adjacent residues in the protein sequence during the sequential assignment process and, therefore, allows the fast manual backbone assignment of small ^{13}C,^{15}N-labeled proteins.

6.5 ACKNOWLEDGMENTS

We thank the H. and J. Weinberg Foundation, the H.N. and F. C. Berger Foundation, the Auen Foundation (R.R.), and American Heart Association (S.C.) for financial support.

Chapter 6 is in part a reprint of the material as it appears in Pegan, S., Kwiatkowski, W., Choe, S., Riek, R. (2003) *High-throughput backbone resonance assignment of small ^{13}C, ^{15}N labeled proteins by a triple resonance experiment with four sequential connectivity pathways using chemical shift-dependent apparent $^{1}J(^{1}H,^{13}C)$: HNCACB^{coded}HAHB*. J. Magn. Reson., **165**: 315-319. The dissertation author was the primary research and author of these publications.

6.6 REFERENCES

Bax, A., and Grzesiek, S. (1993). Methodological advances in protein NMR. Acc Chem Res, 131-138.

Ding, K., and Gronenborn, A. M. (2002). Novel 2D triple-resonance NMR experiments for sequential resonance assignments of proteins. J Magn Reson *156*, 262-268.

Grzesiek, S., and Bax, A. (1993). The importance of not saturating H2O in protein NMR. Application to sensitivity enhancement and NOE measurements. J Am Chem Soc, 12593-12594.

Kay, L. E., Keifer, P., and Saarinen, T. (1992). Pure absorption gradient enhanced heteronuclear single quantum correlation spectroscopy with improved sensitivity. J Am Chem Soc *114*, 10663-10665.

Kim, S., and Szyperski, T. (2003). GFT NMR, a new approach to rapidly obtain precise high-dimensional NMR spectral information. J Am Chem Soc *125*, 1385-1393.

Kwiatkowski, W., and Riek, R. (2003). Chemical shift-dependent apparent scalar couplings: an alternative concept of chemical shift monitoring in multi-dimensional NMR experiments. J Biomol NMR *25*, 281-290.

Marion, D., Ikura, M., Tschudin, R., and Bax, A. (1989). Rapid recording of 2D NMR spectra without phase cycling: application to the study of hydrogen exchange in proteins. J Magn Reson, 393-399.

Marley, J., Lu, M., and Bracken, C. (2001). A method for efficient isotopic labeling of recombinant proteins. J Biomol NMR *20*, 71-75.

Montelione, G. T., Zheng, D., Huang, Y. J., Gunsalus, K. C., and Szyperski, T. (2000). Protein NMR spectroscopy in structural genomics. Nat Struct Biol *7 Suppl*, 982-985.

Morris, G. A., and Freeman, R. (1979). Enhancement of NMR signals by polarization transfer. J Am Chem Soc, 760-762.

Pervushin, K., Riek, R., Wider, G., and Wuthrich, K. (1997). Attenuated T2 relaxation by mutual cancellation of dipole-dipole coupling and chemical shift anisotropy

indicates an avenue to NMR structures of very large biological macromolecules in solution. Proc Natl Acad Sci U S A *94*, 12366-12371.

Pervushin, K., Vogeli, B., and Eletsky, A. (2002). Longitudinal (1)H relaxation optimization in TROSY NMR spectroscopy. J Am Chem Soc *124*, 12898-12902.

Riek, R., Pervushin, K., and Wuthrich, K. (2000). TROSY and CRINEPT: NMR with large molecular and supramolecular structures in solution. Trends Biochem Sci *25*, 462-468.

Ritter, C., Luhrs, T., Kwiatkowski, W., and Riek, R. (2003). 3D TROSYHNCAcodedCB and TROSY-HNCAcodedCO experiments: two triple resonance NMR experiments with two sequential connectivity pathways and high sensitivity. J Biomol NMR.

Salzmann, M., Pervushin, K., Wider, G., Senn, H., and Wuthrich, K. (1999). [13C]-constant-time [15N,1H]-TROSY-HNCA for sequential assignments of large proteins. J Biomol NMR *14*, 85-88.

Sattler, M., Schleucher, J., and Griesinger, C. (1999). Heteronuclear multidimensional NMR experiments for the structure determination of proteins in solution employing pulsed field gradients,. Prog Nucl Magn Reson Spectrosc, 93-158.

Sharma, A., Hanai, R., and Mondragon, A. (1994). Crystal structure of the amino-terminal fragment of vaccinia virus DNA topoisomerase I at 1.6 A resolution. Structure *2*, 767-777.

Szyperski, T., Wider, G., Bushweller, J., and Wuthrich, K. (1993). Reduced dimensionallity in triple-resonance NMR experiments. J AM Chem Soc, 262-268.

Szyperski, T., Yeh, D. C., Sukumaran, D. K., Moseley, H. N., and Montelione, G. T. (2002). Reduced-dimensionality NMR spectroscopy for high-throughput protein resonance assignment. Proc Natl Acad Sci U S A *99*, 8009-8014.

Wider, G. (1998). Technical aspects of NMR spectroscopy with biological macromolecules and studies of hydration in solution. Prog NMR Spectrosc, 193-275.

Witekind, M., and Muller, L. (1993). a high sensitivity 3D NMR experiment to correlate amide-proton and nitrogen resonances with the alpha and beta carbon resonances in proteins. J Magn Reson, 201-205.

Zuiderweg, E. R. (2002). Mapping protein-protein interactions in solution by NMR spectroscopy. Biochemistry *41*, 1-7.

Zweckstetter, M., and Bax, A. (2001). Single-step determination of protein substructures using dipolar couplings: aid to structural genomics. J Am Chem Soc, 9490-9491.